



PHASE EQUILIBRIUM CALCULATIONS FOR HIGH-PRESSURE SYSTEMS
WITH GAS HYDRATES

Matheus Caputo Bello

Dissertação de Mestrado apresentada ao Programa de Pós-graduação em Engenharia Química, COPPE, da Universidade Federal do Rio de Janeiro, como parte dos requisitos necessários à obtenção do título de Mestre em Engenharia Química.

Orientadores: Frederico Wanderley Tavares,
D.Sc.
Iuri Soter Viana Segtovich,
D.Sc.

Rio de Janeiro

Setembro de 2022

PHASE EQUILIBRIUM CALCULATIONS FOR HIGH-PRESSURE SYSTEMS
WITH GAS HYDRATES

Matheus Caputo Bello

DISSERTAÇÃO SUBMETIDA AO CORPO DOCENTE DO INSTITUTO
ALBERTO LUIZ COIMBRA DE PÓS-GRADUAÇÃO E PESQUISA DE
ENGENHARIA DA UNIVERSIDADE FEDERAL DO RIO DE JANEIRO COMO
PARTE DOS REQUISITOS NECESSÁRIOS PARA A OBTENÇÃO DO GRAU
DE MESTRE EM CIÊNCIAS EM ENGENHARIA QUÍMICA.

Orientadores: Frederico Wanderley Tavares, D.Sc.
Iuri Soter Viana Segtovich, D.Sc.

Aprovada por: Prof. Frederico Wanderley Tavares, D.Sc.
Iuri Soter Viana Segtovich, D.Sc.
Prof. Pedro de Alcântara Pessoa Filho, D.Sc.
Prof. Márcio Luis Lyra Paredes

RIO DE JANEIRO, RJ – BRASIL

SETEMBRO DE 2022

Caputo Bello, Matheus

Phase equilibrium calculations for high-pressure systems with gas hydrates/Matheus Caputo Bello. – Rio de Janeiro: UFRJ/COPPE, 2022.

XIX, 106 p.: il.; 29, 7cm.

Orientadores: Frederico Wanderley Tavares, D.Sc.

Iuri Soter Viana Segtovich, D.Sc.

Dissertação (mestrado) – UFRJ/COPPE/Programa de Engenharia Química, 2022.

Referências Bibliográficas: p. 101 – 106.

1. Hydrates. 2. Pressure shift. 3. High pressure.
4. van der Waals and Platteeuw. I. Wanderley Tavares, D.Sc., Frederico *et al.* II. Universidade Federal do Rio de Janeiro, COPPE, Programa de Engenharia Química. III. Título.

*Irmão, você não percebeu
Que você é o único representante
Do seu sonho na face da terra
Se isso não fizer você correr,
chapa
Eu não sei o que vai
– Levanta e anda, de Emicida*

Agradecimentos

Primeiramente, gostaria de agradecer aos meus orientadores que foram essenciais tanto para minha formação enquanto acadêmico quanto para o resultado deste trabalho. Professor Fred e Iuri, além do conhecimento técnico, vocês me transmitiram sua paixão pela Termodinâmica. Obrigado por isso.

É claro que eu não poderia deixar de agradecer às pessoas que me dão estrutura e que me servem de referência. Valdmir, Adriana, Lucas e Anna, eu não teria chegado tão longe sem vocês. Pai e mãe, obrigado por terem estabelecido este alicerce indestrutível o qual eu piso, eu só imagino o quanto vocês renunciaram para construí-lo. Lucas, meu irmão, obrigado por todo seu amor, carinho e parceria. E Anna, minha parceira, obrigado por me inspirar a ser melhor todos os dias. Eu amo vocês.

Além de meus laços sanguíneos, gostaria de agradecer à família que acumulei ao longo da minha trajetória: Bia, Dandara, Filipe, Hyago, Júlia, Lucas Gabriel, Marcio, Natália, Paula, Paulo Vítor, Pedro, Renan, Rodrigo e Vítor. Meus queridos amigos, obrigado por tornarem a minha caminhada tão mais leve e por compartilharem suas vidas comigo.

Agradeço também aos meus colegas de laboratório e pós-graduação, que sempre se mostraram disponíveis para me ajudar nos momentos mais tensos. Mesmo à distância, o ATOMS sempre se preocupou com a formação profissional e o acolhimento de seus integrantes, e por isso, sou muito grato.

Deixo aqui meu agradecimento a todos os outros professores e mestres que participaram da minha formação e que me guiaram através dos caminhos que eu trilhei.

Resumo da Dissertação apresentada à COPPE/UFRJ como parte dos requisitos necessários para a obtenção do grau de Mestre em Ciências (M.Sc.)

CÁLCULOS DE EQUILÍBRIO DE FASES PARA SISTEMAS EM ALTA PRESSÃO ENVOLVENDO HIDRATOS

Matheus Caputo Bello

Setembro/2022

Orientadores: Frederico Wanderley Tavares, D.Sc.

Iuri Soter Viana Segtovich, D.Sc.

Programa: Engenharia Química

Os clatratos são sólidos compostos por uma estrutura cristalina em que as moléculas hospedeiras encontram-se confinadas. Embora os hidratos (clatratos de água) sejam indesejados no setor de óleo e gás por representarem um problema de segurança em cenários de garantia de escoamento, as aplicações industriais recentemente descobertas os tornaram economicamente atraentes para a indústria. O presente trabalho busca expandir os estudos relacionados à modelagem termodinâmica de hidratos de gás natural, principalmente no que concerne à estimação dos parâmetros dos modelos termodinâmicos Intersticial e Pshift para hidratos sII de formador único (um único hóspede), verificar o desempenho desses modelos para descrever a formação e o volume de hidratos sII e estender o escopo do modelo Pshift para a predição de hidratos mistos (mais de um hóspede). Embora os dois modelos tenham sido implementados, o modelo Pshift é o ponto central dessa pesquisa, por ser mais consistente termodinamicamente. Diferentes métodos de parametrização foram usados para estimar os parâmetros dos modelos Intersticial e Pshift. Enquanto os parâmetros do primeiro modelo foram estimados por meio do método de máxima verossimilhança, a parametrização do segundo se deu por uma metodologia mais empírica por conta de sua complexidade. O estudo mostrou que existe uma boa concordância entre os dados experimentais e os calculados pelos modelos para hidratos com um único hóspede. Entretanto, para hidratos mistos, os resultados mostraram que existe necessidade de melhorar a estratégia de estimação para que o modelo Pshift descreva adequadamente os dados experimentais.

Abstract of Dissertation presented to COPPE/UFRJ as a partial fulfillment of the requirements for the degree of Master of Science (M.Sc.)

PHASE EQUILIBRIUM CALCULATIONS FOR HIGH-PRESSURE SYSTEMS WITH GAS HYDRATES

Matheus Caputo Bello

September/2022

Advisors: Frederico Wanderley Tavares, D.Sc.

Iuri Soter Viana Segtovich, D.Sc.

Department: Chemical Engineering

Clathrates are solid-phase composed of a crystalline structure in which guest molecules are confined. Even though gas hydrates (water clathrate) have been treated as villains in the oil and gas industry, the recently discovered applications made them economically attractive to the industry. The present research mainly aspires to expand the investigations concerning gas hydrate thermodynamics modeling. The study aims to obtain Interstitial and Pshift models' parameters for hydrates in sII structure, investigate their performance for pure sII hydrates, and expand the latter methodology to calculate mixed hydrates formation. Although two models have been implemented, the Pshift model is the central point of this research, as it is more thermodynamically consistent. Different parameterization methods were used to estimate the parameters of the Interstitial and Pshift models. While the parameters of the former model were estimated using the maximum likelihood method, the parameterization of the latter was made using a more empirical methodology due to the complexity of the model. The study shows that both models agreed well with the experimental data for pure hydrates. However, we showed that more studies should be carried out for mixed hydrates so that the Pshift model can adequately describe the experimental data.

Contents

Agradecimientos	v
List of Figures	xi
List of Tables	xiii
List of Symbols	xiv
List of Abbreviations	xix
1 Introduction	1
1.1 Gas hydrates research history	2
1.2 Industrial applications	3
1.2.1 Natural methane hydrates reservoirs exploration	3
1.2.2 Natural gas storage	4
1.2.3 Refrigeration cycles	5
1.2.4 Separation processes	6
1.3 New demands, new models	6
1.4 Motivation and objectives	7
1.5 Text structure	8
2 Literature review	9
3 Gas hydrate thermodynamic modeling	15

3.1	The van der Waals and Platteeuw model	15
3.2	Derived macroscopic properties	19
3.3	Hydrate empty lattice and guest molecules contributions	21
3.3.1	Number of guest molecules and cage occupancy	22
3.3.2	Entropy	23
3.3.3	Pressure	24
3.3.4	Host molecules' chemical potential	25
3.3.5	Internal Energy and Enthalpy	26
3.4	Langmuir adsorption coefficient calculation	28
3.4.1	The Langmuir coefficient expression	28
3.4.2	Guest-host adsorption interaction	32
3.4.2.1	Square Well potential	32
3.4.2.2	Kihara potential	33
3.5	The pressure shift phenomenon	36
3.6	Hydrate lattice volumetric properties	39
3.7	Hydrate phase equilibrium	42
4	Phase equilibrium calculation	52
4.1	Guest fugacity calculation	52
4.2	Empty lattice pressure convergence and pressure shift calculation	53
4.3	Phase equilibrium algorithm implementation	54
4.4	The Interstitial model	57
4.5	Parameter estimation and experimental data	58
4.5.1	Maximum likelihood method	58
4.5.2	Estimated parameters	63
4.5.3	Experimental data	65
4.5.4	Parameter optimization methodology	66
4.5.4.1	Interstitial model parameterization	66

4.5.4.2	Pshift model parameterization	69
5	Results and discussion	73
5.1	Thermodynamic model validation	73
5.1.1	Interstitial model validation	74
5.1.2	Pshift model validation	76
5.2	Results for pure sII hydrates	77
5.2.1	Interstitial model	77
5.2.1.1	Interstitial model optimal parameters	77
5.2.1.2	Equilibrium diagrams	78
5.2.2	Pshift model	81
5.2.2.1	Pshift model optimal parameters	81
5.2.2.2	Equilibrium diagrams	84
5.2.2.3	Volume diagrams	86
5.3	Stability analysis	91
5.3.1	Interstitial model mixed hydrates prediction	93
5.3.2	Pshift model mixed hydrates prediction	95
6	Conclusions and suggestions	99
	References	101

List of Figures

1.1	Cage types and clathrates' configurations	2
1.2	World Map of Found NG Hydrate Reservoirs	4
3.1	Graphic representation of Kihara's parameters	34
3.2	Pressure shift visual representation	37
3.3	Phase equilibrium scheme of systems with hydrates	43
4.2	Interstitial model parameter estimation methodology flowchart.	69
4.3	Cell parameter for sII hydrate of propane and empty lattice of structure sII at fixed atmospheric pressure.	71
4.4	Pshift model parameter estimation methodology flowchart.	72
5.1	Phase equilibrium prediction for CH ₄ hydrate using the Interstitial model.	75
5.2	Phase equilibrium prediction for C ₂ H ₆ hydrate using the Interstitial model.	75
5.3	Phase equilibrium prediction for CH ₄ hydrate using the Pshift model.	76
5.4	Phase equilibrium prediction for C ₂ H ₆ hydrate using the Pshift model.	77
5.5	Phase equilibrium prediction for C ₃ H ₈ hydrate using the Interstitial model.	79
5.6	Phase equilibrium prediction for iC ₄ H ₁₀ hydrate using the Interstitial model.	80
5.7	Pshift model's equilibrium and volume prediction of sII empty lattice, propane, and isobutane hydrates for different values of a_0^{uc}	82

5.8	Phase equilibrium prediction for C_3H_8 hydrate using the Pshift model.	85
5.9	Phase equilibrium prediction for iC_4H_{10} hydrate using the Pshift model.	85
5.10	Volume prediction for sII hydrates at 273 K using the Pshift model.	87
5.11	Volume prediction for sII hydrates at 101 325 Pa using the Pshift model.	88
5.12	Pshift model's equilibrium and volume prediction of sII empty lattice, c3, and ic4 hydrates if the guest molecules were not allowed to occupy the small cavities.	92
5.13	Interstitial model's phase equilibrium prediction for a $CH_4 + CO_2$ hydrate (50% mol methane)	94
5.14	Interstitial model's phase equilibrium prediction for a $CH_4 + CO_2$ hydrate (90% mol methane)	94
5.15	Interstitial model's phase equilibrium prediction for a $CH_4 + C_2H_6$ hydrate (90% mol methane)	95
5.16	Pshift model's phase equilibrium prediction for a $CH_4 + CO_2$ hydrate (50% mol methane)	96
5.17	Pshift model's phase equilibrium prediction for a $CH_4 + CO_2$ hydrate (90% mol methane)	97
5.18	Pshift model's phase equilibrium prediction for a $CH_4 + C_2H_6$ hydrate (90% mol methane)	98

List of Tables

4.1	List of estimated parameters.	65
4.2	List of data sets used in the optimization.	66
4.3	Optimization parameters.	68
5.1	Optimal parameters for sII hydrates predicted by the Interstitial model (after simplex method optimization).	78
5.2	Regressed temperature and pressure-related variances.	80
5.3	Optimal parameters for sII hydrates predicted by the Pshift model for $a_0^{uc} = 17.13 \text{ \AA}$	83
5.4	Optimal parameters for sII hydrates predicted by the Pshift model for $a_0^{uc} = 17.03 \text{ \AA}$	84
5.5	Optimal parameters for sII hydrates predicted by the Pshift model for special cases 1 and 2.	90

List of Symbols

A	Absolute extensive Helmholtz free energy, p. 19
C_{ij}	Langmuir adsorption coefficient, p. 29
N	Number of molecules, p. 16
N_A	Avogadro number, p. 42
N_h	Total number of host molecules in the hydrate, p. 17
N_h^{uc}	Number of host molecules in one unit cell, p. 41
N_{ij}	Number of j -type guest molecules in i -type cages, p. 17
N_i^{empty}	Number of empty i -type cages, p. 18
P	Pressure, p. 20
P_j^m	Pressure experimental point after reconciliation of a guest j ., p. 64
P_0	HOLDER <i>et al.</i> (1980)'s notation for dissociation pressure of the reference hydrate at T_0 , p. 10
P_R	HOLDER <i>et al.</i> (1980)'s notation for dissociation pressure of the reference hydrate, p. 10
$P_0^{crystal}$	Experimental reference pressure used to regress the volumetric parameters of crystalline structures, p. 42
Q^H	Canonical partition function of the hydrate, p. 16
Q^{EL}	Canonical partition function of the empty lattice, p. 16
Q^{guest}	Canonical partition function associated with the guest molecules, p. 16
R	Universal gas constant, p. 10

R_i	Spherical cavity radius of a cage i , p. 30
S	Extensive entropy, p. 20
T	Temperature, p. 16
T_0	HOLDER <i>et al.</i> (1980)'s notation for initial's state temperature, p. 10
T_F	HOLDER <i>et al.</i> (1980)'s notation for final's state temperature, p. 10
$T_0^{crystal}$	Experimental reference temperature used to regress the volumetric parameters of crystalline structures, p. 42
U	Extensive internal energy, p. 21
V	Volume, p. 16
V_P	Variance associated with pressure measurement., p. 64
V_T	Variance associated with temperature measurement., p. 64
V_z	Diagonal matrix that contains the variance of the experimental errors., p. 60
W_i	Number of possible permutations in a i -type cavity, p. 17
X_w	HOLDER <i>et al.</i> (1980)'s notation for mole fraction in liquid water phase, p. 10
Z_i	Coordination number of a cavity i , p. 35
Δh_w	HOLDER <i>et al.</i> (1980)'s notation for water's enthalpy difference between the empty lattice and the water-rich solution, p. 10
Δv_w	HOLDER <i>et al.</i> (1980)'s notation for water's volume difference between the empty lattice and the water-rich solution, p. 10
$\Delta \mu_w$	HOLDER <i>et al.</i> (1980)'s notation for water's chemical potential difference between the empty lattice and the water-rich solution, p. 10
$\Delta \mu_w^0$	HOLDER <i>et al.</i> (1980)'s notation for water's chemical potential difference between the empty lattice and the water-rich solution in reference conditions, p. 10

Φ_j	Configurational integral for particle momentum and internal degrees of freedom of a molecule j , p. 29
Ψ	Thermodynamic potential correlated to the semi-grand canonical partition function, p. 19
α_n	Linear coefficient related to isobaric expansivity term of solids' volume calculation, p. 42
\bar{V}^{EL}	Empty lattice's intensive volume, p. 31
\bar{u}_j^{IG}	Intensive internal energy of molecule species j at ideal gas state, p. 31
β	Variable used to represent $\frac{1}{k_B T}$, p. 16
\hat{f}_{ij}	Fugacity of guest component j in a cage i , p. 28
\hat{f}_w^G	Water fugacity in the guest component-rich phase, p. 11
κ_{hyd}	Hydrate lattice compressibility factor, p. 39
κ_w	Water compressibility factor, p. 51
λ_{ij}	Absolute activity of a guest species j in a cavity i , p. 18
\mathcal{H}	System's Hamiltonian, p. 16
\mathcal{H}_{gg}	Hamiltonian associated with guest-guest interaction, p. 16
\mathcal{H}_g	Hamiltonian associated with the internal degrees of freedom of the guest molecules, p. 16
\mathcal{H}_{hg}	Hamiltonian associated with the interaction between host and guest molecules, p. 16
\mathcal{H}_{hh}	Hamiltonian associated with the interaction between two or more host molecules (empty lattice contribution), p. 16
\mathcal{H}_h	Hamiltonian associated with the internal degrees of freedom of the host, p. 16
\mathcal{H}_k	Hamiltonian of a k state, p. 16
μ_h	Chemical potential of the host species, p. 20
μ_{ij}	Chemical potential of guest species j in i cages, p. 18

ν_i	Ratio between the total number of i cages and the number of host molecules in the hydrate, p. 17
σ_j	Combination between the soft-core parameter of a pure light component j and a pure water molecule., p. 35
θ_{ij}	Cage occupancy of guest species j in i cavities, p. 23
\underline{R}	Array which contains the cages radii, p. 39
\underline{R}_0	Array which contains the cages radii obtained experimentally in standard conditions, p. 39
$\underline{\alpha}$	Vector that contains the parameters of the model., p. 59
$\underline{\kappa}_R$	Array which contains the cages compressibility, p. 39
\underline{f}	Array which contains the factor of proportionality that correlates the hydrate compressibility to the cage compressibility, p. 39
\underline{f}_0	Array which contains the factor of proportionality that correlates \underline{R}_0 to a_0^{uc} , p. 39
ε_j	Combination between the depth of the energetic well parameter of a pure light component j and a pure water molecule., p. 35
\wp	Probability of finding the obtained experimental data., p. 60
a^{uc}	Unit cell's edge length, p. 39
a_0^{uc}	Unit cell's edge length parameter (obtained experimentally in standard conditions), p. 39
a_j	Combination between the soft-core parameter of the Kihara's hard-core diameter of a pure light component j and a pure water molecule., p. 35
h_{Planck}	Planck's constant, p. 29
k_B	Boltzmann constant, p. 16
m_j	Extensive mass of a guest j molecule, p. 29
q_{ij}	Internal canonical partition function that describes the motion of a guest j in a cavity i , p. 17

$q_j^{IG,rotational}$	Internal partition function associated with the rotational energy of a guest molecule j in the ideal gas state, p. 29
$q_j^{IG,vibrational}$	Internal partition function associated with the vibrational energy of a guest molecule j in the ideal gas state, p. 29
q_j^{IG}	Canonical partition function of molecule j at ideal gas state, p. 31
r	Radial coordinate, p. 30
w_{ij}	Mean field cage potential on guest species j in cage i , p. 30
x	Dependent variable., p. 59
y	Independent variable., p. 59
z	Vector that contains the dependent and independent variables., p. 60
\hat{f}_w^H	Water fugacity in the hydrate phase , p. 11

List of Abbreviations

CFCs	Chlorofluorocarbons, p. 6
EoS	Equation of State, p. 44
HCFCs	Hydrochlorofluorocarbons, p. 6
HFCs	Hydrofluorocarbons, p. 6
IG	Ideal gas, p. 28
LNG	Liquefied Natural Gas, p. 5
NG	Natural Gas, p. 4
PR	Peng-Robinson, p. 52
PT	Patel-Teja, p. 52
Pshift	Abbreviation for the natural phenomenon of pressure shift, which was also used by SEGTOVICH <i>et al.</i> (2022) to name the proposed model presented in their work, p. 14
RK	Redlich-Kwong, p. 52
SNG	Solidified Natural Gas, p. 5
SRK	Soave-Redlich-Kwong, p. 52
vdWP model	van der Waals and Platteeuw's model, p. 10

Chapter 1

Introduction

Clathrates are solid-phase compounds composed of a crystalline structure in which guest molecules are confined. First observed in laboratory experiments in 1810, clathrates were initially seen as a scientific curiosity. Some reports in the XIX century revealed carbon dioxide, hydrogen sulfide, and light hydrocarbons hydrates. Nonetheless, although these components are commonly encountered in natural gas streams, the industry initially refused to recognize the possibility of pipeline blockage above the water freezing point. Therefore, not only until HAMMERSCHMIDT (1934) attributed these natural gas pipeline blockages to hydrates that these compounds were extensively examined.

Regarding the crystalline structure, clathrates can exist through various configurations. The most thermodynamically stable and commonly observed are sI, sII, and sH. These structures are presented by Figure 1.1.

As illustrated below, the three arrangements mentioned above comprise a combination of five cage types. Usually, these polyhedral cages are identified by the number of polygons that build their surface. For instance, a 5^{12} cage is a polyhedron of 12 pentagonal faces. As illustrated in Figure 1.1, the combination of two 5^{12} cages and six $5^{12}6^2$ cages produces an sI clathrate unit cell. For convenience, the former cage type is typically called "small cavity"; while the latter, "large cavity."

In terms of composition, the clathrates are non-stoichiometric compounds, and their cavities can be occupied by pure guests or mixtures. Customarily, clathrates formed by a single light component are referred to as "single" or "pure"; otherwise, "mixed."

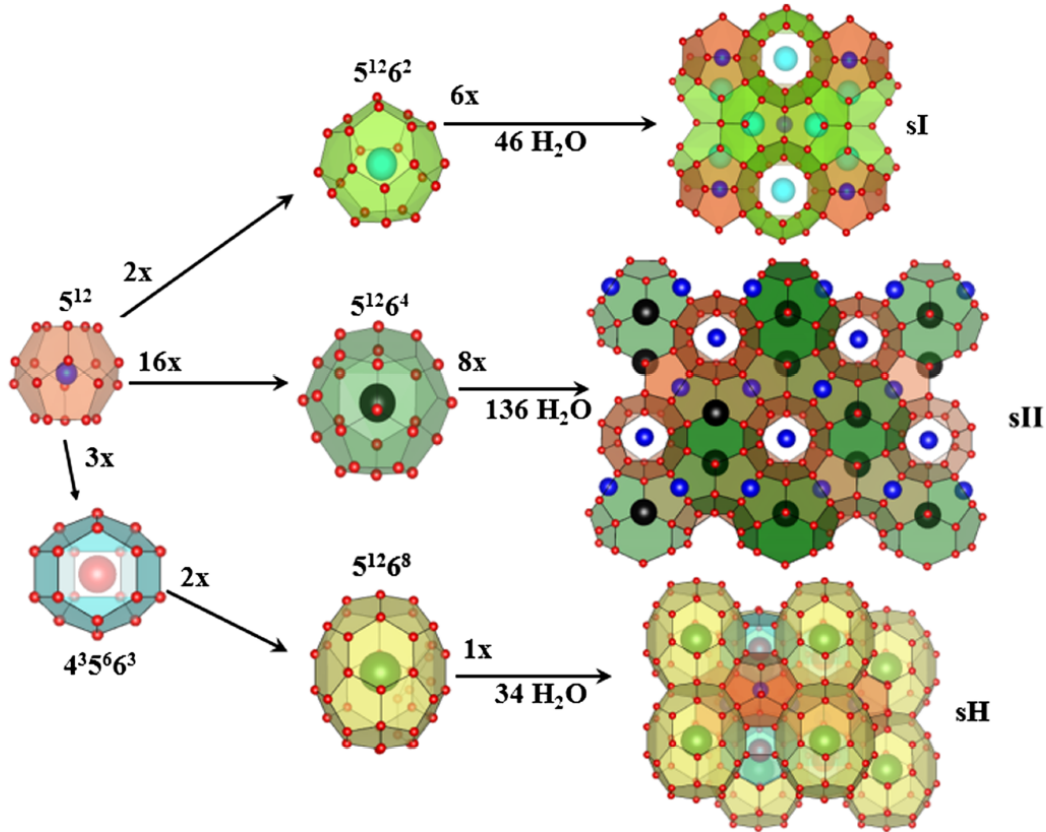


Figure 1.1: Cage types and clathrates' configurations. Reproduced from WARRIER *et al.* (2016)

1.1 Gas hydrates research history

In his groundbreaking work, HAMMERSCHMIDT (1934) details the empirical tests performed to study the leading causes of hydrate formation in natural gas flow systems. Natural gas hydrates, which comprise a specific category within the clathrates class, are crystalline solids composed of water and light components. The water molecules form, through hydrogen bonds, the cages in which the guest molecules are entrapped, which, in turn, stabilizes the hydrate lattice. Since HAMMERSCHMIDT (1934)'s report, natural gas hydrates have been treated as villains in the oil and gas industry for representing a safety concern in flow assurance scenarios. For many years the industry's goal was to identify the possibility of hydrate formation.

In this sense, a myriad of empirical models emerged to predict hydrate formation conditions in natural gas systems pragmatically. However, despite these models' practicality to the industry, their empirical nature limited their applicability. Phenomenological approaches were developed to rectify this restraint; the most eminent model was designed by VAN DER WAALS and PLATTEEUW (1959),

which is considered a milestone in applied statistical thermodynamic and hydrate modeling frameworks. VAN DER WAALS and PLATTEEUW (1959)'s approach can accurately describe hydrate formation in mild conditions when combined with a phase equilibrium algorithm, like the one conceived by PARRISH and PRAUSNITZ (1972) for example. For this reason, their model is still widely used. As it will be explored in Chapter 2, some subsequently proposed modifications enhanced VAN DER WAALS and PLATTEEUW (1959)'s model capability to predict hydrate formation conditions.

1.2 Industrial applications

Initially seen as a scientific curiosity and, later, as a safety issue in flow assurance scenarios, natural gas hydrates have been taking on relevant roles within the energy sector. Since the natural methane hydrates' first observation in Siberian permafrost, its exploration has been profoundly investigated for energetic purposes. The vast energetic potential combined with the search for cleaner alternatives to coal and oil justifies the efforts made by both the academy and industry to make the exploration of natural methane hydrates reservoirs viable.

Moreover, the industrial applications discovered made clathrate hydrates very economically attractive throughout the years. Natural gas storage (SNG technology), secondary refrigerants on refrigeration cycles, and porous media in separation processes are recently discovered industrial applications for gas hydrates.

1.2.1 Natural methane hydrates reservoirs exploration

It is widely known that the population increase and the development of economic activities are two of the primary factors responsible for the global consumption of energy growth. In figures, the World Energy Outlook 2019 estimated that the energy demand should rise progressively by approximately 50 percent between 2018 and 2050 (IEA, 2019), making the Earth's temperature rise control even more challenging as established by the Paris Agreement (COP21). Hence, alternative technologies that match the energetic global demand regarding the carbon emission restrictions imposed by the above agreement must be developed. Furthermore, given that the global energetic matrix transition to renewable energy sources is being carried out at a languid pace, natural gas (NG) – considered the cleanest fossil fuel – emerges as an appealing solution to replace coal and oil. In this sense, it is estimated that the global demand for NG should grow by 44 percent from 2019 to 2040 (YIN

and LINGA, 2019).

Interestingly, as reported by YIN and LINGA (2019), the largest available methane reservoirs, NG main component, are the methane hydrates that occur beneath the seafloor or permafrost region (SLOAN JR and KOH, 2007). It is predicted that such reserves have more than twice the energetic potential of all the fossil fuels combined (MAKOGON, 1997). According to MAKOGON (2010), this potential is so vast that if only 20 percent of its totality is produced, it can be an adequate energy supply for 200 years. Figure 1.2 illustrates the known NG hydrates deposits. In this context, numerous studies about the exploration of these natural reserves have been conducted throughout the years, aiming to make the NG production from methane hydrates economically viable.

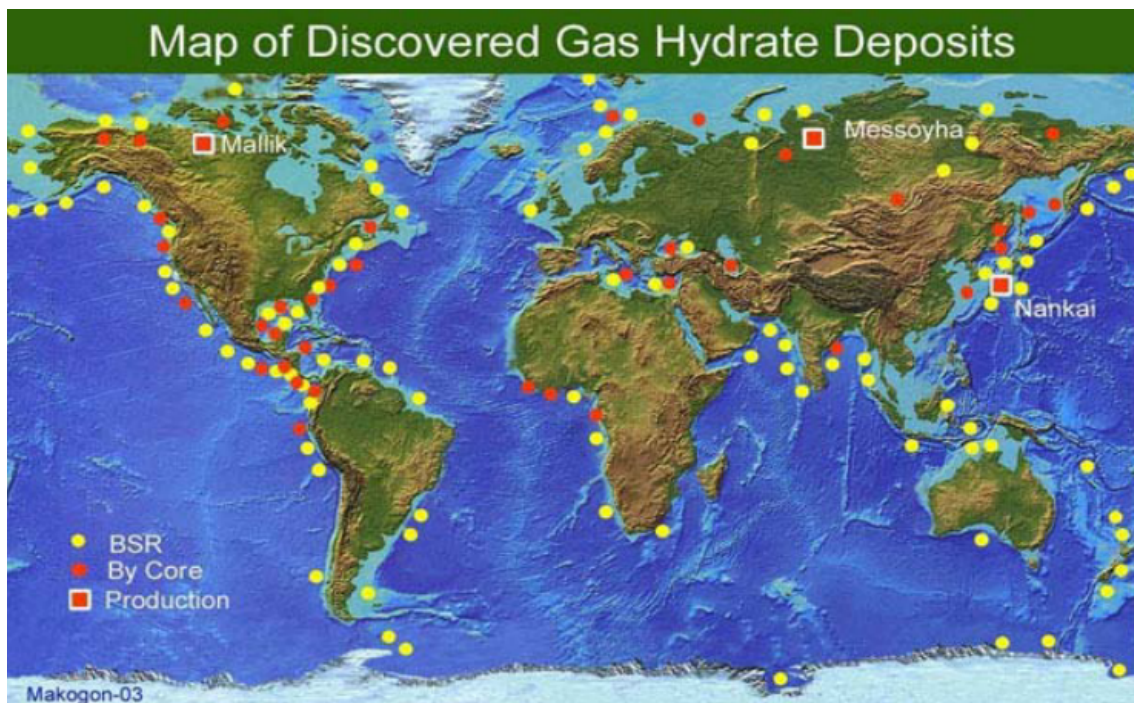


Figure 1.2: World Map of Found NG Hydrate Reservoirs. BSR = deposit located by seismic refraction Reproduced from MAKOGON *et al.* (2004)

1.2.2 Natural gas storage

There are several available technologies within the natural gas storage/transportation field. According to VELUSWAMY *et al.* (2018), although liquefied natural gas (LNG) is considered the natural gas transportation/storage technology with the best cost-benefit ratio, the extreme low-temperature prerequisite, and some other operational issues restrain its employment in large-scale projects. On the other hand, solidified natural gas (SNG) – a promising technique to transport natural gas

in hydrates – has an impressive capability to compress multi-fold volumes of natural gas in relatively compact hydrate structures. Furthermore, in their review, the authors also mentioned some other advantages of this technology’s employment; it provides safe and environmentally friendly NG storage and does not demand severe temperature and pressure conditions.

In this context, there are some initiatives to develop commercially viable techniques, such as the one presented by the Department of Energy of the United States of America (USDOE). In a recent collaborative study between the USDOE, academia, industry, international research organizations, and other U.S. government agencies, a solution for transporting/storing NG through hydrates is introduced. The research consisted of technical and economic analysis of the proposed technique, which comprises transporting NG through gas hydrates filled tanks that can be carried on ships. Even though this technology is still considered unconventional, this study shows that the Hydrastor Modular Platform – the name given to the technique – could potentially cut down shipping costs by half compared to the already established LNG technology (CARSTENS, 2019).

1.2.3 Refrigeration cycles

According to ZHANG *et al.* (2017), the most prominent technologies used to design refrigeration cycles are vapor compression, absorption, and ejector expansion. The refrigerant, which is then used to remove heat from the process stream, naturally has a tremendous influence on the refrigeration cycle’s efficiency. They are categorized into three groups according to their generation. The first generation comprises carbon dioxide, ammonia, and sulfur dioxide. Later, Freon-based refrigerants were developed; CFCs, HCFCs, and HFCs are industrially used. These chemicals comprise the second generation of refrigerants. For the third generation, the refrigerants were designed to work in pairs: lithium bromide-water, lithium chloride-water, and ammonia-water.

Contrary to what one might think, according to ZHANG *et al.* (2017), second-generation refrigerants present a higher coefficient of performance (COP) than those of the third generation. However, as stated by FOURNAISON *et al.* (2004), the exclusive use of these second-generation refrigerants in refrigeration cycles contributes immensely to the depletion of the ozone layer since this operation mode requires large volumes of these chemicals. In order to cut down greenhouse gas emissions, researchers have been investigating the employment of a two-phase secondary refrigerant to reduce the load of primary refrigerants, such as CFCs, HCFCs, and HFCs. A promising alternative involves using hydrate as the phase-change material in the

two-phase secondary refrigerant. As reported by the authors, hydrate dissociation not only presents a higher latent heat than ice but also is more environmentally benign than conventional technologies.

1.2.4 Separation processes

Finally, gas hydrates can also be employed in separation processes. Researchers have recently investigated the clathrate hydrates' potentiality to separate certain compounds from gas mixtures, along with the novel applications reported above. Recent studies have clarified that clathrate hydrates' affinity concerning some components typically present in industrial gas streams enables their capture by hydrate formation. As reported by ESLAMIMANESH *et al.* (2012), hydrogen, nitrogen, and greenhouse gases – such as carbon dioxide, methane, and hydrogen sulfide – are some of the compounds that hydrate formation processes can segregate. Since H_2 and N_2 are profitable components for their properties, and CO_2 , CH_4 and H_2S are the key players in the global warming phenomenon, their separation from flue gas streams is fundamental for the chemical industry. Furthermore, KHAN *et al.* (2019) have written about applying gas hydrates in desalination processes. According to the authors, seawater desalination through hydrate formation is an up-and-coming technique that can be applied on a large scale if its kinetics are thoroughly understood.

1.3 New demands, new models

Bearing in mind the benefits associated with the numerous applications cited above, aside from the elementary prediction of incipient hydrate phase formation, the focal point of hydrate research has shifted to investigate formation and dissociation kinetics. Therefore, more sophisticated methods were required to comply with this new demand.

Novel approaches have been devised to amplify our awareness of hydrate formation/dissociation processes in this context. Ballard and Sloan published a series of papers to present their contribution to hydrate phase equilibrium prediction. The authors have followed the new experimental observations on clathrates' compressibility and cage radii's guest-dependency. Driven by Ballard and Sloan's findings, multiple authors enhanced the existing predictive methodology for determining hydrates' fugacity at and above formation conditions, which, according to BALLARD and SLOAN (2004), is the most suitable variable to describe the driving force.

Aligned with this trend, SEGTOVICH *et al.* (2022) proposed a model which introduces a new phenomenon related to guest molecules adsorption. Analogously to the methodology formulated by BALLARD and SLOAN JR (2002), SEGTOVICH *et al.* (2022)'s model also incorporated lattice compressibility and cage radii variation with guest size. However, the latter noticed some inconsistencies associated with the phase equilibrium calculation in previous models. Even though these novel approaches present promising results, the authors of the former model did not revise van der Waals and Platteuw's equations after modifying the lattice incompressibility hypothesis. Hence, according to SEGTOVICH *et al.* (2022), these models had inconsistencies in their attempt to represent the influence of guest adsorption on host chemical potential and lattice volume. In virtue of the lattice guest-dependency, the author states that the pressure of the hydrate ought to differ from its reference state (empty lattice) in a calculation at a specified volume, which is the case for the semi-grand canonical partition function approach. SEGTOVICH *et al.* (2022), then named this phenomenon "Pressure shift" and presented their interpretation of how the phase equilibrium calculation should be carried out.

1.4 Motivation and objectives

Driven by the recently unveiled promising potential of gas hydrates, this work mainly aspires to expand the investigations concerning its modeling at and above phase equilibrium conditions. Furthermore, since SEGTOVICH *et al.* (2022)'s approach appears to be the most promising, the undertaken study shall be based on this model, with the necessary adjustments.

In this sense, the undertaken study's goal is to implement the Pshift model (SEGTOVICH *et al.*, 2022) to represent sII hydrates equilibrium condition and volume, as well as to adjust it to available experimental data through parameter estimation. More specifically, we intend to:

- implement the hydrate thermodynamic modelling through the Interstitial (KLAUDA and SANDLER, 2000) and Pshift (SEGTOVICH *et al.*, 2022) models;
- perform phase equilibrium calculations;
- estimate parameters for pure sII hydrates;
- produce phase equilibrium and volume diagrams for pure hydrates;
- generate phase equilibrium diagrams for mixed hydrates.

1.5 Text structure

This document is segmented into six sections. Subsequently to the introduction, the literature review is presented in Chapter 2. Afterward, the methodology is demonstrated in the two succeeding chapters; the thermodynamic concepts supporting the gas hydrate modeling are scrutinized in Chapter 3, while the computation details are given in Chapter 4. Then, the outcomes and repercussions are closely examined in Chapter 5. Ultimately, Chapter 6 presents the final considerations and the outlined prospects for this field of research.

Chapter 2

Literature review

Hydrates have been known for over two centuries, yet the first complete phenomenological characterization method is only about 60 years old. According to MEDEIROS *et al.* (2020), this setback was caused by various reasons. To name a couple, not only the statistical thermodynamics foundations were not well established in the XIX century, but also there was not enough experimental microscopic information on clathrates.

Sustained by the breakthroughs made in crystallographic studies, the first complete phenomenological models based on statistical thermodynamics emerged in the late 1950s. Previously, compelled by HAMMERSCHMIDT (1934)'s report, some empirical models had already been devised. However, the latter is somewhat limited to predicting hydrate formation in various conditions because of its empirical nature.

Even though the approach devised by VAN DER WAALS and PLATTEEUW (1959) is the most eminent methodology for hydrate prediction, it was not the first to use statistical thermodynamics to represent clathrates. This position belongs to the model conceived by BARRER and STUART (1957). In their paper, the authors presented a thorough statistical thermodynamic interpretation of hydrates' properties. However, their most relevant contribution was the combinatorial analysis to deal with all the possible ways of guest occupation. Two years later, van der Waals and Platteeuw would publish the paper to impact statistical thermodynamics and hydrate modeling framework irreversibly.

In the paper entitled "Clathrate Solutions", VAN DER WAALS and PLATTEEUW (1959) presented a general model – called the "vdWP model" from now on – that can be used to describe clathrates with any number of guest and cage types. Furthermore, their approach could deal with non-ideal fluid phase equilibria since

the guests were represented by their fugacity (MEDEIROS *et al.* (2020)). Under these qualities, this model is universally used to predict hydrate formation. Nevertheless, some adjustments were necessary to make it produce more reliable results at high pressures. Thus, efforts have been made to broaden its range of applicability.

A myriad of derived models was developed throughout the years to improve the limited approach proposed by van der Waals and Platteeuw (vdWP model) to deal with the phase equilibrium calculation in systems with natural gas hydrates. Since the authors did not describe the reference state – namely, the empty hydrate lattice – directly from statistical thermodynamics, the proper computation of its properties (i.e., the chemical potential of the host molecule in the empty lattice and empty lattice volume) depended on parameter estimation. According to BALLARD and SLOAN JR (2002), the deviation of the vdWP model’s predictions from experimental data at high pressures indicates that the hydrate reference state’s properties were not well defined. In this context, the proposed modifications to the vdWP model aspired mainly to calculate these properties.

The earliest adjustments to the vdWP model consisted of extending the reference state for the host component. In this sense, MARSHALL *et al.* (1964) acknowledged the possibility that the water and the hydrate-forming compound could have some degree of miscibility. Hence, the phase equilibrium calculation could be carried out with a non-pure aqueous phase as a reference to chemical potential in the empty lattice. Analogously, PARRISH and PRAUSNITZ (1972) also considered this scenario in their work, in which a set of estimated parameters associated with the thermodynamic properties of the empty lattice and liquid water relative to ice are presented. Furthermore, the authors contributed with an iterative method that enabled statistical thermodynamics application in an industrial setting, a turning point in the field.

In 1980, HOLDER *et al.* (1980) used experimental data to generate chemical potential, enthalpy, and heat capacity functions for sI hydrates. Interestingly, in their research, the authors proposed a more straightforward equation to compute the chemical potential difference between the empty lattice and the water-rich solution. Originally, this variable was calculated by the expression given by Equation 2.1.

$$\frac{\Delta\mu_w(T_F, P)}{RT_F} = \frac{\Delta\mu_w^0(T_0, 0)}{RT_0} + \int_0^{P_0} \frac{\Delta v_w}{RT_0} dP - \int_{T_0}^{T_F} \frac{\Delta h_w}{RT^2} dT + \int_{P_0}^{P_R} \frac{\Delta v_w}{RT} dP_R + \int_{P_R}^P \frac{\Delta v_w}{RT_F} dP - \ln X_w \quad (2.1)$$

According to the authors,

The first term on the right is an experimentally determined chemical potential difference between the unoccupied hydrate and pure water at some reference temperature, usually 0 °C, and zero absolute pressure. The second term corrects the chemical potential of pure water from zero pressure to the dissociation pressure of a reference hydrate (at T_0). The third and fourth terms correct the chemical potential for changes in temperature and pressure along the reference hydrate curve. The temperature dependence of Δh_w and reference pressure are needed in these integrations. The terms Δh_w and Δv_w are the enthalpy and volume differences, respectively, between the empty hydrate and pure ice or liquid water phases. The fifth term corrects the chemical potential from the dissociation pressure of the reference hydrate to the final pressure, P . This is an isothermal integration. The last term corrects the chemical potential from that of a pure water or ice phase to that water-rich solution. At temperatures below 273 K, X_w is unity. (HOLDER *et al.* (1980), pp. 283).

The equation introduced above is reproduced with the original. Later, a more modern notation is employed in the methodology section to represent the same terms.

Thus, to eliminate the reference equilibrium curve dependence, HOLDER *et al.* (1980) proposed a new approach to perform this calculation. Their contribution is illustrated in Equation 2.2.

$$\frac{\Delta\mu_w}{RT_F} = \frac{\Delta\mu_w^0}{RT_0} - \int_{T_0}^{T_F} \left(\frac{\Delta h_w}{RT^2} \right)_{P=0} dT + \int_0^P \left(\frac{\Delta v_w}{RT_F} \right)_{T_F} dP - \ln X_w \quad (2.2)$$

Computing fugacity instead of chemical potential has some practical advantages. The former variable's employment allows us to describe a system without the presence of a condensed phase. This feature can be handy, for instance, in cases in which all water is dissolved in non-polar fluids, especially in the case of NG with low water content. Under these circumstances, the most convenient equilibrium condition criterion is given by Equation 2.3.

$$\hat{f}_w^H = \hat{f}_w^G \quad (2.3)$$

In which \hat{f}_w^H represents the water fugacity in the hydrate phase, and \hat{f}_w^G depicts the water fugacity in the guest component-rich phase.

In this sense, SLOAN *et al.* (1976) were the first to use water fugacity to perform phase equilibrium calculations in systems with hydrates; this was achieved by applying the intrinsic correlation between chemical potential and fugacity. Then, the authors derived an equation to compute water fugacity in the empty lattice regarding water sublimation pressure, its fugacity coefficient, and a Poynting correction term. A few years later, NG and ROBINSON (1980) published their approach on water content estimation in natural gas systems in equilibrium with a hydrate. In the undertaken study, the authors used the equilibrium condition criterion based on fugacity and extended this methodology for single and mixed hydrates of both sI and sII structures. Nonetheless, in their approach, the parameters were not guest-dependent, which later was shown to be inconsistent with future experimental results.

Driven by the repercussions of the latest experimental developments, researchers incorporated these new traits into their phenomenological models. In this context, HOLDER *et al.* (1988) published a review on the existing technologies within the hydrate characterization framework. In their study, the authors commented on the influence that guest-dependent parameters and lattice distortion could have on empty lattice properties calculation. Following this trend, HWANG *et al.* (1993) showed, via molecular dynamics, that the lattice unit cell parameter was guest-dependent, corroborating with experimental observation.

Later, KLAUDA and SANDLER (2000) would propose a fugacity based-model capable of estimating the formation of hydrates with different guests and structures that do not need the reference energy parameter used in the vdWP model. Furthermore, the authors removed the assumption of constant crystal lattice for guests of different sizes and lowered the number of fitted parameters by using quantum mechanical calculations. Despite the promising results presented in their paper and the efforts to devise a more practical method, Klauda and Sandler's model is inaccurate. Even though their approach assumes possible volume variations with lattice pressure, it neglects cage deformation. In other words, their modeling predicts a compressible lattice with cages with a constant radius. For that reason, henceforth, this model will be referred to as being part of the "Interstitial model" group.

Aware of this inaccuracy, BALLARD and SLOAN JR (2002) proposed a model capable of accounting for volume lattice temperature-, pressure- and guest-dependency, including a linear correlation between the cage radii and the hydrate lattice parameter. The authors made the Langmuir adsorption coefficient – commonly referred to as the 'Langmuir coefficient' – lattice volume-dependent so that the lattice deformation is recognized at high pressures. In addition, a non-ideality assumption was introduced by including a water activity coefficient, correlating the

non-ideal hydrate to the idealized one. The authors observed encouraging results at high-pressure conditions with these modifications, including the hydrate lattice retrograde behavior. Also motivated by the aspiration to appropriately model hydrates at high pressures, HSIEH *et al.* (2012) idealized a fugacity-based model that combines the vdWP model with a pressure- and temperature-dependent Langmuir adsorption constant. Unlike the approach devised by KLAUDA and SANDLER (2000), which includes a distorted empty lattice as a reference state, the reference phase for the equilibrium calculation of the two latter models is an undistorted empty lattice.

Nonetheless the models formulated by BALLARD and SLOAN JR (2002) and HSIEH *et al.* (2012) are thermodynamically inconsistent, as noticed by SEGTOVICH *et al.* (2022). According to SEGTOVICH *et al.* (2022), a revision of phase equilibrium equations must follow the Langmuir adsorption coefficient expression modification. Since BALLARD and SLOAN JR (2002) and HSIEH *et al.* (2012) did not revise the derived expressions for the water chemical potential and fugacity, the correlation between the Langmuir coefficient and the lattice volume was neglected.

As a sequence for the part I of the series, BALLARD and SLOAN (2004) published their work on mixed hydrates modeling through Gibbs energy minimization formalism. In this part III of the series, the authors aim to employ a Gibbs energy minimization routine for multiple phases and execute a multi-phase flash calculation. Even though this methodology is not limited to hydrate phase equilibrium calculations, it is an alternative to the prominent algorithm proposed by PARRISH and PRAUSNITZ (1972) to predict mixed hydrate formation.

Based on BALLARD and SLOAN JR (2002)'s model, HIELSCHER *et al.* (2018) proposed an approach focused on mixed hydrate modeling. Unlike the former, the latter applies a simpler mixing rule for the volume calculation with no adjustable parameters. Furthermore, the model devised by HIELSCHER *et al.* (2018) presents results in good agreement with experimental data.

In order to rectify the inconsistency introduced by BALLARD and SLOAN JR (2002)'s approach, SEGTOVICH *et al.* (2022) proposed a model capable of accounting for hydrate compressibility and cage deformation due to temperature and pressure conditions and guest size. The distinction between BALLARD and SLOAN JR (2002)'s and SEGTOVICH *et al.* (2022)'s approaches is that the former derived a water chemical potential expression that embodies the Langmuir adsorption constant lattice volume-dependency. Hence, their model not only incorporates important experimental observations but also yields thermodynamically consistent results. In addition, the authors observed another relevant consequence related to

the correlation involving the Langmuir coefficient: the reference state (empty lattice) pressure is different from the hydrate pressure at a derivation with constant volume – as is the case for the semi-grand canonical partition function approach. SEGTOVICH *et al.* (2022) attributed this phenomenon to a natural pressure shift generated by the guest adsorption into the empty hydrate lattice. For this reason, the authors often refer to the new model as the "Pshift" model. Further details about the Pshift model are given in the next chapter.

Chapter 3

Gas hydrate thermodynamic modeling

In Chapter 2, the hydrate modeling framework was outlined chronologically, from the first phenomenological model to the most sophisticated interpretation of the vdWP model’s hypothesis. Here, the model idealized by VAN DER WAALS and PLATTEEUW (1959) is thoroughly investigated. Firstly, we present the premises and the theory on which the model is built. Next, some macroscopic properties’ equations are derived. Then, a brief discussion about the hydrate’s reference state is carried out, and the Langmuir adsorption coefficient calculation methodology is presented. Eventually, the Pshift approach (SEGTOVICH *et al.*, 2022) is scrutinized, and the hydrate phase equilibrium calculation is disclosed.

It is worth highlighting that we are not attempting to reproduce the thermodynamic modeling developed by other authors. Instead, we intend to implement our interpretation of the approaches.

3.1 The van der Waals and Platteeuw model

The model devised by VAN DER WAALS and PLATTEEUW (1959) is a statistical thermodynamic-based model which utilizes a solution theory to describe clathrate phase behavior. The vdWP model is based on three fundamental – letters (a) to (c) – and three complementary hypotheses – letters (d) to (f). Here we present our interpretation of the original assumptions.

- a. Given an *a priori* description of the lattice, the guest molecules can only be placed within the clathrate cavities, and each cage can only host one guest

molecule.

- b. Guest-guest interactions are negligible.
- c. The partition function associated with guest molecules' internal degrees of freedom is independent of the number of guest types.
- d. Classical statistical mechanics is sufficient to predict all relevant properties.
- e. Solute (guest) molecules can rotate freely within their cages.
- f. The potential energy of a guest molecule located at a distance r from its cage center is given by the spherically symmetric potential proposed by Lennard-Jones and Devonshire.

As stated in the first hypothesis, the lattice is characterized by an *a priori* description so that the empty lattice potential energy is not a function of guests' positions. Therefore, the system's potential energy can be separated into two contributions: one related to the empty lattice and the other the individual guest molecules. Mathematically, the effect of this assumption can be illustrated by Equation 3.1.

$$Q^H = Q^{EL}Q^{guest} \quad (3.1)$$

Q^H represents the hydrate's canonical partition function, Q^{EL} is the empty lattice canonical partition function, and Q^{guest} is the canonical partition function associated with the guest molecules.

According to the approach developed by HILL (1986), the formal definition of the canonical partition function of a system can be represented by Equation 3.2.

$$Q(T, V, N) = \sum_k \exp(-\beta\mathcal{H}_k) \quad (3.2)$$

In which β is $\frac{1}{k_B T}$, and \mathcal{H}_k represents the Hamiltonian of a k state. The latter variable can be decomposed as shown by Equation 3.3.

$$\mathcal{H} = \mathcal{H}_h + \mathcal{H}_g + \mathcal{H}_{hh} + \mathcal{H}_{gg} + \mathcal{H}_{hg} \quad (3.3)$$

In this expression, the subscript indicates the source of each energy contribution. In this manner, the first two terms refer to the energy associated with the host and guest molecules' internal degrees of freedom, respectively. The third term represents the energy contribution from the interaction between two or more host

molecules (empty lattice contribution). The fourth term illustrates the Hamiltonian from the interaction between guest molecules in different cages, which is neglected by assumption (b). The last term symbolizes energy contribution from the interaction between host and guest molecules.

Assumption (c) states that the guest molecules' motion is independent of the number of types of guests. In other words, the guest molecules' modes of occupation are independent of each other, so their contributions can be separated. Consequently, Equation 3.1 can be rewritten as Equation 3.4 to discriminate the contribution of the motion of each solute molecule.

$$Q^H = Q^{EL} \prod_i \prod_j q_{ij}^{N_{ij}} \quad (3.4)$$

In which q_{ij} represents an internal partition function that describes the motion of a guest j in a cavity i , and N_{ij} the number of j -type guest molecules in i -type cages. However, since the guest molecules are differentiable and can occupy the lattice in multiple ways, permutations must be considered. Equation 3.5 includes the combinatorial term W_i , representing the number of possible permutations in a i -type cavity.

$$Q^H = Q^{EL} \prod_i W_i \prod_j q_{ij}^{N_{ij}} \quad (3.5)$$

Thermodynamically, W_i can be understood as the entropy associated with the possible permutations. This variable is a function of the number of host molecules (N_h), the number of guests j in cages i (N_{ij}), and the ratio between the number of i -type cavities and the number of host molecules – defined as ν_i . Equation 3.6 shows how W_i is calculated.

$$W_i = \frac{(\nu_i N_h)!}{\left[(\nu_i N_h - \sum_{j=1}^{n_{guest}} N_{ij})! \right] \prod_{j=1}^{n_{guest}} (N_{ij}!)} \quad (3.6)$$

Where:

$$\nu_i = \frac{N_i^{cages}}{N_h} \quad (3.7)$$

The partition function equation shown above was devised for a system whose temperature, volume, and the number of host and guest molecules were specified, thus, corresponding to a canonical ensemble. Nevertheless, for systems with hy-

drates, the most convenient ensemble, according to VAN DER WAALS and PLATTEEUW (1959), has temperature, volume, number of host molecules, and absolute activity of guest species as independent variables. In their review, MEDEIROS *et al.* (2020) justify this choice by listing its advantages. According to the authors, the hydrate's volume is chosen as an independent variable because it also defines the volume of the clathrate structure in which the solute molecules are trapped, namely the empty lattice volume. In addition, they pointed out that the empty lattice and the hydrate have a well-characterized structure with a known number of host molecules. Eventually, they also mentioned that the hydrates are non-stoichiometric compounds since the number of guest molecules that stabilize the crystalline structure is a function of other properties. Hence, MEDEIROS *et al.* (2020) claim that specifying the guest species' chemical potential is more valuable than defining the number of guest molecules.

This new ensemble created by VAN DER WAALS and PLATTEEUW (1959) is currently referred to as the semi-grand canonical, and it is represented by the Greek letter Ξ . It is possible to rewrite the hydrate's partition function using this new set of independent variables by performing a Laplace transformation, illustrated by Equation 3.8.

$$\Xi(T, V, N_h, \underline{\lambda}) = Q^{EL} \sum_{N_{1,1}=0}^{N_1^{cages}} \sum_{N_{2,1}=0}^{N_2^{cages}} \cdots \sum_{N_{n_{cage}, n_{guest}}=0}^{N_{n_{cage}}^{cages}} \prod_{i=1}^{n_{cage}} \left[W_i \prod_{j=1}^{n_{guest}} \left(q_{ij}^{N_{ij}} \lambda_{ij}^{N_{ij}} \right) \right] \quad (3.8)$$

The expression above is subject to the restriction imposed by assumption (a), which says there can be as many guest species molecules as cages in the lattice. Equation 3.9 summarizes this corollary.

$$\sum_{j=1}^{n_{guest}} (N_{ij}) + N_i^{empty} = N_i^{cages} \quad \forall \quad i = 1, 2, 3, \dots, n_{cage} \quad (3.9)$$

Where N_i^{empty} represents the number of empty i -type cages.

Furthermore, the absolute activity of a guest species j in a cavity i , given by λ_{ij} , is defined in Equation 3.10.

$$\lambda_{ij} = \exp \left(\frac{\mu_{ij}}{k_B T} \right) \quad (3.10)$$

After expanding W_i and comparing the outcome in contrast with the multinomial theorem, Equation 3.8 can be rewritten as follows:

$$\Xi(T, V, N_h, \underline{\lambda}) = Q^{EL} \prod_{i=1}^{n_{cage}} \left[1 + \sum_{j=1}^{n_{guest}} (q_{ij} \lambda_{ij}) \right]^{\nu_i N_h} \quad (3.11)$$

The partition function derived above (Equation 3.11) was devised by van der Waals and Platteeuw in their 1959 paper.

3.2 Derived macroscopic properties

Several macroscopic properties can be obtained from Equation 3.11. However, it is necessary first to correspond the semi-grand canonical partition function to its correlative thermodynamic potential, represented by the Greek symbol Ψ . The mathematical definition of this variable is given by Equation 3.12.

$$\Psi(T, V, N_h, \underline{\lambda}) = -k_B T \ln \Xi(T, V, N_h, \underline{\lambda}) \quad (3.12)$$

Once more, with the aid of the Legendre transform technique, it was possible to derive an expression for $\Psi(T, V, N_h, \underline{\lambda})$ from its canonical ensemble equivalent $A(T, V, N_h, N^{guest})$. This expression is illustrated by Equation 3.13.

$$\Psi = A - \sum_{j=1}^{n_{guest}} \left\{ \sum_{i=1}^{n_{cage}} \left[N_{ij} \left(\frac{\partial A}{\partial N_{ij}} \right)_{T, V, N_h, N_{mn} \neq N_{ij}} \right] \right\} = A - \sum_{j=1}^{n_{guest}} \sum_{i=1}^{n_{cage}} N_{ij} \mu_{ij} \quad (3.13)$$

Using the definition of absolute activity, expressed by Equation 3.10, the hydrate thermodynamic potential above can be rewritten as a function of its natural coordinates.

$$\Psi = A - \sum_{j=1}^{n_{guest}} \sum_{i=1}^{n_{cage}} N_{ij} k_B T \ln \lambda_{ij} \quad (3.14)$$

Equation 3.15, below, illustrates the differential form of Equation 3.14.

$$d\Psi = -SdT - PdV + \mu_h dN_h - k_B \left(\sum_{j=1}^{n_{guest}} \sum_{i=1}^{n_{cage}} N_{ij} T d \ln \lambda_{ij} + \sum_{j=1}^{n_{guest}} \sum_{i=1}^{n_{cage}} N_{ij} \ln \lambda_{ij} dT \right) \quad (3.15)$$

Which, for convenience, can be displayed as Equation 3.16.

$$d\Psi = - \left(S + k_B \sum_{j=1}^{n_{guest}} \sum_{i=1}^{n_{cage}} N_{ij} \ln \lambda_{ij} \right) dT - PdV + \mu_h dN_h - k_B T \sum_{j=1}^{n_{guest}} \sum_{i=1}^{n_{cage}} N_{ij} d \ln \lambda_{ij} \quad (3.16)$$

The correlation between Equations 3.12 and 3.16 enables us to derive expressions for some macroscopic properties from microscopic ones easily. The total number of guest molecules, hydrate's entropy and pressure, and the host molecules' chemical potential are the macroscopic properties directly obtained by differentiation of the clathrate's potential.

$$N_{ij} = -\frac{1}{k_B T} \left(\frac{\partial \Psi}{\partial \ln \lambda_{ij}} \right)_{T, V, N_h, \lambda_{mn \neq ij}} = -\frac{\lambda_{ij}}{k_B T} \left(\frac{\partial \Psi}{\partial \lambda_{ij}} \right)_{T, V, N_h, \lambda_{mn \neq ij}} \quad (3.17)$$

$$S = - \left(\frac{\partial \Psi}{\partial T} \right)_{V, N_h, \lambda} - k_B \sum_{j=1}^{n_{guest}} \sum_{i=1}^{n_{cage}} N_{ij} \ln \lambda_{ij} \quad (3.18)$$

$$P = - \left(\frac{\partial \Psi}{\partial V} \right)_{T, N_h, \lambda} \quad (3.19)$$

$$\mu_h = \left(\frac{\partial \Psi}{\partial N_h} \right)_{T, V, \lambda} \quad (3.20)$$

Where the total number of molecules of a guest species j is given by:

$$N_j = \sum_{i=1}^{n_{cage}} N_{ij} \quad (3.21)$$

Moreover, since the system is in equilibrium, the absolute activities for a guest j in any cage i are the same regardless of occupation mode.

$$\lambda_j = \lambda_{ij} \quad \forall \quad i = 1, 2, 3, \dots, n_{cage} \quad (3.22)$$

In addition, with some effort, one can deduce the remaining macroscopic properties' expressions. Both internal energy and enthalpy expressions derive from the differentiation of $\Psi/(k_B T)$. Equation 3.23 demonstrates the application of the chain rule.

$$d\left(\frac{\Psi}{k_B T}\right) = \frac{1}{k_B T} d\Psi - \frac{\Psi}{k_B T^2} dT \quad (3.23)$$

Combining Equations 3.14, 3.16, and 3.23, the differential form of $\Psi/(k_B T)$ can be written as:

$$d\left(\frac{\Psi}{k_B T}\right) = -\frac{U}{k_B T^2} dT - \frac{P}{k_B T} dV + \frac{\mu_h}{k_B T} dN_h - \sum_{j=1}^{n_{guest}} N_j d \ln \lambda_j \quad (3.24)$$

Applying the same reasoning used to derive the other properties' expressions, the internal energy of the hydrate can be calculated by differentiating $\Psi/(k_B T)$ for temperature, as demonstrated by Equation 3.25.

$$\frac{U}{k_B T^2} = - \left[\frac{\partial (\Psi/k_B T)}{\partial T} \right]_{V, \lambda, N_h} \quad (3.25)$$

Finally, the hydrate enthalpy is given by:

$$H = U + PV = -k_B T^2 \left[\frac{\partial (\Psi/k_B T)}{\partial T} \right]_{V, \lambda, N_h} - V \left(\frac{\partial \Psi}{\partial V} \right)_{T, N_h, \lambda} \quad (3.26)$$

3.3 Hydrate empty lattice and guest molecules contributions

One of the effects of van der Waals and Platteuw's assumptions was the segregation of empty lattice and guest molecules' contributions to the partition function. This section exhibits the separation process of these contributions at a macroscopic level. Equation 3.12 above shows us that the thermodynamic potential of the hydrate is proportional to the natural logarithm of the associated partition function.

Hence, the logarithmic form of $\Xi(T, V, N_h, \underline{\lambda})$ is crucial to further developments. This expression is displayed by Equation 3.27.

$$\ln \Xi = \ln Q^{EL} + \sum_{i=1}^{n_{cage}} \nu_i N_h \ln \left[1 + \sum_{j=1}^{n_{guest}} (q_{ij} \lambda_{ij}) \right] \quad (3.27)$$

One can correlate the hydrate partition function from Equation 3.27 and the derived expressions for the macroscopic properties presented in Section 3.2. This correlation is essential to identify empty lattice and guest molecules' contributions to macroscopic properties. The subsequent subsections will address each property.

3.3.1 Number of guest molecules and cage occupancy

From Equation 3.17, it is known that:

$$N_{ij} = -\frac{\lambda_{ij}}{k_B T} \left(\frac{\partial \ln \Psi}{\partial \lambda_{ij}} \right)_{T, V, N_h, \lambda_{im \neq ij}} = -\frac{\lambda_{ij}}{k_B T} \left[\frac{\partial (-k_B T \ln \Xi)}{\partial \lambda_{ij}} \right]_{T, V, N_h, \lambda_{im \neq ij}} \quad (3.28)$$

which can be expressed as:

$$N_{ij} = \lambda_{ij} \left(\frac{\partial \ln \Xi}{\partial \lambda_{ij}} \right)_{T, V, N_h, \lambda_{im \neq ij}} \quad (3.29)$$

The differentiation of the right side of Equation 3.27 with respect to λ_{ij} results in:

$$\left(\frac{\partial \ln \Xi}{\partial \lambda_{ij}} \right)_{T, V, N_h, \lambda_{im \neq ij}} = \frac{\nu_i N_h q_{ij}}{1 + \sum_{j=1}^{n_{guest}} (q_{ij} \lambda_{ij})} \quad (3.30)$$

Hence, Equation 3.29 can be rewritten as Equation 3.31.

$$N_{ij} = \frac{\nu_i N_h q_{ij} \lambda_{ij}}{1 + \sum_{j=1}^{n_{guest}} (q_{ij} \lambda_{ij})} = \frac{\nu_i N_h q_{ij} \lambda_j}{1 + \sum_{j=1}^{n_{guest}} (q_{ij} \lambda_j)} \quad (3.31)$$

or even, according to Equation 3.21:

$$N_j = \sum_{i=1}^{n_{cage}} \frac{\nu_i N_h q_{ij} \lambda_j}{1 + \sum_{j=1}^{n_{guest}} (q_{ij} \lambda_j)} \quad (3.32)$$

Nevertheless, the number of guest molecules trapped within the crystalline structure is a less practical property than the cage occupancy. The latter property is defined as the ratio between the number of guest species j within cages i and the total number of i -type cages, as illustrated by Equation 3.33.

$$\theta_{ij} = \frac{N_{ij}}{\nu_i N_h} \quad (3.33)$$

Equation 3.34 describes the cage occupancy in terms of the natural coordinates of the semi-grand canonical ensemble.

$$\theta_{ij} = \frac{q_{ij} \lambda_j}{1 + \sum_{j=1}^{n_{guest}} (q_{ij} \lambda_j)} \quad (3.34)$$

3.3.2 Entropy

Analogously, the development of Equation 3.18 gives:

$$S = - \left[\frac{\partial (-k_B T \ln \Xi)}{\partial T} \right]_{V, N_h, \lambda} - k_B \sum_{j=1}^{n_{guest}} \sum_{i=1}^{n_{cage}} N_{ij} \ln \lambda_{ij} \quad (3.35)$$

$$S = k_B \left[\ln \Xi \left(\frac{\partial T}{\partial T} \right)_{V, N_h, \lambda} + T \left(\frac{\partial \ln \Xi}{\partial T} \right)_{V, N_h, \lambda} \right] - k_B \sum_{j=1}^{n_{guest}} \sum_{i=1}^{n_{cage}} N_{ij} \ln \lambda_{ij} \quad (3.36)$$

Where the differentiation of $\ln \Xi$ with respect to temperature gives:

$$\left(\frac{\partial \ln \Xi}{\partial T} \right)_{V, N_h, \lambda} = \left(\frac{\partial \ln Q^{EL}}{\partial T} \right)_{V, N_h, \lambda} + \sum_{i=1}^{n_{cage}} \nu_i N_h \frac{\sum_{j=1}^{n_{guest}} [\lambda_{ij} (\partial q_{ij} / \partial T)]}{1 + \sum_{j=1}^{n_{guest}} (q_{ij} \lambda_{ij})} \quad (3.37)$$

$$\begin{aligned} \left(\frac{\partial \ln \Xi}{\partial T} \right)_{V, N_h, \lambda} = & - \left[\frac{\partial (A^{EL} / k_B T)}{\partial T} \right]_{V, N_h, \lambda} + \\ & + \sum_{i=1}^{n_{cage}} \nu_i N_h \frac{\sum_{j=1}^{n_{guest}} [\lambda_{ij} (q_{ij} / q_{ij}) (\partial q_{ij} / \partial T)]}{1 + \sum_{j=1}^{n_{guest}} (q_{ij} \lambda_{ij})} \end{aligned} \quad (3.38)$$

$$\begin{aligned} \left(\frac{\partial \ln \Xi}{\partial T} \right)_{V, N_h, \lambda} = & - \frac{1}{k_B} \left[\frac{1}{T} \left(\frac{\partial A^{EL}}{\partial T} \right)_{V, N_h, \lambda} - \frac{A^{EL}}{T^2} \right] \\ & + \sum_{i=1}^{n_{cage}} \nu_i N_h \frac{\sum_{j=1}^{n_{guest}} [\lambda_{ij} q_{ij} (\partial \ln q_{ij} / \partial T)]}{1 + \sum_{j=1}^{n_{guest}} (q_{ij} \lambda_{ij})} \end{aligned} \quad (3.39)$$

$$\left(\frac{\partial \ln \Xi}{\partial T}\right)_{V, N_h, \Delta} = \frac{1}{k_B T} \left[\frac{TS^{EL} + A^{EL}}{T} \right] + \sum_{i=1}^{n_{cage}} \sum_{j=1}^{n_{guest}} \left[N_{ij} \left(\frac{\partial \ln q_{ij}}{\partial T} \right) \right] \quad (3.40)$$

The combination of Equations 3.36 and 3.40 results in Equation 3.41, shown below.

$$S = k_B \left\{ -\frac{A^{EL}}{k_B T} + \sum_{i=1}^{n_{cage}} \nu_i N_h \ln \left[1 + \sum_{j=1}^{n_{guest}} (q_{ij} \lambda_{ij}) \right] + \frac{S^{EL}}{k_B} + \frac{A^{EL}}{k_B T} + T \sum_{i=1}^{n_{cage}} \sum_{j=1}^{n_{guest}} \left[N_{ij} \left(\frac{\partial \ln q_{ij}}{\partial T} \right) \right] \right\} - k_B \sum_{i=1}^{n_{cage}} \sum_{j=1}^{n_{guest}} N_{ij} \ln \lambda_{ij} \quad (3.41)$$

$$S = S^{EL} + k_B \sum_{i=1}^{n_{cage}} \left\{ \nu_i N_h \ln \left[1 + \sum_{j=1}^{n_{guest}} (q_{ij} \lambda_{ij}) \right] + T \sum_{j=1}^{n_{guest}} \left[N_{ij} \left(\frac{\partial \ln q_{ij}}{\partial T} \right)_{V, N_h, \Delta} \right] - \sum_{j=1}^{n_{guest}} N_{ij} \ln \lambda_{ij} \right\} \quad (3.42)$$

The first term on the right-hand side of Equation 3.42 corresponds to the empty lattice's entropy, whereas the second term represents the guest molecules' enclathration's contribution.

3.3.3 Pressure

Equation 3.19 gives us the correlation between the hydrate's pressure and Ψ . Through Equation 3.12, it is possible to calculate the system's pressure as a function of microscopic properties.

$$P = - \left[\frac{\partial (-k_B T \ln \Xi)}{\partial V} \right]_{T, N_h, \Delta} \quad (3.43)$$

$$P = k_B T \left(\frac{\partial \ln \Xi}{\partial V} \right)_{T, N_h, \Delta} \quad (3.44)$$

where the differentiation of $\ln \Xi$ concerning the hydrate's volume gives:

$$\left(\frac{\partial \ln \Xi}{\partial V}\right)_{T, N_h, \lambda} = \left(\frac{\partial \ln Q^{EL}}{\partial V}\right)_{T, N_h, \lambda} + \sum_{i=1}^{n_{cage}} \nu_i N_h \frac{\sum_{j=1}^{n_{guest}} [\lambda_{ij} (\partial q_{ij} / \partial V)]}{1 + \sum_{j=1}^{n_{guest}} (q_{ij} \lambda_{ij})} \quad (3.45)$$

$$\left(\frac{\partial \ln \Xi}{\partial V}\right)_{T, N_h, \lambda} = - \left[\frac{(A^{EL} / k_B T)}{\partial V} \right]_{T, N_h, \lambda} + \sum_{i=1}^{n_{cage}} \nu_i N_h \frac{\sum_{j=1}^{n_{guest}} [\lambda_{ij} (q_{ij} / q_{ij}) (\partial q_{ij} / \partial V)]}{1 + \sum_{j=1}^{n_{guest}} (q_{ij} \lambda_{ij})} \quad (3.46)$$

$$\left(\frac{\partial \ln \Xi}{\partial V}\right)_{T, N_h, \lambda} = \frac{P^{EL}}{k_B T} + \sum_{i=1}^{n_{cage}} \nu_i N_h \frac{\sum_{j=1}^{n_{guest}} [q_{ij} \lambda_{ij} (\partial \ln q_{ij} / \partial V)]}{1 + \sum_{j=1}^{n_{guest}} (q_{ij} \lambda_{ij})} \quad (3.47)$$

$$\left(\frac{\partial \ln \Xi}{\partial V}\right)_{T, N_h, \lambda} = \frac{P^{EL}}{k_B T} + \sum_{i=1}^{n_{cage}} \sum_{j=1}^{n_{guest}} N_{ij} \left(\frac{\partial \ln q_{ij}}{\partial V}\right)_{T, N_h, \lambda} \quad (3.48)$$

The substitution of the derived expression for $(\partial \ln \Xi / \partial V)$ in Equation 3.44 results in Equation 3.49.

$$P = P^{EL} + k_B T \sum_{i=1}^{n_{cage}} \sum_{j=1}^{n_{guest}} N_{ij} \left(\frac{\partial \ln q_{ij}}{\partial V}\right)_{T, N_h, \lambda} \quad (3.49)$$

The first term on the right-hand side corresponds to the empty lattice's pressure, while the second represents the contribution of guest molecules enclathration.

3.3.4 Host molecules' chemical potential

Finally, for the host's chemical potential, the expansion of Equation 3.20 gives:

$$\mu_h = -k_B T \left[\frac{\partial (\ln \Xi)}{\partial N_h} \right]_{T, V, \lambda} \quad (3.50)$$

Where the differentiation of $\ln \Xi$ concerning the number of host molecules results in:

$$\left(\frac{\partial \ln \Xi}{\partial N_h}\right)_{T, V, \lambda} = \left(\frac{\partial \ln Q^{EL}}{\partial N_h}\right)_{T, V, \lambda} + \frac{\partial}{\partial N_h} \left\{ N_h \sum_{i=1}^{n_{cage}} \nu_i \ln \left[1 + \sum_{j=1}^{n_{guest}} (q_{ij} \lambda_{ij}) \right] \right\} \quad (3.51)$$

$$\left(\frac{\partial \ln \Xi}{\partial N_h}\right)_{T,V,\lambda} = -\frac{1}{k_B T} \left(\frac{\partial A^{EL}}{\partial N_h}\right)_{T,V,\lambda} + \sum_{i=1}^{n_{cage}} \nu_i \left\{ \ln \left[1 + \sum_{j=1}^{n_{guest}} (q_{ij} \lambda_{ij}) \right] + N_h \frac{\sum_{j=1}^{n_{guest}} \lambda_{ij} (\partial q_{ij} / \partial N_h)}{1 + \sum_{j=1}^{n_{guest}} (q_{ij} \lambda_{ij})} \right\} \quad (3.52)$$

$$\left(\frac{\partial \ln \Xi}{\partial N_h}\right)_{T,V,\lambda} = -\frac{\mu_h^{EL}}{k_B T} + \sum_{i=1}^{n_{cage}} \nu_i \left\{ \ln \left[1 + \sum_{j=1}^{n_{guest}} (q_{ij} \lambda_{ij}) \right] + N_h \frac{\sum_{j=1}^{n_{guest}} q_{ij} \lambda_{ij} (\partial \ln q_{ij} / \partial N_h)}{1 + \sum_{j=1}^{n_{guest}} (q_{ij} \lambda_{ij})} \right\} \quad (3.53)$$

Replacing the expression above (Equation 3.53) in Equation 3.50 generates:

$$\mu_h = \mu_h^{EL} - k_B T \sum_{i=1}^{n_{cage}} \left\{ \nu_i \ln \left[1 + \sum_{j=1}^{n_{guest}} (q_{ij} \lambda_{ij}) \right] + \sum_{j=1}^{n_{guest}} N_{ij} \left(\frac{\partial \ln q_{ij}}{\partial N_h} \right)_{T,V,\lambda} \right\} \quad (3.54)$$

Again, contributions from the empty lattice and the guest species can be adequately distinguished.

3.3.5 Internal Energy and Enthalpy

For the internal energy and enthalpy, the same procedure is performed.

$$U = k_B T^2 \left[\frac{\partial (\ln \Xi)}{\partial T} \right]_{V,\lambda,N_h} \quad (3.55)$$

Where the differentiation of $\ln \Xi$ with respect to temperature results in:

$$\left(\frac{\partial \ln \Xi}{\partial T}\right)_{V,\lambda,N_h} = \left(\frac{\partial \ln Q^{EL}}{\partial T}\right)_{V,\lambda,N_h} + \sum_{i=1}^{n_{cage}} \nu_i N_h \frac{\sum_{j=1}^{n_{guest}} \lambda_{ij} (\partial q_{ij} / \partial T)}{1 + \sum_{j=1}^{n_{guest}} q_{ij} \lambda_{ij}} \quad (3.56)$$

$$\left(\frac{\partial \ln \Xi}{\partial T}\right)_{V,\lambda,N_h} = -\frac{1}{k_B} \left[\frac{\partial (A^{EL}/T)}{\partial T} \right]_{V,\lambda,N_h} + \sum_{i=1}^{n_{cage}} \nu_i N_h \frac{\sum_{j=1}^{n_{guest}} q_{ij} \lambda_{ij} (\partial \ln q_{ij} / \partial T)}{1 + \sum_{j=1}^{n_{guest}} q_{ij} \lambda_{ij}} \quad (3.57)$$

$$\left(\frac{\partial \ln \Xi}{\partial T}\right)_{V,\lambda,N_h} = -\frac{1}{k_B} \left[\frac{1}{T} \left(\frac{\partial A^{EL}}{\partial T}\right)_{V,\lambda,N_h} - \frac{A^{EL}}{T^2} \right] + \sum_{i=1}^{n_{cage}} \sum_{j=1}^{n_{guest}} N_{ij} \left(\frac{\partial \ln q_{ij}}{\partial T}\right) \quad (3.58)$$

$$\left(\frac{\partial \ln \Xi}{\partial T}\right)_{V,\lambda,N_h} = \frac{U^{EL}}{k_B T^2} + \sum_{i=1}^{n_{cage}} \sum_{j=1}^{n_{guest}} N_{ij} \left(\frac{\partial \ln q_{ij}}{\partial T}\right)_{V,\lambda,N_h} \quad (3.59)$$

Substituting the derived expression for $(\partial \ln \Xi / \partial T)$ depicted above in Equation 3.55 we arrive at:

$$U = U^{EL} + k_B T^2 \sum_{i=1}^{n_{cage}} \sum_{j=1}^{n_{guest}} N_{ij} \left(\frac{\partial \ln q_{ij}}{\partial T}\right)_{V,\lambda,N_h} \quad (3.60)$$

For the enthalpy, we have:

$$H = U + PV = U^{EL} + k_B T^2 \sum_{i=1}^{n_{cage}} \sum_{j=1}^{n_{guest}} N_{ij} \left(\frac{\partial \ln q_{ij}}{\partial T}\right)_{V,N_h,\lambda} + P^{EL}V + k_B TV \sum_{i=1}^{n_{cage}} \sum_{j=1}^{n_{guest}} N_{ij} \left(\frac{\partial \ln q_{ij}}{\partial V}\right)_{T,N_h,\lambda} \quad (3.61)$$

And since

$$H^{EL} = U^{EL} + P^{EL}V \quad (3.62)$$

Equation 3.61 can be simplified into:

$$H = H^{EL} + k_B T \left\{ \sum_{i=1}^{n_{cage}} \sum_{j=1}^{n_{guest}} N_{ij} \left[T \left(\frac{\partial \ln q_{ij}}{\partial T}\right)_{V,N_h,\lambda} + V \left(\frac{\partial \ln q_{ij}}{\partial V}\right)_{T,N_h,\lambda} \right] \right\} \quad (3.63)$$

Through Equations 3.60 and 3.63, it is possible to clearly distinguish both empty lattice's and guest's contributions (a melting and a heat of adsorption effect, respectively).

3.4 Langmuir adsorption coefficient calculation

In order to segregate the empty lattice's contribution from the guest species' contribution, it was necessary to write the macroscopic properties as functions of microscopic coordinates. So, from the derived expressions presented in Section 3.3, it is evident the macroscopic properties' dependence on λ_{ij} and q_{ij} . Nevertheless, these variables are not the most convenient ones.

The Langmuir adsorption coefficient – henceforth called Langmuir coefficient – is a key property within thermodynamic calculations involving the adsorption phenomenon since it describes how the adsorbate interacts with the adsorbent's surface. In the context of hydrate phase equilibrium prediction, we need to compute the Langmuir coefficient to contemplate the guest-host adsorption interaction within the thermodynamic modeling.

3.4.1 The Langmuir coefficient expression

Regarding the guest species representation in a coupled model scenario (vdWP model and fluid phase equation of state), the fugacity is a more appropriate variable to be employed as a substitute for λ_{ij} . The guest molecules' fugacity is defined by Equation 3.64.

$$\hat{f}_{ij} = P \exp\left(\frac{\mu_{ij} - \mu_j^{IG}}{k_B T}\right) \quad (3.64)$$

As in Equation 3.22, the chemical potential of guest species j in cages i will be expressed simply as μ_j from now on. It is worth highlighting that, in this work, the abbreviation "IG" always refers to a pure ideal gas, never to a mixture. In addition, we dropped the index i from the fugacity because we assume equilibrium between small and large as well as between each cage and bulk.

Since both fugacity and absolute activity are representations of the chemical potential in an exponential scale, the replacement of λ_j for \hat{f}_j is rather straightforward. Combining Equations 3.10 and 3.64 we arrive at:

$$\lambda_j = \frac{\hat{f}_j}{P} \exp\left(\frac{\mu_j^{IG}}{k_B T}\right) \quad (3.65)$$

According to MCQUARRIE (1976), the ideal gas (IG) state's chemical potential can be written as:

$$\mu_{ij}^{IG} = -k_B T \ln(k_B T \Phi_j) + k_B T \ln P \quad (3.66)$$

In which Φ_j portrays the configurational integral for particle momentum and internal degrees of freedom. This variable represents the product of intramolecular partition functions associated with translational, rotational, and vibrational energies. It should be noted that Φ_j is component-specific and exclusively dependent on temperature. Moreover, Φ_j can be described as the ratio between the internal partition function of a guest molecule j in the ideal gas state and its volume, as follows.

$$\Phi_j = \left(\frac{2\pi m_j k_B T}{h_{Planck}^2} \right)^{3/2} q_j^{IG,rotational} q_j^{IG,vibrational} \quad (3.67)$$

Hence, Equation 3.66 enables us to write the absolute activity of a guest j in terms of its fugacity.

$$\lambda_j = \frac{\hat{f}_j}{k_B T \Phi_j} \quad (3.68)$$

Likewise, the internal partition function q_{ij} is not the most suitable way to describe the molecules' behavior. Since the hydrate's formation is, essentially, an adsorption phenomenon, it is more convenient to calculate the guest's Langmuir adsorption coefficient (C_{ij}). Therefore, we must find means of writing q_{ij} as a function of C_{ij} . One method consists of substituting the λ_{ij} in Equation 3.34 for the right-hand side of Equation 3.68.

$$\theta_{ij} = \frac{q_{ij} \hat{f}_j / (k_B T \Phi_j)}{1 + \sum_{j=1}^{n_{guest}} \left[q_{ij} \hat{f}_j / (k_B T \Phi_j) \right]} \quad (3.69)$$

If closely examined, this is identical to a Langmuir adsorption isotherm, as depicted by Equation 3.70.

$$\theta_{ij} = \frac{C_{ij} f_j}{1 + \sum_{j=1}^{n_{guest}} (C_{ij} f_j)} \quad (3.70)$$

In which f_j represents the fugacity of component j in the fluid phase.

Comparing Equations 3.69 and 3.70, it is easy to correlate the Langmuir adsorption coefficient to the internal partition function.

$$C_{ij} = \frac{q_{ij}}{k_B T \Phi_j} \quad (3.71)$$

Worth noticing that, because of assumption (e), the internal partition function of a guest j in a cage i gets the same contribution Φ_j that this molecule would get in the ideal gas state. In other words, since the cage does not interfere with guest molecules' rotation and vibration, the internal degrees of freedom contribution is the same as if the ideal gas state condition was imposed.

Furthermore, as a result of assumptions (e) and (f), an expression for the internal partition function (q_{ij}) can be formulated. Equation 3.72, below, illustrates this expression.

$$q_{ij} = \Phi_j \int_0^{R_i} \left[\exp\left(\frac{-w_{ij}}{k_B T}\right) 4\pi r^2 \right] dr \quad (3.72)$$

In which the second term of the right-hand side of Equation 3.72 expresses the configurational integral for the free volume in spherical coordinates. R_i represents the spherical cavity radius of a cage i – which can be a mean radius or the actual distance between host and guest molecules, depending on the assumptions –, w_{ij} expresses the interaction potential function on a guest species j in a cage i , and r is the radial coordinate.

Now we can devise a more handy expression for the Langmuir coefficient, depicted below by Equation 3.73.

$$C_{ij} = \frac{1}{k_B T} \int_0^{R_i} \left[\exp\left(\frac{-w_{ij}}{k_B T}\right) 4\pi r^2 \right] dr \quad (3.73)$$

Moreover, with Equations 3.68 and 3.71 it is possible to arrange a clearer correlation between the original variables (λ_j and q_{ij}) and the most convenient ones (\hat{f}_j and C_{ij}).

$$\lambda_j q_{ij} = \hat{f}_j C_{ij} \quad (3.74)$$

Nonetheless, to use \hat{f}_j and C_{ij} to compute the macroscopic properties, we still need to make some adjustments. Through algebraic manipulation Equation 3.34 can be rewritten as:

$$1 + \sum_{j=1}^{n_{guest}} (q_{ij} \lambda_j) = \frac{1}{1 - \sum_{j=1}^{n_{guest}} \theta_{ij}} \quad (3.75)$$

With Equation 3.75, the logarithm form of Ξ is revised.

$$\ln \Xi = \ln Q^{EL} - \sum_{i=1}^{n_{cage}} \left[\nu_i N_h \ln \left(1 - \sum_{j=1}^{n_{guest}} \theta_{ij} \right) \right] \quad (3.76)$$

It should be noted that every derived property presented in Section 3.3 depends on the differential form of $\ln q_{ij}$, depicted by Equation 3.77.

$$d \ln q_{ij} = d \ln (C_{ij} k_B T \Phi_j) = d \ln (C_{ij} k_B T) + d \ln \Phi_j \quad (3.77)$$

As previously mentioned, Φ_j can be defined as the ratio between the internal partition function of a molecule j at the ideal gas state and its volume. Mathematically, this variable can be depicted as:

$$\Phi_j (T) = \frac{q_j^{IG} (T)}{\bar{V}_j^{IG}} \quad (3.78)$$

$$\ln [\Phi_j (T)] = \ln [q_j^{IG} (T)] - \ln \bar{V}_j^{IG} \quad (3.79)$$

Thus, the differential form of $\ln [\Phi_j (T)]$ is given by:

$$d \ln (\Phi_j) = \left[\frac{\partial \ln (q_j^{IG})}{\partial T} \right] dT = \frac{\bar{u}_j^{IG}}{k_B T^2} dT \quad (3.80)$$

Being \bar{u}_j^{IG} the internal energy of a guest species j at ideal gas state, i.e., solely function of temperature. Unlike the Langmuir adsorption coefficients, which also depend on the lattice's intensive volume. Therefore, the differential form of C_{ij} is represented by:

$$dC_{ij} = \left(\frac{\partial C_{ij}}{\partial \bar{V}^{EL}} \right)_T d\bar{V}^{EL} + \left(\frac{\partial C_{ij}}{\partial T} \right)_{\bar{V}^{EL}} dT \quad (3.81)$$

Where:

$$\bar{V}^{EL} = \frac{V}{N_h} \quad (3.82)$$

The differential form of C_{ij} in natural coordinates, thus, can be expressed as:

$$dC_{ij} = \left[\frac{\partial C_{ij}}{\partial \left(\frac{V}{N_h} \right)} \right]_T \left(\frac{dV}{N_h} - \frac{V}{N_h^2} dN_h \right) + \left(\frac{\partial C_{ij}}{\partial T} \right)_{V, N_h} dT \quad (3.83)$$

The first parcel of the first term on the right-hand side of Equation 3.83 is directly connected to the geometric relations between cages radii and intensive lattice volume. Therefore, the assumptions regarding the Langmuir coefficients' dependence on intensive lattice volume, and the latter's relation with cage radii, will dictate the model's capability to predict the influence of temperature, pressure, and guest size on the phase equilibrium calculation.

3.4.2 Guest-host adsorption interaction

Now that the Langmuir coefficient expression (Equation 3.73) has been devised, we should focus on how the guest-host interaction due to guest adsorption is computed.

According to MEDEIROS *et al.* (2020), one of the most common approaches to modifying the vdWP model consists of changing the Langmuir coefficient expression, which includes interaction potential between host and guest molecules. Since we are not concerned with describing every variation, we will limit our discussion to studying the Langmuir coefficient expressions that use a spherically symmetrical potential function. More specifically, we will focus on two possible variations of the LENNARD-JONES and DEVONSHIRE (1937) model: the Square Well and the Kihara potentials.

3.4.2.1 Square Well potential

Conceptually, a square well potential can be defined as a potential-energy function to which a particle is subjected which is infinite everywhere except for a specified portion of space (LEVINE, 2014). For a spherically symmetrical system such as the one used to model clathrates' cages, BARRER and EDGE (1967) proposed the following mathematical definition to describe guest adsorption:

$$w_{ij}(r) = \begin{cases} -w_0, & 0 < r < R_i \\ +\infty & \end{cases} \quad (3.84)$$

The substitution of Equation 3.84 on Equation 3.73 produces:

$$C_{ij} = \frac{4\pi R_i^3}{3k_B T} \exp\left(-\frac{w_{0,ij}}{k_B T}\right) \quad (3.85)$$

A close examination of Equation 3.85 reveals that its right-hand side contains the volume of the spherical cavity. Moreover, one can also notice that, except for T , all the other variables are parameters estimated from equilibrium data. Thus, conveniently, the above expression can be rewritten as follows:

$$C_{ij} = \frac{A_{ij}}{T} \exp\left(\frac{B_{ij}}{T}\right) \quad (3.86)$$

The equation above is the empirical relation used by PARRISH and PRAUSNITZ (1972) to calculate the Langmuir coefficients within the temperature range of 260K–300K. Nevertheless, the authors pointed out that for calculations outside the mentioned temperature range, Equation 3.73 should be used along with the Kihara potential. Using Equation 3.86 PARRISH and PRAUSNITZ (1972) and MUNCK *et al.* (1988) estimated A_{ij} and B_{ij} for some guest species, for both sI and sII configurations. e

3.4.2.2 Kihara potential

As shown in MCKOY and SINANOĞLU (1963) 's work, the original potential function devised by Kihara looks identical to the prominent 12-6 Lennard-Jones potential equation, and both can be written as follows.

$$w(d) = 4\varepsilon \left[\left(\frac{\sigma}{d}\right)^{12} - \left(\frac{\sigma}{d}\right)^6 \right] \quad (3.87)$$

However, while the Lennard-Jones considered d as the distance between interaction points in each particle, Kihara used the same variable to embody the shortest distance between the hard cores of interacting species (MEDEIROS *et al.*, 2020). To avoid misinterpretations, the Kihara potential function is generally written as:

$$w(d) = 4\varepsilon \left[\left(\frac{\sigma}{d-a}\right)^{12} - \left(\frac{\sigma}{d-a}\right)^6 \right] \quad (3.88)$$

where d represents the distance between interaction points in each particle, σ is the distance for which the potential is 0 – also called the soft-core parameter –, ε represents the depth of the energetic well located at $d = 2^{1/6}\sigma$ and a , the molecule's

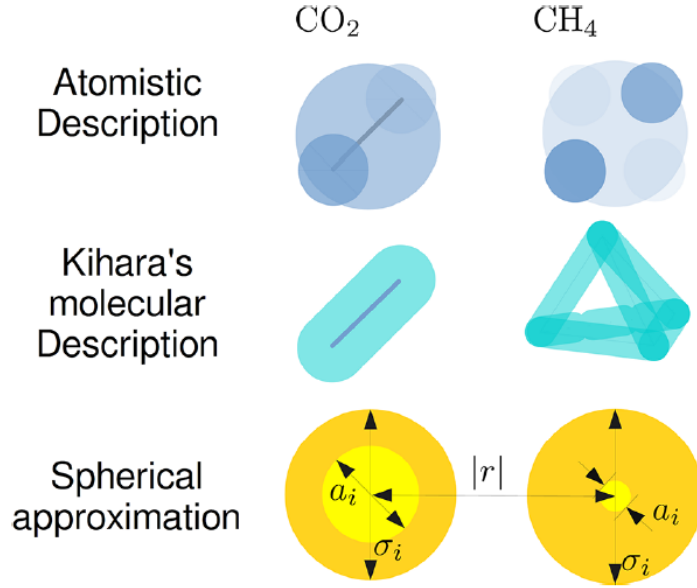


Figure 3.1: Graphic representation of Kihara's parameters for carbon dioxide and methane molecules. Reproduced from MEDEIROS *et al.* (2020)

hard-core radius. Figure 3.1 illustrates a graphic representation of these parameters for carbon dioxide and methane molecules.

In this sense, $(d - a)$ is an alternative, straightforward way of representing the shortest distance between the hard cores of interacting species, as intended by Kihara. It is worth mentioning that, for multi-component systems, the parameters a , σ , and ε are the outcome of some combining rule application, usually the Lorentz-Berthelot rules. Specifically for gas hydrates, the Lorentz-Berthelot combining rule applied to combine each guest and water of the shell yields:

$$\bar{a} = \frac{a_j^0 + a_w^0}{2} \quad (3.89)$$

$$\bar{\sigma} = \frac{\sigma_j^0 + \sigma_w^0}{2} \quad (3.90)$$

$$\bar{\varepsilon} = \sqrt{\varepsilon_j^0 \varepsilon_w^0} \quad (3.91)$$

Where superscript 0 indicates pure component parameters, the subscripts represent either the guest (j) or the host – w stands for water. In Equations 3.89 - 3.91 the combined parameters are indicated with a bar. However, since we are only dealing with natural gas hydrates, in which the host is always water and the guest is a light component j , for simplicity, the bar will be omitted, and the resulting parameter will be accompanied by the subscript j to indicate the guest. Therefore, for instance, the combination between the soft-core parameter of the pure light

component j (σ_j^0) and the pure water (σ_w^0) will be represented as σ_j .

According to VAN DER WAALS and PLATTEEUW (1959), the LENNARD-JONES and DEVONSHIRE (1937) 's approach, which comprised of the application of the 12-6 Lennard-Jones potential equation to the cell theory archetype, provides a robust method for the quantitative assessment of the partition function of a guest species within its cage. Nonetheless, MCKOY and SINANOĞLU (1963) 's study revealed that Lennard-Jones and Devonshire's methodology's effectiveness is restricted to spherical molecules, such as methane. According to the authors, the Kihara potential was the most suitable for rod-like molecules.

A variation of the original Kihara's potential was used in this work. The modification, proposed by JOHN *et al.* (1985) to improve the original Kihara's potential performance, introduces new parameters as portrayed in Equations 3.92.

$$w_{ij} = 2\varepsilon_j Z_i \left[\frac{\sigma_j^{12}}{R_i^{11} r} \left(\delta_{10} + \frac{a_j}{R_i} \delta_{11} \right) - \frac{\sigma_j^6}{R_i^5 r} \left(\delta_4 + \frac{a_j}{R_i} \delta_5 \right) \right] \quad (3.92)$$

Where:

$$\delta_n = \frac{1}{n} \left[\left(1 - \frac{r}{R_i} - \frac{a_j}{R_i} \right)^{-n} - \left(1 + \frac{r}{R_i} - \frac{a_j}{R_i} \right)^{-n} \right] \quad (3.93)$$

Z_i represents the coordination number of a cage i , and a_j , σ_j , and ε_j are the Kihara pair interaction potential parameters between a host molecule from the lattice and a guest species j .

In their paper, PRATT *et al.* (2001) pointed out that the physical meaning of $r = R_i - a_j$ for the Kihara potential is the guest molecule's spherical core touching the cage's edge. For this reason, according to the authors, the evaluation of the integrand of Equation 3.72 in $r > R_i - a_j$ does not physically make sense. Therefore, the upper limit of the integrand mentioned above should be changed to $R_i - a_j$.

$$C_{ij} = \frac{1}{k_B T} \int_0^{R_i - a_j} \left[\exp \left(\frac{-w_{ij}}{k_B T} \right) 4\pi r^2 \right] dr \quad (3.94)$$

The Equation 3.94 presents the final form of the expression applied to calculate the Langmuir coefficients whenever the Kihara parameters (a_j , σ_j , and ε_j) were available.

3.5 The pressure shift phenomenon

In their 1959’s paper, VAN DER WAALS and PLATTEEUW (1959) suggested that the host lattice, supposedly a rigid structure, would not be affected by the guest molecules. In addition, the authors neglected cage radii variation. Nevertheless, through recent experiments, it is known that both assumptions are at least inaccurate. Not only do we know that the lattice is compressible and its parameters in the original vdWP framework are guest-dependent, but the hydrate’s cavities do not have a constant radius. In this context, several models emerged to enhance hydrate formation prediction’s reliability.

The first phenomenological model to assimilate these new features was the one devised by KLAUDA and SANDLER (2000). In their paper, the authors acknowledged variations of hydrate volume with temperature and pressure for a specific guest species and hydrate lattice distortions caused by guest size. However, their approach still assumed that the cages’ radii were constant. Unlike BALLARD and SLOAN JR (2002) and HSIEH *et al.* (2012), whose models included both hydrate lattice compressibility and cavities radii variation. The latter assumption was carried out through Langmuir adsorption coefficients’ dependence on the lattice intensive volume. In their work, SEGTOVICH *et al.* (2022) noticed that, as a consequence of the correlation between C_{ij} and \bar{V}^{EL} , the hydrate should have a different pressure value from the empty lattice with the same volume. The authors attributed this phenomenon to a natural pressure shift generated by the isochoric enclathration of guest molecules into the hydrate’s crystalline structure. Mathematically, this phenomenon can be observed by rewriting Equation 3.49 and employing the correlations presented in Equations 3.73 and 3.86.

$$P - P^{EL} = k_B T \sum_{i=1}^{n_{cage}} \sum_{j=1}^{n_{guest}} \nu_i \theta_{ij} \left[\frac{\partial (\ln C_{ij})}{\partial \left(\frac{V}{N_h} \right)} \right]_T \quad (3.95)$$

where the difference $P - P^{EL}$ represents the pressure shift caused by guests’ enclathration; here, we will address this difference by using ΔP^{H-EL} , similarly to SEGTOVICH *et al.* (2022).

Visually, this phenomenon can be represented by Figure 3.2, which presents the enclathration of small and large guests through two perspectives: an isobaric and an isochoric.

In Figure 3.2, the letter D represents the empty lattice (EL), which, despite being hypothetical, is the hydrate reference state at reference volume (V_0) and pres-

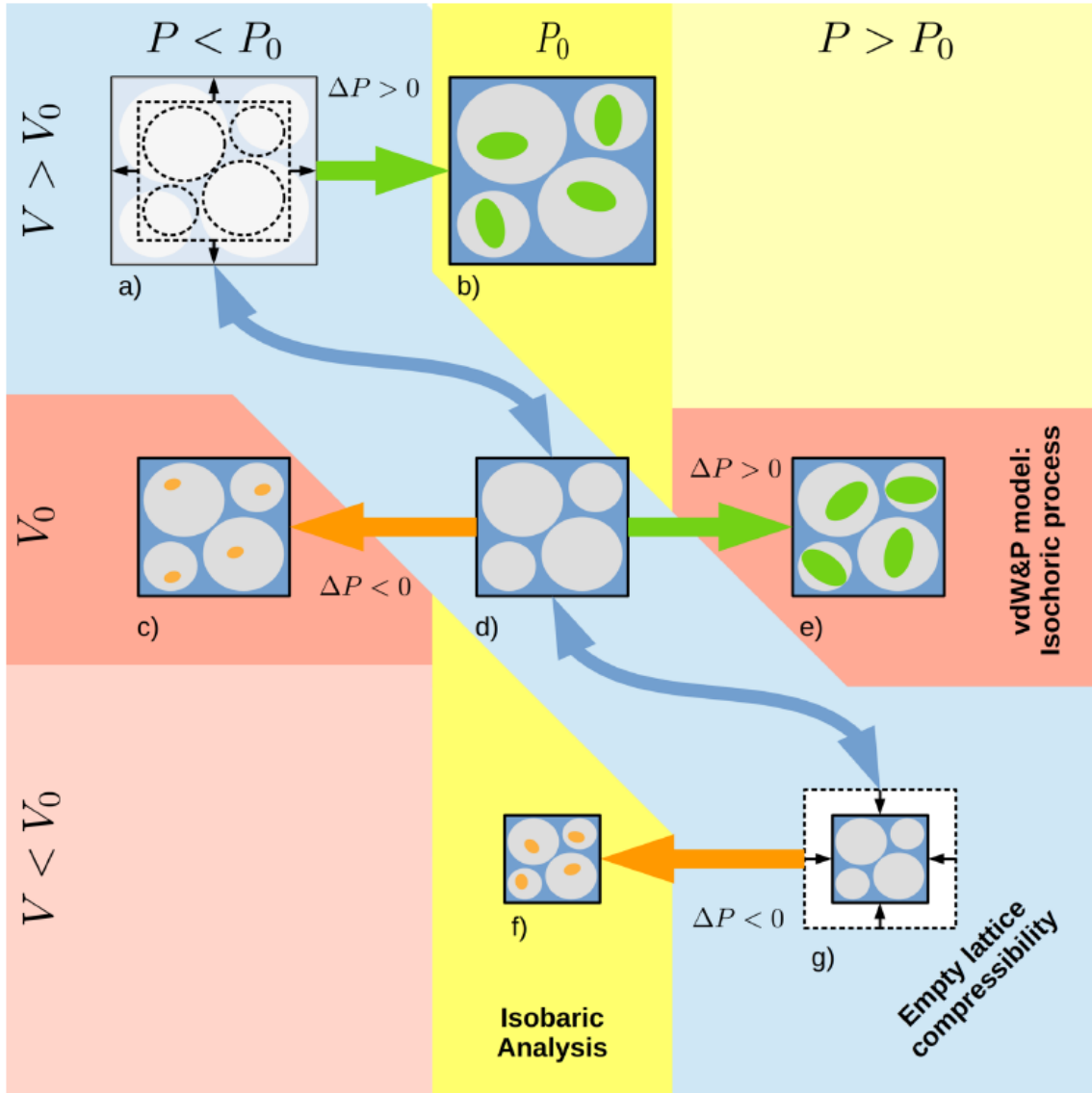


Figure 3.2: Graphic representation of the pressure shift phenomenon through both isochoric and isobaric perspectives. The blue squares and gray circles depict the hydrate lattice and its cavities, respectively. The green particles represent a component of large molecular size, whereas the orange particles are a component of small molecular size. Reproduced from SEGTOVICH *et al.* (2022).

sure (P_0). The transition depicted by $D \rightarrow E$ describes the isochoric enclathration process of large guests (green particles) as they fit tightly within the cavities. After the enclathration, the hydrate illustrated by letter E in Figure 3.2 would still have a volume of V_0 since the system volume is specified. However, according to the new model's premises, there is a computable pressure shift between the states D and E. In this case, the calculation shows a positive pressure shift ($\Delta P^{H-EL} > 0$), so that $P > P_0$. With this reasoning, to compute the volume that this hydrate would have at P_0 , we must assume that the reference state – i.e., the empty lattice – exists at a pressure lower than P_0 ($P^{EL} > P_0$) so that $P^{EL} + \Delta P^{(+)} = P_0$. This new reference state is given by letter A and, by virtue of the EL's intrinsic compressibility, its volume is greater than V_0 ($V^{EL} > V_0$) since it is assumed to exist in a pressure lower than P_0 . Thus, considering a hydrate whose guests fit tightly within its cages (letter B), its volume is greater than V_0 at P_0 .

The reasoning behind the enclathration process of small guests (orange particles) is very similar. At constant volume (V_0), this process is given by $D \rightarrow C$ and a pressure shift can be computed by implementing the Pshift model. Nonetheless, contrarily to what was observed for large guests, the pressure shift associated with the path $D \rightarrow C$ is negative ($P < P_0$). Now, to analyze this enclathration from an isobaric perspective regarding P_0 , the EL must be assumed to exist at a pressure $P^{EL} > P_0$, so that $P^{EL} + \Delta P^{(-)} = P_0$. In Figure 3.2, this new reference state is represented by the letter G, and, since it occurs at a pressure greater than P_0 , it has a volume $V^{EL} < V_0$. Hence, at reference pressure (P_0), a hydrate whose guests fit loosely within its cavities (letter F) has a lower volume when compared to an empty lattice with V_0 (letter D).

To summarize, from the reasoning employed to interpret the phenomena illustrated by Figure 3.2, it can be observed that the Pshift model offers a perspective that corroborates with the experimental observations that the enclathration of prominent guests expands the hydrate lattice, whereas small guests shrink it.

Even though the Pshift approach appears to conflict with the assumptions used by VAN DER WAALS and PLATTEEUW (1959), SEGTOVICH *et al.* (2022)'s proposition is a new interpretation of the vdWP model's hypotheses. Conversely to what one might think, no assumptions are violated by stating that the actual hydrate must have a different pressure from the empty lattice. These two states are not in thermodynamic equilibrium. The vdWP model only requires that both states have the same volume.

3.6 Hydrate lattice volumetric properties

In Section 3.4, it was demonstrated that the Langmuir adsorption coefficients depend on temperature and lattice intensive volume. Hence, to accurately represent the crystalline structure of a compressible hydrate, we must correlate the cages' radii variation to the lattice intensive volume. Some geometric relations between the crystalline structure's unit cell and the whole hydrate will be addressed in this section. Similar to SEGTOVICH *et al.* (2022), the cage radius deformation is considered to be isotropic.

It is known that sI and sII hydrates are of cubic symmetry. In this manner, the volume of a cubic unit cell is given by:

$$V^{uc} = (a^{uc})^3 \quad (3.96)$$

Where a^{uc} represents the cubic unit cell's edge length.

The correlation between the unit cell's edge and the cages radii (\underline{R}) is experimental by nature. Here, following SEGTOVICH *et al.* (2022)'s approach, we correlated a^{uc} and \underline{R} via Equation 3.97.

$$\underline{R} = \underline{f}_0 a^{uc} \underline{f} \quad (3.97)$$

The factor of proportionality \underline{f}_0 depicts the array that correlates \underline{R}_0 to a_0^{uc} . The latter variables are experimental parameters representing the cages' radii and the unit cell's edge length, respectively.

$$\underline{f}_0 = \frac{\underline{R}_0}{a_0^{uc}} \quad (3.98)$$

Likewise, \underline{f} is another proportionality factor; however, its computation is not as straightforward as the former.

$$\underline{f} = \exp \left[\left(\frac{\underline{\kappa}_R}{\kappa_{hyd}} \right) \ln \left(\frac{a^{uc}}{a_0^{uc}} \right) \right] \quad (3.99)$$

$$\underline{f} = \exp \left\{ \ln \left[\left(\frac{a^{uc}}{a_0^{uc}} \right) \left(\frac{\underline{\kappa}_R}{\kappa_{hyd}} \right) \right] \right\} = \left(\frac{a^{uc}}{a_0^{uc}} \right) \left(\frac{\underline{\kappa}_R}{\kappa_{hyd}} \right) \quad (3.100)$$

In Equation 3.99 κ_{hyd} and $\underline{\kappa}_R$ portrays the unit cell and cages compressibility factors, respectively. The array $\underline{\kappa}_R$ has as many elements as there are cage types.

The differential form of the Langmuir adsorption coefficient presented in Section 3.4 indicated its variable's dependency with the lattice intensive volume. Since the latter is the ratio between V and N_h , the Langmuir coefficient is a function of these two variables. Decomposing the partial derivative $\partial C_{ij}/\partial\left(\frac{V}{N_h}\right)$ in terms of the lattice geometric parameters, we have:

$$\frac{\partial C_{ij}}{\partial\left(\frac{V}{N_h}\right)} = \frac{\partial C_{ij}}{\partial R_i} \frac{\partial R_i}{\partial a^{uc}} \frac{\partial a^{uc}}{\partial V^{uc}} \frac{\partial V^{uc}}{\partial\left(\frac{V}{N_h}\right)} \quad (3.101)$$

From Equation 3.73, the first term on the right-hand side of Equation 3.101 can be calculated by:

$$\frac{\partial C_{ij}}{\partial R_i} = \frac{1}{k_B T} \int_0^{R_i - a_i} \left[\frac{-4\pi r^2}{k_B T} \left(\frac{\partial w_{ij}}{\partial R_i} \right) \exp\left(\frac{-w_{ij}}{k_B T}\right) dr \right] \quad (3.102)$$

The second term of 3.101 is obtained through the application of the chain rule, as shown below.

$$\frac{\partial R_i}{\partial a^{uc}} = \frac{\partial}{\partial a^{uc}} \left[\underline{f}_0 a^{uc} \underline{f}(a^{uc}) \right] \quad (3.103)$$

Since \underline{f}_0 is not a function of a^{uc} , the former can be withdrawn from the derivation.

$$\frac{\partial R_i}{\partial a^{uc}} = \underline{f}_0 \frac{\partial}{\partial a^{uc}} \left[a^{uc} \underline{f}(a^{uc}) \right] \quad (3.104)$$

$$\frac{\partial R_i}{\partial a^{uc}} = \underline{f}_0 \left(\underline{f} + a^{uc} \frac{\partial \underline{f}}{\partial a^{uc}} \right) \quad (3.105)$$

Where:

$$\frac{\partial \underline{f}}{\partial a^{uc}} = \left(\frac{\underline{\kappa}_R}{\kappa_{hyd}} \right) \left(\frac{1}{a_0^{uc}} \right) \left(\frac{a^{uc}}{a_0^{uc}} \right)^{\left(\frac{\underline{\kappa}_R}{\kappa_{hyd}} - 1 \right)} \quad (3.106)$$

The multiplication of the right-hand side on Equation 3.106 by (a^{uc}/a_0^{uc}) results in:

$$\frac{\partial \underline{f}}{\partial a^{uc}} = \left(\frac{\underline{\kappa}_R}{\kappa_{hyd}} \right) \left(\frac{1}{a^{uc}} \right) \left(\frac{a^{uc}}{a_0^{uc}} \right) \left(\frac{\underline{\kappa}_R}{\kappa_{hyd}} \right) \quad (3.107)$$

The variable \underline{f} is recovered in the right-hand side's last term.

$$\frac{\partial \underline{f}}{\partial a^{uc}} = \left(\frac{\underline{\kappa}_R}{\kappa_{hyd}} \right) \left(\frac{1}{a^{uc}} \right) \underline{f} \quad (3.108)$$

Substituting the $(\partial \underline{f} / \partial a^{uc})$ expression on Equation 3.105 we have:

$$\frac{\partial R_i}{\partial a^{uc}} = \underline{f}_0 \left[\underline{f} + a^{uc} \left(\frac{\underline{\kappa}_R}{\kappa_{hyd}} \right) \left(\frac{1}{a^{uc}} \right) \underline{f} \right] \quad (3.109)$$

Through some algebraic manipulation, Equation 3.109 turns into:

$$\frac{\partial R_i}{\partial a^{uc}} = \underline{f}_0 \left(\frac{\underline{\kappa}_R}{\kappa_{hyd}} \right) \underline{f} \quad (3.110)$$

As for the third term on Equation's 3.101 right-hand side, we have:

$$\frac{\partial a^{uc}}{\partial V^{uc}} = \frac{1}{3} (V^{uc})^{-2/3} = \frac{(a^{uc})^{-2}}{3} \quad (3.111)$$

Before we deduce the expression for the last term of $\partial C_{ij} / \partial \left(\frac{V}{N_h} \right)$ decomposition, a consideration must be made. The hydrate and its unit cells have the same specific volume since, by definition, the crystalline structure of the former is assembled by the replication of the latter. Therefore:

$$\frac{V}{N_h} = \frac{V^{uc}}{N_h^{uc}} = \bar{V}^{EL} \quad (3.112)$$

Finally, we have:

$$\frac{\partial V^{uc}}{\partial \left(\frac{V}{N_h} \right)} = N_h^{uc} \quad (3.113)$$

Now the partial derivative of C_{ij} in terms of lattice intensive volume can be obtained through some lattice parameters $(\kappa_{hyd}, \underline{\kappa}_R, a_0^{uc}, N_h^{uc}, \underline{R}_0)$ and the calculation of a^{uc} , which, in turn, is a function of temperature, pressure and composition of hydrate-forming phase. Interestingly, the correlation displayed by Equation 3.112 shows us that a^{uc} – which is tied to V^{uc} – can be computed through \bar{V}^{EL} .

The expression used to calculate the empty lattice volume is given by:

$$\begin{aligned} \bar{V}^{EL}/(\text{m}^3\text{mol}^{-1}) = & \left[a_0^{uc} + \alpha_1 \left(T - T_0^{crystal} \right) + \alpha_2 \left(T - T_0^{crystal} \right)^2 + \right. \\ & \left. + \alpha_3 \left(T - T_0^{crystal} \right)^3 \right]^3 \frac{10^{-30} N_A}{N_h^{uc}} \exp \left[-\kappa_{hyd} \left(P^{EL} - P_0^{crystal} \right) \right] \end{aligned} \quad (3.114)$$

Where α_1 , α_2 and α_3 are the linear parameters from a cubic fit for the thermal expansion term; N_A is the Avogadro number; κ_{hyd} is the hydrate compressibility; $T_0^{crystal}$ and $P_0^{crystal}$ are the experimental reference temperature and pressure of the experiments used to regress the volumetric parameters of crystalline structures. Usually, $T_0^{crystal} = 0$ K and $P_0^{crystal} = 101\,325$ Pa. In addition, to calculate \bar{V}^{EL} in m^3/mol , a_0^{uc} must be provided in \AA .

It should be emphasized that a_0^{uc} , α_1 , α_2 , α_3 , κ_{hyd} and $\underline{\kappa}_R$ are parameters that will be estimated from experimental data promptly.

Although Equation 3.114 describes how the empty lattice's pressure and volume are correlated, it is known that it is virtually impossible to reproduce such a state in the laboratory. Therefore, the parameters related to crystallographic measures – henceforth called volumetric parameters – exhibited in Equation 3.114 must be regressed from hydrates' experimental data. This approximation is not an issue, since

$$V^H (P^H) = V^{EL} (P^{EL}) \quad (3.115)$$

for a hydrate modeled by the vdWP model considering the pressure shift phenomenon.

In conclusion, the above mathematical modelling informs that the computation of $\left[\partial C_{ij} / \partial \left(\frac{V}{N_h} \right) \right]$ depends on the value of P^{EL} , which, in turn, according to Equation 3.95, is a function of the former. Therefore, to calculate P^{EL} and, consequently, \bar{V}^{EL} , we need an iterative algorithm. Here, we used the convergence method designed by SEGTOVICH *et al.* (2022). Further details will be addressed in Chapter 4.

3.7 Hydrate phase equilibrium

The aim of thermodynamic calculations of systems with clathrates usually consists of building a phase equilibrium problem. More specifically, a three-phase

equilibrium problem composed of a pure, non-volatile phase containing the host species; a solid solution phase; a hydrate-forming fluid phase containing the guest molecules. It is worth mentioning that the mutual solubility between the phases which contain the host and guest species is neglected in the calculation. Therefore, the activity coefficients are unity.

The scheme replicated from SEGTOVICH *et al.* (2022) displayed in Figure 3.3 portrays the states involved in the phase equilibrium calculation. In addition, this diagram also shows how the physical states – such as pure liquid water (PW), pure ice (I), hydrate (H), and vapor (V) – are correlated to their respective reference state – namely, the empty hydrate lattice (EL) and the pure ideal gas state (PIG). It is worth noticing that the hydrate-forming phase will not always be present in the equilibrium as a vapor. Depending on the compound’s nature and the conditions, this phase can stabilize as a liquid or vapor.

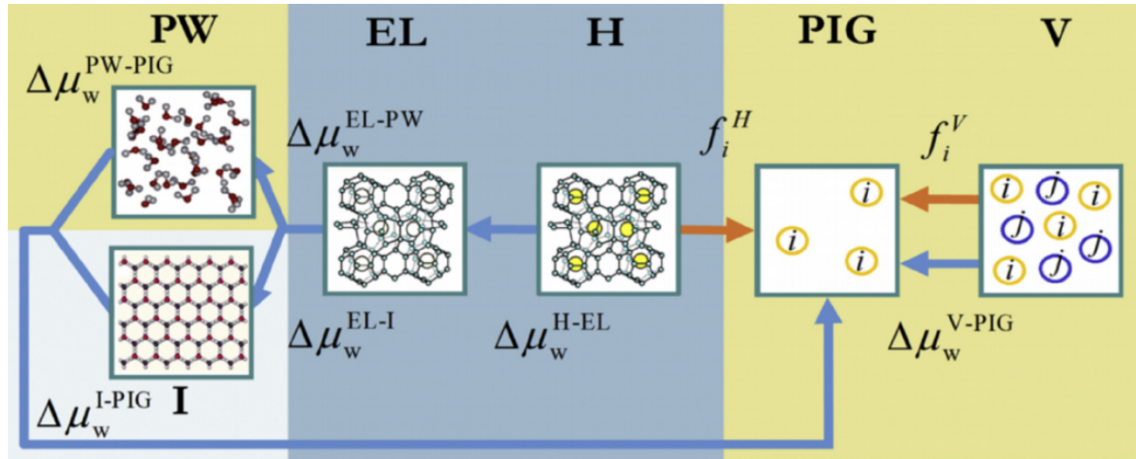


Figure 3.3: Diagram that presents the states involved in hydrate phase equilibrium calculations. The arrows depict the chemical potential difference between the two states. For phase transitions from the pure ideal gas state (PIG), the chemical potential difference is represented by its fugacity. Reproduced from SEGTOVICH (2018).

As mentioned in Chapter 2, the phase coexistence computation can be either based on fugacities or chemical potential differences. For an approach based on the former property, the necessary condition for the equilibrium is:

$$\hat{f}_w^H = \hat{f}_w^{PW} \quad (3.116)$$

Using the latter criterion, the necessary condition is given by:

$$\Delta\mu_w^{H-EL} = \Delta\mu_w^{PW-EL} \quad (3.117)$$

The subscripts of the variables displayed by Equations 3.116 and 3.117 represent a component within the phase equilibrium, which, in this case, is the water. While the superscripts represent the phase to which the water molecules belong. Here, the initials "PW" (pure water) can serve as liquid water as well as ice.

It is worth highlighting that the equality between μ_w^H and μ_w^{PW} does not define the chemical potential-based criterion because the former variable's calculation depends on μ_w^{EL} , for which there is no statistical thermodynamic-based expression. Hence, the hydrate's chemical potential is evaluated relative to the empty lattice reference state. In order to maintain equality, the pure water chemical potential must be calculated as a variation concerning the same reference state.

In both approaches cited above (Equations 3.116 and 3.117), the hydrate modeling must be combined with condensed phase modeling (for host molecules) and a fluid phase equation of state (for guest species). Fortunately, since the non-volatile and the hydrate-forming phases are considered immiscible, the latter phase's modeling is rather straightforward. The representation of guest molecules within the phase equilibrium calculation is implemented by its fugacity, estimated through an EoS application. This property is essential to compute its cage occupancy (θ_{ij}) and, therefore, other fundamental macroscopic properties, as shown in previous sections.

Following SEGTOVICH *et al.* (2022)'s approach, this work aspires to perform phase equilibrium calculations using chemical potential differences. Thus, we shall address the further developments of Equation 3.117, starting with a thorough investigation concerning its variables: $\Delta\mu_w^{H-EL}$ and $\Delta\mu_w^{EL-PW}$.

According to the reasoning presented in Section 3.3.4, $\Delta\mu_w^{H-EL}$ can be estimated through the manipulation of Equation 3.54 combined with the application of the mathematical modeling developed in Section 3.4.

$$\Delta\mu_w^{H-EL} = \mu_w^H - \mu_w^{EL} = k_B T \sum_{i=1}^{n_{cage}} \left[\nu_i \ln \left(1 - \sum_{j=1}^{n_{guest}} \theta_{ij} \right) - \sum_{j=1}^{n_{guest}} N_{ij} \left(\frac{\partial \ln q_{ij}}{\partial N_w} \right)_{T,V,\lambda} \right] \quad (3.118)$$

As we are dealing with a specific class of clathrates whose crystalline structure is composed of the hydrogen bond between water molecules, the generic subscript "h" for the host has been replaced by "w" for water.

Even though the modeling matured in Section 3.3.4 enabled us to replace the

term $[1 + \sum_{j=1}^{n_{guest}} (q_{ij}\lambda_{ij})]$ for a more convenient one, it does not help us to rewrite the partial derivative in more handy variables. Therefore, we now turn our attention to the Equation 3.49, which can be rewritten as:

$$P^H - P^{EL} = \Delta P^{H-EL} = k_B T \sum_{i=1}^{n_{cage}} \sum_{j=1}^{n_{guest}} N_{ij} \left(\frac{1}{q_{ij}} \right) \left(\frac{\partial q_{ij}}{\partial V^H} \right)_{T, N_w, \lambda} \quad (3.119)$$

We still do not have an expression to properly represent the last term on the right-hand side of Equation 3.119, so this gap must be filled before further progress.

At this point, it is known that q_{ij} is a function of T , V^H and N_w . Hence, assuming constant temperature, the differential form of the former variable can be written as the sum of contributions from the partial derivatives concerning the two latter variables.

$$dq_{ij}(T, V^H, N_w) = \left(\frac{\partial q_{ij}}{\partial V^H} \right)_{T, N_w} dV^H + \left(\frac{\partial q_{ij}}{\partial N_w} \right)_{T, V^H} dN_w \quad (3.120)$$

It should be mentioned that the temperature was fixed at a constant value because both hydrate pressure and water chemical potential in the hydrate phase are properties derived at a constant temperature. This hypothesis must not be assumed for other properties like hydrate internal energy.

Moreover, in Section 3.4 it has been established that C_{ij} , which is directly correlated to q_{ij} , can be expressed exclusively as a function of \bar{V}^{EL} and T . Thus, assuming constant temperature, the Equation 3.120 can be rewritten as:

$$dq_{ij} = \left[\frac{\partial q_{ij}}{\partial (V^H/N_w)} \right]_T d \left(\frac{V^H}{N_w} \right) \quad (3.121)$$

Analogously, the last term of the right-hand side of Equation 3.121 can be written as a function of its partial derivatives.

$$d \left(\frac{V^H}{N_w} \right) = \left[\frac{\partial (V^H/N_w)}{\partial V^H} \right]_{N_w} dV^H + \left[\frac{\partial (V^H/N_w)}{\partial N_w} \right]_{V^H} dN_w \quad (3.122)$$

The computation of the partial derivatives yields:

$$d\left(\frac{V^H}{N_w}\right) = \frac{1}{N_w}dV^H - \frac{V^H}{N_w^2}dN_w \quad (3.123)$$

By substituting the last term on the right-hand side of Equation 3.121 for the expression derived in Equation 3.123 we have:

$$dq_{ij} = \left(\frac{\partial q_{ij}}{\partial \bar{V}^{EL}}\right)_T \left(\frac{1}{N_w}dV^H - \frac{V^H}{N_w^2}dN_w\right) \quad (3.124)$$

Finally, the comparison between Equations 3.120 and 3.124 enable us to deduce that:

$$\left(\frac{\partial q_{ij}}{\partial V^H}\right)_{T, N_w} = \left(\frac{\partial q_{ij}}{\partial \bar{V}^{EL}}\right)_T \left(\frac{1}{N_w}\right) \quad (3.125)$$

$$\left(\frac{\partial q_{ij}}{\partial N_w}\right)_{T, V^H} = \left(\frac{\partial q_{ij}}{\partial \bar{V}^{EL}}\right)_T \left[\frac{(-V^H)}{N_w^2}\right] \quad (3.126)$$

In possession of these new equations, we can infer it is possible to replace the partial derivative term of Equation 3.119 with a more handy one.

$$\Delta P^{H-EL} = k_B T \sum_{i=1}^{n_{cage}} \sum_{j=1}^{n_{guest}} N_{ij} \left(\frac{1}{q_{ij}}\right) \left(\frac{1}{N_w}\right) \left(\frac{\partial q_{ij}}{\partial \bar{V}^{EL}}\right)_T \quad (3.127)$$

Rearranging the terms of Equation 3.126 it is possible to isolate $(\partial q_{ij}/\partial \bar{V}^{EL})_{T, N_w}$. This procedure enables us to rewrite the above equation as:

$$\Delta P^{H-EL} = -k_B T \sum_{i=1}^{n_{cage}} \sum_{j=1}^{n_{guest}} N_{ij} \left(\frac{1}{q_{ij}}\right) \left(\frac{N_w}{V^H}\right) \left(\frac{\partial q_{ij}}{\partial N_w}\right)_{T, V^H} \quad (3.128)$$

Eventually, the Equation 3.128 can be reorganized to a more convenient form, which is illustrated below by Equation 3.129.

$$\bar{V}^{EL} \Delta P^{H-EL} = -k_B T \sum_{i=1}^{n_{cage}} \sum_{j=1}^{n_{guest}} N_{ij} \left(\frac{\partial \ln q_{ij}}{\partial N_w}\right)_{T, V^H} \quad (3.129)$$

Therefore, comparing Equation 3.129 with the last term of Equation's 3.118 right-hand side, and changing k_B for R , $\Delta \mu_w^{H-EL}$ (in molar basis) can be described

by:

$$\Delta\mu_w^{H-EL} = RT \sum_{i=1}^{n_{cage}} \left[\nu_i \ln \left(1 - \sum_{j=1}^{n_{guest}} \theta_{ij} \right) \right] + \bar{V}^{EL} \Delta P^{H-EL} \quad (3.130)$$

Regarding the chemical potential difference between the pure water and the empty lattice phases, VAN DER WAALS and PLATTEEUW (1959) did not devise a statistical thermodynamics-based expression to estimate this variable. Hence, $\Delta\mu_w^{PW-EL}$ at a certain T and P is calculated from $\Delta\mu_w^{PW-EL}$ at a reference T_0 and P_0 ($\Delta\mu_{w,00}^{PW-EL}$) through classical thermodynamics.

The differential form of $(\Delta\mu_w^{PW-EL}/RT)$ is given by Equation 3.131.

$$d \left(\frac{\Delta\mu_w^{PW-EL}}{RT} \right) = \left[\frac{\partial}{\partial T} \left(\frac{\Delta\mu_w^{PW-EL}}{RT} \right) \right]_P dT + \left[\frac{\partial}{\partial P} \left(\frac{\Delta\mu_w^{PW-EL}}{RT} \right) \right]_T dP \quad (3.131)$$

From Van't Hoff's equation, we have:

$$- \left[\frac{\partial}{\partial T} \left(\frac{\Delta\bar{G}}{RT} \right) \right]_P = \frac{\Delta\bar{H}}{RT^2} \quad (3.132)$$

Moreover, from classical thermodynamics, it is known that:

$$\left[\frac{\partial}{\partial P} \left(\frac{\Delta\bar{G}}{RT} \right) \right]_T = \left[\frac{\partial}{\partial P} \left(\frac{\Delta\mu}{RT} \right) \right]_T = \frac{\Delta\bar{V}}{RT} \quad (3.133)$$

Using Equations 3.132 and 3.133, the integral form of Equation 3.131 can be written as a line integral – an integral in which the integrand is evaluated along a curve:

$$\int_{\mu_0(T_0, P_0)}^{\mu_f(T_f, P_f)} d \left(\frac{\Delta\bar{\mu}_w^{PW-EL}}{RT} \right) = \int_{T_0}^{T_f} \left[\frac{\partial}{\partial T} \left(\frac{\Delta\bar{\mu}_w^{PW-EL}}{RT} \right) \right]_P dT + \int_{P_0}^{P_f} \left[\frac{\partial}{\partial P} \left(\frac{\Delta\bar{\mu}_w^{PW-EL}}{RT} \right) \right]_T dP \quad (3.134)$$

$$\begin{aligned} \frac{\Delta\mu_w^{PW-EL}(T_f, P_f)}{RT_f} - \frac{\Delta\mu_w^{PW-EL}(T_0, P_0)}{RT_0} &= \int_{T_0}^{T_f} \left(-\frac{\Delta\bar{H}_w^{PW-EL}}{RT^2} \right)_P dT + \\ &+ \int_{P_0}^{P_f} \left(\frac{\Delta\bar{V}_w^{PW-EL}}{RT} \right)_T dP \end{aligned} \quad (3.135)$$

In phase equilibrium calculations, a $P \times T$ diagram is constructed through an algorithm whose convergence criterion is based on an alternative arrangement of Equation 3.117, as shown below.

$$\Delta\mu_w^{H-EL} + \Delta\mu_w^{EL-PW} = 0 \quad (3.136)$$

Where:

$$\Delta\mu_w^{EL-PW} = -\Delta\mu_w^{PW-EL} \quad (3.137)$$

Thus, the chemical potential difference between pure water and empty lattice states is preferably represented by $\Delta\mu_w^{EL-PW}$.

Via the Pshift model, SEGTOVICH *et al.* (2022) proposed a new hydrate and empty lattice pressure paradigm. As mentioned in Section 3.5, since these two phases are not in equilibrium, there are no restrictions concerning their pressures. Therefore, differently from HOLDER *et al.* (1980)'s proposition – displayed by Equation 2.2 – , in a phase transition whose final state is the empty lattice, the final pressure (P_f) is P^{EL} for \bar{V}_w^{EL} and P^H for \bar{V}_w^{PW} .

Therefore,

$$\begin{aligned} \Delta\mu_w^{EL-PW} &= RT_f \left[\frac{\Delta\mu_{w,00}^{EL-PW}}{RT_0} - \int_{T_0}^{T_f} \left(\frac{\Delta\bar{H}_w^{EL-PW}}{RT^2} \right)_{P_0} dT + \right. \\ &\left. + \int_{P_0}^{P^{EL}} \left(\frac{\bar{V}_w^{EL}}{RT} \right)_{T_f} dP - \int_{P_0}^{P^H} \left(\frac{\bar{V}_w^{PW}}{RT} \right)_{T_f} dP \right] \end{aligned} \quad (3.138)$$

Where $\Delta\bar{H}_w^{EL-PW}$ represent molar enthalpy of dissociation. Since it is impossible to measure the dissociation enthalpy directly, the same procedure used to derive an expression for $\Delta\mu_w^{EL-PW}$ will be applied here. From classical thermodynamics, we have:

$$\Delta\bar{H}_w^{EL-PW}(T_f, P_0) = \Delta\bar{H}_w^{EL-PW}(T_0, P_0) + \int_{T_0}^{T_f} \Delta\bar{C}_{P_w}^{EL-PW} dT \quad (3.139)$$

Where $\Delta\bar{H}_w^{EL-PW}(T_0, P_0)$ is the molar dissociation enthalpy at a reference state (T_0, P_0) – also designated by $\Delta\bar{H}_{w,00}^{EL-PW}$ –, and $\Delta\bar{C}_{P_w}^{EL-PW}$ represents the dissociation specific heat capacity. Here, the latter variable is fixed to a value that is assumed to be equal to the experimental $\Delta\bar{C}_{P_w,00}^{EL-PW}$ of actual hydrate in a given structure. Likewise, $\Delta\bar{H}_{w,00}^{EL-PW}$ is also expected to be close to experimental hydrate dissociation, while the actual value concerning the empty lattice is estimated from phase equilibrium data. Hence,

$$\Delta\bar{H}_w^{EL-PW}(T_f, P_0) = \Delta\bar{H}_{w,00}^{EL-PW} + \Delta\bar{C}_{P_w,00}^{EL-PW}(T_f - T_0) \quad (3.140)$$

In conclusion, Equation 3.138 can be rewritten as:

$$\frac{\Delta\mu_w^{EL-PW}}{RT_f} = \left\{ \frac{\Delta\mu_{w,00}^{EL-PW}}{RT_0} + \int_{P_0}^{P^{EL}} \left(\frac{\bar{V}_w^{EL}}{RT} \right)_{T_f} dP - \int_{P_0}^{P^H} \left(\frac{\bar{V}_w^{PW}}{RT} \right)_{T_f} dP - \int_{T_0}^{T_f} \left[\frac{\Delta\bar{H}_{w,00}^{EL-PW} + \Delta\bar{C}_{P_w,00}^{EL-PW}(T_f - T_0)}{RT^2} \right]_{P_0} dT \right\} \quad (3.141)$$

Depending on the temperature, \bar{V}_w^{PW} can either represent the liquid water molar volume (\bar{V}_w^{LW}) or the ice molar volume (\bar{V}_w^I). Similarly to the lattice molar volume, \bar{V}_w^{LW} and \bar{V}_w^I expressions – depicted by Equations 3.142 and 3.143, respectively – come from empirical correlations. On the other hand, since the pure water molar volume modeling has been exhaustively validated, its parameters do not require estimation.

$$\bar{V}_w^{LW} / (\text{m}^3 \text{mol}^{-1}) = \left[2.61517 \times 10^{-5} - 5.71157 \times 10^{-8} (T - T_0^{crystal}) + 1.00453 \times 10^{-10} (T - T_0^{crystal})^2 \right] \exp \left[3.30859 \times 10^{-10} (P - P_0^{crystal}) \right] \quad (3.142)$$

$$\begin{aligned} \bar{V}_w^I / (\text{m}^3 \text{mol}^{-1}) = & 1.912 \times 10^{-5} + 8.387 \times 10^{-10} (T - T_0^{crystal}) + \\ & + 4.016 \times 10^{-12} (T - T_0^{crystal})^2 \end{aligned} \quad (3.143)$$

The former correlation was reproduced from MEDEIROS (2018), while the latter was proposed by KLAUDA and SANDLER (2000).

For the model implementation, the volume correlations must be integrated in relation to pressure with the temperature fixed at T_f . However, since our program cannot perform symbolic calculations, these expressions were integrated separately, and the results were included in the algorithm later. Equations 3.144, 3.145 and 3.146 depict the outcome of the symbolic integration of Equations 3.114, 3.142 and 3.143, respectively.

$$\begin{aligned} \int_{P_0}^{P^{EL}} \left[\frac{\bar{V}_w^{EL}(T, P)}{RT} \right]_{T_f} dP = & \left[a_0^{uc} + \alpha_1(T_f - T_0^{crystal}) + \right. \\ & \left. + \alpha_2(T_f - T_0^{crystal})^2 + \alpha_3(T_f - T_0^{crystal})^3 \right]^3 \frac{10^{-30} N_A}{N_h^{uc} RT_f} \\ & \exp(\kappa_{hyd} P_0^{crystal}) \left(-\frac{1}{\kappa_{hyd}} \right) [\exp(-\kappa_{hyd} P^{EL}) - \exp(-\kappa_{hyd} P_0)] \end{aligned} \quad (3.144)$$

$$\begin{aligned} \int_{P_0}^{P^H} \left[\frac{\bar{V}_w^{LW}(T, P)}{RT} \right]_{T_f} dP = & \frac{1}{RT_f} \left[2.61517 \times 10^{-5} - 5.71157 \times \right. \\ & \left. 10^{-8} (T_f - T_0^{crystal}) + 1.00453 \times 10^{-10} (T_f - T_0^{crystal})^2 \right] \\ & \left[-\frac{\exp(\kappa_w P_0^{crystal})}{\kappa_w} \right] [\exp(-\kappa_w P^H) - \exp(-\kappa_w P_0)] \end{aligned} \quad (3.145)$$

$$\begin{aligned} \int_{P_0}^{P^H} \left[\frac{\bar{V}_w^I(T)}{RT} \right]_{T_f} dP = & \frac{(P^H - P_0)}{RT_f} \left[1.912 \times 10^{-5} + \right. \\ & \left. + 8.387 \times 10^{-10} (T_f - T_0^{crystal}) + 4.016 \times 10^{-12} (T_f - T_0^{crystal})^2 \right] \end{aligned} \quad (3.146)$$

where $\kappa_w =$, $T_0^{crystal} = 0$ K, and $P_0^{crystal} = 101\,325$ Pa.

Parameter estimation is required to adequate the model to the available experimental data properly. The details concerning the estimation of $\Delta\mu_{w,00}^{EL-PW}$, $\Delta\bar{H}_{w,00}^{EL-PW}$ and $\Delta\bar{C}_{P,w,00}^{EL-PW}$ will be discussed in the subsequent topics.

Chapter 4

Phase equilibrium calculation

Now that the modeling has been formally presented, this chapter unveils how the calculation was conducted. Even though the Pshift model was scrupulously examined in Chapter 3, some gaps must be filled before the exhibition of the results.

The present chapter has been divided into five sections, organized according to the calculation implementation sequence. Python was chosen to reproduce and validate the Pshift model because of its simplicity and dynamism.

4.1 Guest fugacity calculation

Hydrate-forming fluid phase modeling is one of the most fundamental aspects of hydrate phase equilibrium calculation. Since the guest molecules are usually light hydrocarbons, equations of state (EoS) are extensively used to model the phase to which they belong. Furthermore, as multiple guest species can be enclathrated within the same lattice, their fugacity is the most suitable property to express their contribution.

According to the literature, many EoS can estimate guest fugacity. In this context, BHAWANGIRKAR *et al.* (2018) investigate the influence of different EoS in hydrate phase equilibrium calculation. The authors compared the performance of three commonly used EoS: Peng-Robinson-Stryjek-Vera (PRSV), Patel-Teja (PT), and Soave-Redlich-Kwong (SRK). PARRISH and PRAUSNITZ (1972), for instance, chose a simpler course and resorted to the modified Redlich-Kwong (RK) EoS to compute guest fugacity. The guest fugacity calculation is executed in the undertaken study by implementing the Peng-Robinson (PR) equation.

As previously mentioned in Chapter 3, the mutual solubility between the liquid

water and the hydrate-forming fluid phase – either gas or liquid – is neglected. For that reason, the interaction between the polar and non-polar phases' molecules is not considered in the PVT calculations. Concerning the water molecules, its PVT behavior is modeled through empirical volume correlations corrected by the Poynting factor rather than the employment of an EoS. Therefore, the PR equation's renowned capability to predict light components' properties, added to its robustness and uncomplicated implementation, makes the model devised by Peng-Robinson the optimal choice.

4.2 Empty lattice pressure convergence and pressure shift calculation

The discussion disclosed in Section 3.5 attempted to present the main features of the pressure shift phenomenon. This topic aspires to address the numerical solution devised to calculate its associated variables.

At some point in Chapter 3 it has become evident that the pressure shift calculation (ΔP^{H-EL}) depended on the partial derivative of the Langmuir adsorption coefficients with respect to the lattice intensive volume ($\partial C_{ij}/\partial \bar{V}^{EL}$), and vice-versa. In this sense, SEGTOVICH *et al.* (2022) suggested that this loop problem should be resolved using an iterative method. As a solution, the authors thus proposed two functions: "calcPshift" and "convergePEL." The former takes temperature (T), empty lattice pressure (P^{EL}), and guest fugacity (\hat{f}_j) as input and calculates ΔP^{H-EL} .

Function calcPShift(T, P^{EL}, \hat{f}_j):

- $\bar{V}^{EL} \leftarrow$ Equation 3.114
- $R_i \leftarrow$ Equations 3.97 to 3.100
- $C_{ij} \leftarrow$ Equation 3.73
- $\theta_{ij} \leftarrow$ Equations 3.34 and 3.74
- $(\partial C_{ij}/\partial \bar{V}^{EL})_T \leftarrow$ Equations 3.101 to 3.111
- $\Delta P^{H-EL} \leftarrow$ Equation 3.95
- return** $\Delta P^{H-EL}, \underline{\theta}$

Nonetheless, since P^{EL} is unknown and depends on a recursive calculation, a numerical method must be implemented to estimate this variable. Therefore, the latter consists of an algorithm that receives T , P^H and \hat{f}_j as input and, through successive substitution, converges the ΔP^{H-EL} to obtain P^{EL} . In other words, the algorithms must be used simultaneously: more specifically, the "convergePEL"

algorithm makes a call recursively to the "calcPshift" function.

```

Function convergePEL( $T, P^H, \hat{f}_j$ ):
   $(\Delta P^{H-EL})_{[k]} \leftarrow 0$ 
  while abs(res) > tolerance do
     $P^{EL} \leftarrow P^H - (\Delta P^{H-EL})_{[k]}$ 
     $(\Delta P^{H-EL})_{[k+1]}, \underline{\theta} \leftarrow \text{calcPshift}(T, P^{EL}, \hat{f}_j)$ 
    res  $\leftarrow \left[ \frac{(\Delta P^{H-EL})_{[k+1]} - (\Delta P^{H-EL})_{[k]}}{P^H} \right]$ 
     $(\Delta P^{H-EL})_{[k]} \leftarrow (\Delta P^{H-EL})_{[k+1]}$ 
  end
  return  $P^{EL}, \underline{\theta}$ 

```

Even though VAN DER WAALS and PLATTEEUW (1959) have established T , V , N_h , and $\underline{\lambda}$ as independent variables, pressure is a much more convenient variable to determine, in many engineering applications, than volume. Hence, we specify the hydrate's pressure instead of its volume.

4.3 Phase equilibrium algorithm implementation

With all the hydrate equilibrium participant phases modeled, the phase coexistence problem can be resolved by employing a suitable numerical method. More specifically, a root-finding problem must be addressed in order to calculate the equilibrium properties.

In the undertaken study, we chose to specify the hydrate's pressure and light fluid-phase composition. By establishing the pressure value, and the fugacity provided by an EoS, the only remaining unknown variable is the temperature. Conceptually, this procedure can be illustrated by rewriting Equation 3.136 as

$$\text{Res}(T) = \Delta\mu_w^{H-EL}(T) + \Delta\mu_w^{EL-PW}(T) \quad (4.1)$$

where $\text{Res}(T)$ represents the residue function that indicates the present state's distance to the equilibrium. In other words, when $\text{Res}(T) = 0$, phase coexistence is reached. Therefore, to determine the equilibrium temperature, we need a one-dimensional solver capable of finding the temperature that serves as a root for Equation 4.1.

The function depicted below details the residue function computation.

```

Function calcRes( $T$ ,  $P^H$ ,  $y$ ):
   $\hat{f} \leftarrow$  Peng-Robinson ( $T$ ,  $P^H$ ,  $y$ )
   $P^{EL}$ ,  $\theta \leftarrow$  convergePEL ( $T$ ,  $P^H$ ,  $\hat{f}$ )
   $\bar{V}^{EL} \leftarrow \bar{V}^{EL}(T, P^{EL})$  [Equation 3.114]
   $\Delta\mu_w^{H-EL} \leftarrow \Delta\mu_w^{H-EL}(T, P^H, P^{EL}, \bar{V}^{EL}, \theta)$  [Equation 3.130]
  intVEL  $\leftarrow \int_{P_0}^{P^{EL}} \left[ \frac{\bar{V}_w^{EL}(T, P)}{RT} \right]_{T_f} dP$  [Equation 3.144]
  if  $T < 273$  K then
     $\bar{V}_w^{PW} \leftarrow \bar{V}_w^I(T)$  [Equation 3.143]
    intVI  $\leftarrow \int_{P_0}^{P^H} \left[ \frac{\bar{V}_w^I(T)}{RT} \right]_{T_f} dP$  [Equation 3.146]
     $\Delta\mu_w^{EL-PW} \leftarrow \Delta\mu_w^{EL-I}(T, P^H, P^{EL}, \text{intVEL}, \text{intVI})$  [Equation 3.141]
  else
     $\bar{V}_w^{PW} \leftarrow \bar{V}_w^{LW}(T, P)$  [Equation 3.142]
    intVLW  $\leftarrow \int_{P_0}^{P^H} \left[ \frac{\bar{V}_w^{LW}(T, P)}{RT} \right]_{T_f} dP$  [Equation 3.145]
     $\Delta\mu_w^{EL-PW} \leftarrow$ 
       $\Delta\mu_w^{EL-LW}(T, P^H, P^{EL}, \text{intVEL}, \text{intVLW})$  [Equation 3.141]
  end
  Res  $\leftarrow \Delta\mu_w^{H-EL} + \Delta\mu_w^{EL-PW}$ 
  return Res

```

Since both $\Delta\mu_w^{H-EL}$ and $\Delta\mu_w^{EL-PW}$ are functions of temperature implicitly, a numerical method must be implemented. We used the function "root" from the "optimize" package within the scientific library SciPy, which only requires an initial guess to find the equilibrium temperature.

One relevant aspect of hydrate phase equilibrium calculations is that the host's crystalline structure configuration must be previously defined. Otherwise, there would be ambiguity in selecting the appropriate set of parameters. On the one hand, in single hydrate phase equilibrium computations, guessing the most thermodynamically stable configuration is relatively straightforward. On the other hand, this process can be pretty complicated for mixed hydrates since we do not know beforehand the most stable lattice configuration for clathrates with multi-component guests. In this context, PARRISH and PRAUSNITZ (1972) presented an algorithm that eliminates this speculation.

In summary, the PARRISH and PRAUSNITZ (1972)'s methodology consists of calculating the dissociation pressure using the parameters' sets of sI and sII structures – after checking that both are possible – and comparing the results for the two structures. The configuration that presents the lower dissociation pressure is considered the most thermodynamically stable structure for the analyzed conditions. In

other words, for a given temperature and composition, the configuration that yields the lowest dissociation pressure is the most stable.

After calculating the equilibrium temperature for both sI and sII structures, the PARRISH and PRAUSNITZ (1972)'s computational algorithm was employed to determine the most stable configuration under the given conditions. It is worth mentioning that the adopted procedure to implement this algorithm is distinctive from the original. Since we decided to compute the equilibrium temperature rather than pressure, the PARRISH and PRAUSNITZ (1972)'s pressure-based criterion does not apply to our study. Alternatively, the preferred strategy was to define the most stable structure by taking the highest equilibrium temperature. This procedure is illustrated in Figure 4.1 that shows a $P \times T$ diagram for two different equilibria for a water/methane/ethane system:

- Water - sI Hydrate - vapor with molar composition: 0.95 methane/0.05 ethane;
- Water - sII Hydrate - vapor with molar composition: 0.95 methane/0.05 ethane.

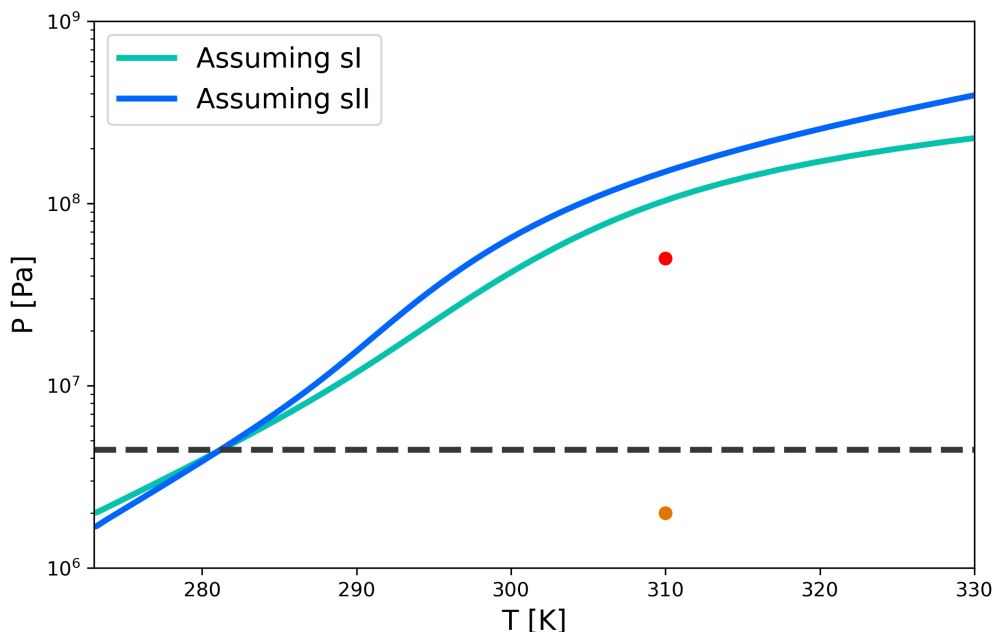


Figure 4.1: Phase equilibrium prediction for a CH₄ (0.95 mol) + C₂H₆ (0.05 mol) hydrate. The solid green line represents the equilibrium curve assuming sI structure for the hydrate, whereas the solid blue line represents the equilibrium curve assuming sII structure for the hydrate. The dashed grey line indicates the limit pressure where the hydrate's most stable configuration changes, i.e., the structural transition point.

In order to explain the reasoning behind this method, two arbitrary points at $T = 310$ K have been drawn: a red one (high pressure) and an orange one (moderate

pressure). Starting from a hypothetical system located at the orange mark, which was submitted to an isobaric cooling, the diagram depicted in Figure 4.1 shows us that an sII hydrate should occur when T is approximately 275 K. With further cooling at constant pressure, all the liquid water is converted into sII hydrate. Now the system is composed of an equilibrium between the sII hydrate and the remaining vapor. It is believed that further isobaric cooling would not produce an sI hydrate phase since the sII configuration is the most stable in this region. This procedure corroborates with PARRISH and PRAUSNITZ (1972) original approach since, for temperatures below 281 K, the sII structure curve presents lower pressure values when compared to the sI curve at the same temperature.

Similarly, taking the red mark as the hypothetical initial stage of the isobaric cooling process, according to the diagram mentioned above, an sI hydrate phase should occur near $T = 300$ K. The sII structure that would supposedly appear with further cooling is a meta-stable one at best. Once more, the same result would be obtained if the original algorithm were to be used, as sI configuration hydrates present a lower equilibrium pressure when compared to sII hydrates at the same temperature.

4.4 The Interstitial model

As aforementioned, one of this work's goals is to validate and improve SEGTOVICH *et al.* (2022)'s approach to sII hydrate formation prediction. However, since there is no data in the literature concerning the Pshift model parameters for sII hydrates, another approach was used to generate the necessary data to validate the Pshift model. In the undertaken study, the selected approach is the one devised by KLAUDA and SANDLER (2000), also called the Interstitial model. Even though their model is not the most sophisticated, it is thermodynamically consistent and uncomplicated to implement. On account of its qualities, the Interstitial model was chosen as a preliminary work to aid in the Pshift model parameter optimization and to serve as a reliable fallback option when the Pshift model fails to converge. The Interstitial model can be used in the simulation for a reasonable range of conditions.

The Interstitial model implementation is similar to the Pshift approach, with a few variations. On the one hand, like SEGTOVICH *et al.* (2022), KLAUDA and SANDLER (2000) acknowledged the lattice compressibility. On the other hand, the latter authors assumed constant cage radii, and their model did not contemplate the Langmuir coefficient variation concerning the lattice volume. Hence, the Interstitial model recognizes the lattice compressibility - thus predicting the retrograde

behavior at high pressures - but fails to foresee the effect of guest adsorption on the hydrate volume. In this context, the KLAUDA and SANDLER (2000)'s approach is implemented with some modifications.

Mathematically, the hypotheses assumed by KLAUDA and SANDLER (2000) can be translated to:

$$\left(\frac{\partial C_{ij}}{\partial \bar{V}^{EL}} \right)_T = 0 \quad (4.2)$$

Therefore, tracing a parallel with the Pshift model methodology, we have that:

$$\Delta P^{H-EL} = k_B T \sum_{i=1}^{n_{cage}} \sum_{j=1}^{n_{guest}} \nu_i \theta_{ij} \left[\frac{\partial (\ln C_{ij})}{\partial \bar{V}^{EL}} \right]_T = 0 \quad (4.3)$$

As illustrated in Equation 4.3, for the Interstitial model implementation, the empty lattice pressure is assumed to be the same as the hydrate pressure. In other words, the algorithms "calcPshift" and "convergePEL" are bypassed. Consequently, the implementation of the equivalent to KLAUDA and SANDLER (2000)'s approach is much more straightforward and has a lower computational cost when compared to the Pshift model. Furthermore, its parameters can be, to some extent, helpful in validating the Pshift model parameter estimation methodology.

4.5 Parameter estimation and experimental data

Following the procedure used by SEGTOVICH *et al.* (2022), which is an adaptation of the methodology introduced by MEDEIROS (2018), a parameterization was carried out to adjust the model to the experimental data associated with sII hydrates.

4.5.1 Maximum likelihood method

Prior to presenting the parameterization methodology, it is essential to discuss some aspects of the technique used to adjust the model to the experimental data: the maximum likelihood method.

As further explained in the following sections, parameter tuning is carried out via objective function minimization in the present work. In this sense, it is necessary to formulate objective functions compatible with the modeling and the experimental

data set available in the literature.

The least squares method is a prominent technique on which objective functions are based because of its simplicity and effectiveness when employed to parameterize linear models regarding the parameters (SCHWAAB and PINTO, 2007). The implementation of this approach to define an objective function results in the expression portrayed by Equation 4.4.

$$F_{obj} = \sum_{k=1}^{n_{exp}} [y_k^e - y_k^m(x_k, \underline{\alpha})]^2 \quad (4.4)$$

Where y is an arbitrary dependent variable; the superscripts indicate the variable's nature: e for experimental, and m for values obtained from the model; x represents an arbitrary independent variable; $\underline{\alpha}$ represents the parameters vector of the model.

Nevertheless, in consonance with SCHWAAB and PINTO (2007), the least squares function is somewhat limited since it considers that all variables are measured with the same accuracy regardless of the experimental conditions, which is an inadequate generalization. Not only the equipment performance substantially influences the measurement errors, but also the measurement of the variables can be co-dependent. In this context, still according to the authors, it is possible to weigh these features by implementing the maximum likelihood method.

Fundamentally, the maximum likelihood method is guided by three assumptions:

1. the experimental deviations distributions within the experimentation region are known;
2. the perfect model hypothesis is valid;
3. the experiments are considered to be well-administered.

A consequence of the second assumption is that the model is perfectly capable of reproducing the experimental data. Nonetheless, each parameter set yields a different curve. Thus, our goal is to find the parameter set that maximizes the probability of reproducing the experimental data through modeling. By maximizing the data probability, we maximize the likelihood of a curve.

According to SCHWAAB and PINTO (2007), as a result of the third assumption, it is reasonable to assume that the experimental data must be located within

the region of maximum probability. Therefore, to find the optimal parameters, the parameter estimation problem must be defined by the maximization of the function, which describes the probability of finding the obtained experimental data. If the experimental deviations are submitted to a normal probability distribution and independent, this function is illustrated by Equation 4.5.

$$\wp(z^e; z, V_z) = \frac{1}{\sqrt{(2\pi)^n \det(V_z)}} \exp \left[-\frac{1}{2} (z - z^e)^T V_z^{-1} (z - z^e) \right] \quad (4.5)$$

Where \wp represents the probability of finding the obtained experimental data (z^e), z is a vector that contains the dependent (x) and independent (y) variables, and V_z is a diagonal matrix that contains the variance of the experimental errors.

As mentioned before, z is a vector containing independent and dependent variables. Assuming that the measurements of both types of variables are not correlated, we have:

$$\wp(z^e; z, V_z) = \prod_{k=1}^{n_{exp}} [\wp_{x,k}(x_k^e; x_k, V_{x,k}) \wp_{y,k}(y_k^e; y_k, V_{y,k})] \quad (4.6)$$

$$\wp(z^e; z, V_z) = \prod_{k=1}^{n_{exp}} \left\{ \frac{1}{\sqrt{2\pi \det(V_{x,k})}} \exp \left[-\frac{1}{2} (x_k^e - x_k)^T V_{x,k}^{-1} (x_k^e - x_k) \right] \right. \\ \left. \frac{1}{\sqrt{2\pi \det(V_{y,k})}} \exp \left[-\frac{1}{2} (y_k^e - y_k)^T V_{y,k}^{-1} (y_k^e - y_k) \right] \right\} \quad (4.7)$$

It is worth highlighting that the difference between the value obtained experimentally and the one provided by the model is simply the experimental error. According to SCHWAAB and PINTO (2007), it is reasonable to assume that the values of the independent variables are known with good accuracy, which enables us to infer that $(x^e - x) \approx 0$. In other words, the experimental error for the independent variable is negligible. By applying this reasoning on Equation 4.8, we have:

$$\wp(z^e; z, V_z) = \prod_{k=1}^{n_{exp}} \left\{ \frac{1}{\sqrt{2\pi \det(V_{y,k})}} \exp \left[-\frac{1}{2} (y_k^e - y_k)^T V_{y,k}^{-1} (y_k^e - y_k) \right] \right\} \quad (4.8)$$

Since V_y is a diagonal matrix, its determinant is the product of the diagonal elements. In addition, the term within the exponential results in:

$$(y_k - y^e)^T V_{y,k}^{-1} (y_k - y_k^e) = \frac{(y_k - y_k^e)^2}{V_{y,kk}} \quad (4.9)$$

Hence, Equation 4.5 can be rewritten as:

$$\varphi(z^e; z, V_z) = \prod_{k=1}^{n_{exp}} \left[\frac{1}{\sqrt{2\pi V_{y,kk}}} \exp \left[-\frac{1}{2} \frac{(y_k - y_k^e)^2}{V_{y,kk}} \right] \right] \quad (4.10)$$

Equation 4.10 illustrates the form of the probability function, which is maximized in the parameterization procedure of the maximum likelihood method. However, some algebraic manipulation is necessary to optimize this function maximization.

It is known that the maximum point of the function φ is the same as the maximum point of $\ln \varphi$, as the latter is a monotonic ascending function of the former. Thus, to maximize $\ln \varphi$ is the same as maximizing φ , and vice-versa. In addition, finding the point of maximum of a function is equivalent to calculating the minimum point of the same function multiplied by -1. Mathematically, these manipulations can be represented by:

$$\max(\varphi) = \max(\ln \varphi) = \min[-\ln(\varphi)] \quad (4.11)$$

Now we can rewrite Equation 4.10 as:

$$-\ln(\varphi) = -\sum_{k=1}^{n_{exp}} \left\{ \ln \left[\frac{1}{\sqrt{2\pi V_{y,kk}}} \exp \left(-\frac{1}{2} \frac{(y_k - y_k^e)^2}{V_{y,kk}} \right) \right] \right\} \quad (4.12)$$

$$-\ln(\varphi) = -\sum_{k=1}^{n_{exp}} \left\{ \ln \left(\frac{1}{\sqrt{2\pi V_{y,kk}}} \right) + \ln \left[\exp \left(-\frac{1}{2} \frac{(y_k - y_k^e)^2}{V_{y,kk}} \right) \right] \right\} \quad (4.13)$$

$$-\ln(\varphi) = -\sum_{k=1}^{n_{exp}} \left[-\frac{1}{2} \ln(2\pi V_{y,kk}) - \frac{1}{2} \frac{(y_k - y_k^e)^2}{V_{y,kk}} \right] \quad (4.14)$$

Another important realization is that the multiplication or division of φ by any constant would not alter the function's maximum (or minimum) point location. By eliminating the constants (for simplicity) and, Equation 4.14 becomes:

$$-\ln(\varphi) = \sum_{k=1}^{n_{exp}} \left[\ln(V_{y,kk}) + \frac{(y_k - y_k^e)^2}{V_{y,kk}} \right] \quad (4.15)$$

Assuming constant variance regarding the dependent variable measurement, we have:

$$-\ln(\varphi) = \sum_{k=1}^{n_{exp}} \ln(V_y) + \sum_{k=1}^{n_{exp}} \left[\frac{(y_k - y_k^e)^2}{V_y} \right] \quad (4.16)$$

$$-\ln(\varphi) = n \ln(V_y) + \sum_{k=1}^{n_{exp}} \left[\frac{(y_k - y_k^e)^2}{V_y} \right] \quad (4.17)$$

Where n is the number of experiments related to variable y .

The first term from the right-hand side of Equation 4.17 is a constant. Therefore, searching for the minimum point of $(-\ln \varphi)$ above is equivalent to searching for the minimum point of the following expression.

$$Fobj = -\ln(\varphi) = \sum_{k=1}^{n_{exp}} \left[\frac{(y_k - y_k^e)^2}{V_y} \right] \quad (4.18)$$

Equation 4.18 is an objective function that can be used to estimate a model's optimal parameters when the maximum likelihood method is applied. Customarily, this function is referred to as the weighted least squares function. In agreement with SCHWAAB and PINTO (2007), this function is the natural approach when the experimental deviations are normally distributed.

In the present work, we intend to use a variation of the Equation 4.18 to estimate the optimal parameters of the Interstitial model. However, the reasoning presented so far concerns a generic minimization problem. The independent variable (x) must be associated with the system's pressure (P) and the dependent variable (y) with the system's temperature (T) to represent the minimization problem prescribed by the thermodynamic modeling adequately.

Furthermore, since the parameterization of the Interstitial model is performed with data reconciliation, we should disregard the previous hypothesis, which stated that the experimental deviation associated with the independent value was negligible, i.e., $(x^e - x) \neq 0$. By doing so, the objective function employed to optimize the Interstitial model's parameters is given by Equation 4.19.

$$\text{Fobj} = n \ln (V_y) + \sum_{k=1}^{n_{exp}} \left[\frac{(y_k - y_k^e)^2}{V_y} \right] + n \ln (V_x) + \sum_{k=1}^{n_{exp}} \left[\frac{(x_k - x_k^e)^2}{V_x} \right] \quad (4.19)$$

After substituting the generic variables for their equivalent and doing some algebraic manipulations, Equation 4.19 turns into Equation 4.20, depicted below. In the current approach, the terms $\ln V_x$ and $\ln V_y$ are not constant; rather, the variances are inferred from the available data along with the parameters.

$$\text{Fobj} = n \ln (V_T) + \sum_{k=1}^{n_{exp}} \left[\frac{(T_k^m - T_k^e)^2}{\exp(\ln V_T)} \right] + n \ln (V_P) + \sum_{k=1}^{n_{exp}} \left[\frac{(P_k^m - P_k^e)^2}{\exp(\ln V_P)} \right] \quad (4.20)$$

Finally, Equation 4.20 illustrates the expression used to solve the maximum likelihood problem with data reconciliation and variance inference so that the Interstitial model's optimal parameters are estimated.

4.5.2 Estimated parameters

This section scrutinizes the parameters that took part in the parameterization process. In other words, here we present the parameters for sII hydrate promoting guests and formation properties, as well as volumetric parameters for sII hydrates.

Since many parameters (around 10) needed to be optimized, we sorted them into four categories to facilitate the implementation of the parameterization methodology. The first set contains the Kihara pair interaction potential parameters, which solely depend on the nature of the guest species since the host is always the same throughout the present research: water. The next set consists of the parameters associated with hydrate dissociation, i.e., transition lattice-liquid, which is used to calculate phase equilibrium. The third group comprehends the parameters that characterize the crystalline structure of the hydrate. Finally, the last category contains the estimated parameters in the data reconciliation procedure, that is, reconciled pressure values (\underline{P}^m), discussed in the following paragraph. In addition, the variances associated with pressure and temperature measurements – V_P and V_T , respectively – were included in the parameter estimation because there was no information in the literature about the experimental data standard deviation for any equilibrium experiment.

Furthermore, since we intend to perform a data reconciliation along with the

parameterization, we also incorporated the pressure values estimated as a parameter in the maximum likelihood approach, which corresponds to the pressure at which the experiment occurred, and which is used in the model to calculate the equilibrium temperature $T^m(P^m)$ at given model parameters. For a guest j , there are as many P_j^m parameters as experimental points available in the literature. Table 4.1 illustrates these categories and its parameters.

As it can be seen from Table 4.1, the volumetric and equilibrium data from propane and isobutane hydrates were used to perform the parameter regression computations. These compounds were selected not only because they form sII hydrates – when pure – but also due to their greater data availability than other sII-hydrate-forming species.

As explained in Section 3.4, our approach is to describe guest-host interaction through the Kihara potential. However, MEDEIROS (2018) reported that the strong correlation between the parameters a, σ and ε significantly interferes in parameter estimation, producing unsatisfactory results. Therefore, although all the expressions in the section mentioned above have been derived for the Kihara potential, we decided to fix the hard-core parameters of the Kihara potential to zero, which means that the potential effectively used in this work was the Lennard-Jones potential – following the adopted procedure by the authors. Furthermore, it should be noted that the cavities compressibility (κ_R) parameter optimization was managed through its logarithmic form. This strategy was adopted to prevent negative estimation results associated with this variable, which could produce numerical issues within the model.

In addition, it is also worth highlighting that, although there is a decent number of experimental measurements of other pure sII clathrates, such as oxygen and nitrogen hydrates, the current model is not suitable to represent that data. In virtue of the N_2 molecular size, sII hydrates that contain it as a guest often have their large cavities occupied by two N_2 molecules – especially at high pressures –, which characterize the double occupancy phenomenon. This was proved by KUHS *et al.* (1997), who also recognized that the same behavior could be expected for oxygen molecules (RASOOLZADEH and SHARIATI, 2016). The double occupancy phenomenon substantially impacts hydrate phase equilibrium prediction since its consideration conflicts with one of the vdWP model’s fundamental assumptions: "each cage can only host one guest molecule." Moreover, since the double occupancy phenomenon is significant for O_2 and N_2 hydrates at high pressures according to RASOOLZADEH and SHARIATI (2016), we should consider it when analyzing the results generated by the Pshift model, which follows the same premise that the vdWP model does. To summarize, because of the substantial possibility of the

double occupation phenomenon occurrence and the Pshift model’s deficiency in predicting it, we did not use the available experimental data of N₂ and O₂ hydrates. The same criterion discarded argon and krypton pure hydrates’ experimental data.

Table 4.1: List of estimated parameters.

Parameter List		
Guest-dependent parameters	Propane (c3)	σ_{c3}
		ε_{c3}/k_B
	Isobutane (ic4)	σ_{ic4}
		ε_{ic4}/k_B
Dissociation parameters	$\Delta\mu_{w,00}^{EL-PW}$	
	$\Delta\bar{H}_{w,00}^{EL-PW}$	
Lattice parameters	a_0^{uc}	
	$\ln(\kappa_{R,small})$	
	$\ln(\kappa_{R,large})$	
Reconciliation parameters	$\ln(V_P)$	
	$\ln(V_T)$	
	\underline{P}_{-c3}^m	
	\underline{P}_{-ic4}^m	

It is worth mentioning that sI hydrates parameter regression is not within this dissertation’s scope. Kihara parameters for methane, ethane, and xenon, as well as formation properties for the sI structure and volumetric properties for the sI empty lattice, are available in SEGTOVICH *et al.* (2022).

4.5.3 Experimental data

In order to propose a practical parameter estimation procedure, we have categorized the experimental data according to the measured properties. The experiments were divided into two broad groups: those that measure the unit cell edge length at a fixed temperature or pressure – henceforth called volumetric experiments – and those that provide a set of equilibrium pressure and temperature – henceforth called equilibrium experiments. Regarding the former data set, we gathered the volumetric data from propane and isobutane hydrates, further subdivided into two subsets: isothermal and isobaric data. Propane and isobutane hydrates equilibrium data were compiled from the literature for the latter data set.

Table 4.2 shows the data sets used in the calculation along with their availability, number of experiments, and reference.

Table 4.2: List of data sets used in the optimization.

Comp.	Data sets	Availability	Number of experiments	References
C3	Equilibrium data	Yes	94	NIST
	Isothermal data	Yes	1	KOH <i>et al.</i> (1996)
	Isobaric data	Yes	4	BELOSLUDOV <i>et al.</i> (2002) KIRCHNER <i>et al.</i> (2004) HESTER <i>et al.</i> (2007)
iC4	Equilibrium data	Yes	59	NIST
	Isothermal data	No	-	-
	Isobaric data	No	-	-

4.5.4 Parameter optimization methodology

The preferred approach to carry out the parameter optimization in this work was through the minimization of objective functions, which were designed in consonance with the parameters' characteristics, the thermodynamic models, and current algorithm robustness regarding convergence. We developed a more statistically complete parameter estimation method for the simplest model, whereas more straightforward objective functions were devised for the most sophisticated model. Therefore, the adopted strategy consisted of regressing the Interstitial model parameters using a more complex and robust methodology, whose results would later serve as initial guesses to the – much simpler – Pshift model parameterization. Both methodologies are scrutinized in the upcoming subsections.

4.5.4.1 Interstitial model parameterization

For the Interstitial model parameterization, no parameter estimation was performed concerning the lattice parameters; those were taken from the KLAUDA and SANDLER (2000)'s empty lattice volume correlation. The authors' a_0^{uc} , $\underline{\alpha}$ and κ_{hyd} were used as input for the equilibrium parameters optimization. It is worth mentioning that, since the Interstitial model (KLAUDA and SANDLER, 2000) does not predict a compressible lattice cavity, κ_R is zero for both cages.

With the a_0^{uc} , $\underline{\alpha}$ and κ_{hyd} provided by KLAUDA and SANDLER (2000), the parameters related to the equilibrium experimental data were regressed in two steps, with different parameter sets being optimized in each stage. Firstly, a heuristic op-

timization method was employed to minimize a preliminary equilibrium adjustment objective function. Its outcome served as an initial guess for a second step, which consists of minimizing an objective function of weighted least-squares – derived from the maximum likelihood method (SCHWAAB and PINTO, 2007) – with data reconciliation. The former objective function is illustrated by the Equation 4.21, whereas the latter, by the Equation 4.22, henceforth referred as "Fobj_1" and "Fobj_2", respectively.

$$\begin{aligned} \text{Fobj_1}_j^{eq} = \sum_{k=1}^{n_{exp}} \left[\Delta\mu_{w,k}^{H-EL} \left(T_k^{exp}, P_k^{exp}, \sigma_j, \frac{\varepsilon_j}{k_B}, a_0^{uc}, \kappa_{hyd}, \ln \underline{\kappa}_R \right) + \right. \\ \left. + \Delta\mu_{w,k}^{EL-PW} \left(T_k^{exp}, P_k^{exp}, \Delta\mu_{w,00}^{EL-PW}, \Delta\bar{H}_{w,00}^{EL-PW} \right) \right]^2 \quad (4.21) \\ \forall \quad j = c3, ic4 \end{aligned}$$

Where n_{exp} is the number of experiments. Inside the parenthesis are highlighted the input temperature and pressure followed by the optimizable parameters.

$$\begin{aligned} \text{Fobj_2}_j^{eq} = \sum_{k=1}^{n_{exp}} \left\{ \frac{[T_k^m(P_k^m) - T_k^{exp}]^2}{\exp(\ln V_T)} \right\} + n_{exp} (\ln V_T) + \\ + \sum_{k=1}^{n_{exp}} \left[\frac{(P_k^m - P_k^{exp})^2}{\exp(\ln V_P)} \right] + n_{exp} (\ln V_P) \quad \forall \quad j = c3, ic4 \end{aligned} \quad (4.22)$$

As explained in Section 4.5.1, the implementation of Fobj_2 allows us to contemplate the measurement inaccuracy inherent to every experimental practice in the parameter estimation. Through this technique, we have adjusted the measured temperature and pressure.

Our phase equilibrium algorithm was designed to generate an equilibrium temperature from a specified pressure. Thus, the measured equilibrium temperature after reconciliation (\underline{T}^m) is calculated with the routines presented in Sections 4.2 and 4.3, using \underline{P}^m as input. In other words, \underline{P}^m is an independent variable, and \underline{T}^m is a dependent one.

All the sII hydrates' shared parameters are estimated by minimizing a global objective function, which is the sum of the guest-specific objective functions. In this manner, no data set is prioritized. The global objective function is presented by Equation 4.23.

$$\text{Fobj}_{global}^{eq} = \text{Fobj}_{c3}^{eq} + \text{Fobj}_{ic4}^{eq} \quad (4.23)$$

Using this notation, $\text{Fobj}_{1_{global}}^{eq}$ means Fobj_{c3}^{eq} and Fobj_{ic4}^{eq} are both of the Fobj_{1} kind; and $\text{Fobj}_{2_{global}}^{eq}$ means they are both of the Fobj_{2} kind.

About the optimization techniques, Fobj_{1} was minimized through the implementation of the particle swarm optimization (PSO) method, while Fobj_{2} was minimized by using the Nelder-Mead technique, a direct search method that is commonly called downhill simplex method. Table 4.3 summarizes the optimization parameters used in both methods.

Table 4.3: Optimization parameters.

Method	Parameter	Value
Nelder-Mead	Tolerance	1e-9
	Number of particles	10
PSO	Number of generations	1000

The algorithm below explains how the Interstitial model parameterization methodology was implemented.

1. Estimate σ_j , ε_j/k_B , $\Delta\mu_{w,00}^{EL-PW}$, and $\Delta\bar{H}_{w,00}^{EL-PW}$ for $j = c3, ic4$ by minimizing $\text{Fobj}_{1_{global}}^{eq}$ via PSO.
2. Estimate σ_j , ε_j/k_B , $\Delta\mu_{w,00}^{EL-PW}$, and $\Delta\bar{H}_{w,00}^{EL-PW}$ for $j = c3, ic4$ by minimizing $\text{Fobj}_{2_{global}}^{eq}$ via Simplex.
- 3a. Estimate \underline{P}_{c3}^m , $\ln V_T$, and $\ln V_P$ by minimizing $\text{Fobj}_{2_{c3}}^{eq}$ via Simplex.
- 3b. Estimate \underline{P}_{ic4}^m , $\ln V_T$, and $\ln V_P$ by minimizing $\text{Fobj}_{2_{ic4}}^{eq}$ via Simplex.
4. If necessary, return to step 2 until convergence.

In the first step, guest-dependent and dissociation parameters were regressed against the equilibrium experimental data by minimizing the so-called preliminary equilibrium adjustment objective function using the PSO method. Despite its empirical nature, the implementation of Equation 4.21 allows us to estimate the parameters at the thermodynamic equilibrium without running the equilibrium algorithm for each experiment. Since this step's goal consists of finding a good initial guess for the next stage, we were not overly concerned about its accuracy.

In the second step of the parameterization, guest-dependent and dissociation parameters were estimated by minimizing the maximum likelihood objective functions using the preliminarily estimated parameters in the first step as initial guesses.

Noticeably, this step of the Interstitial model parameterization is considerably more robust than the previous since Fobj_2 is based on statistical principles. In virtue of the high number of parameters involved within this stage, the parameterization was performed iteratively to reduce the computational cost of estimating multiple parameters simultaneously. Hence, not all parameters are optimized at once: while some are regressed, the other portion remains at a fixed value.

Afterward, the experimental data were reconciled through the Fobj_2 minimization. It should be emphasized that steps 3a and 3b are independent, so their execution order does not matter. However, the number of parameters involved in this step is so great that it was necessary to subdivide this step into two sub-steps: one dedicated to reconciling the experimental equilibrium pressure values for propane hydrate and the other for the isobutane hydrate. Since these substeps are not correlated, as explained above, 3a and 3b are interchangeable.

After some parameters subsets estimation cycles, the parameters' values converged, and the procedure was terminated.

The flowchart displayed by Figure 4.2 resumes the method purported above.

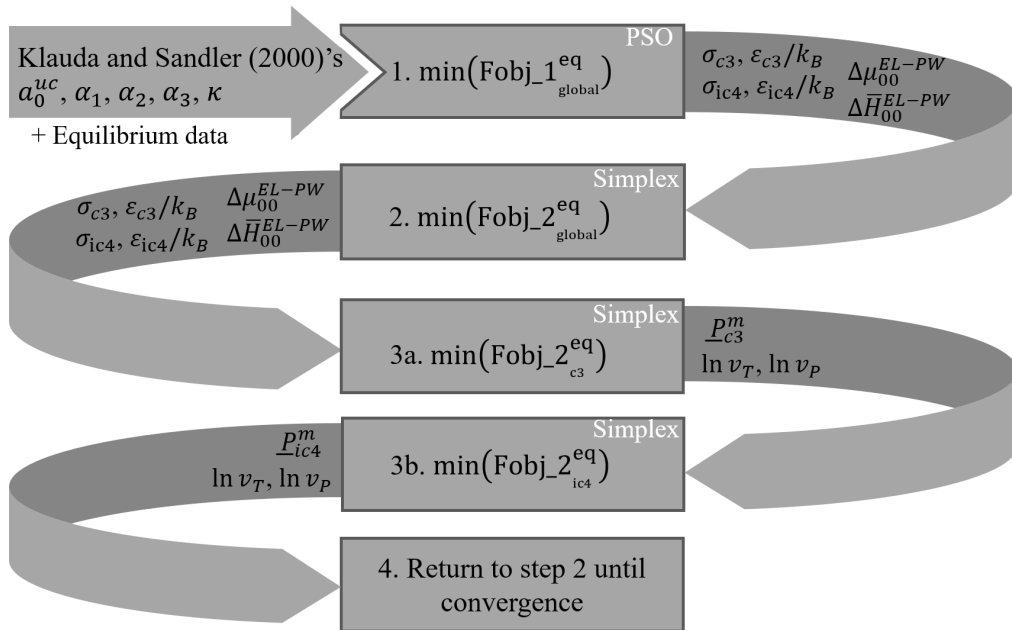


Figure 4.2: Interstitial model parameter estimation methodology flowchart.

4.5.4.2 Pshift model parameterization

Optimizing the Pshift model's parameters is more straightforward than the implemented methodology to adjust the Interstitial model to the experimental data. On account of the intrinsic difficulty of converging the algorithm that calculates

the pressure shift, the objective function based on the maximum likelihood method application would cost a substantial computational effort. In this sense, for the Pshift model parameterization, we have regressed the guest-dependent and dissociation parameters against the experimental data by minimizing only Fobj_1 using the Nelder-Mead optimization method. No data reconciliation was performed here, thus:

$$\underline{P}_j^m = \underline{P}_j^{exp} \quad \forall \quad j = c3, ic4 \quad (4.24)$$

Analogous to the Interstitial model parameterization methodology, the KLAUDA and SANDLER (2000)'s empty lattice volume correlation was used. However, instead of incorporating the all the parameters provided by the authors, a_0^{uc} was estimated, as well as $\ln(\kappa_{R,small})$ and $\ln(\kappa_{R,large})$. The rest of the lattice parameters remained fixed.

It should be mentioned that KLAUDA and SANDLER (2000)'s empty lattice data was not the only one used to perform the lattice parameters estimation. Instead, we have indirectly used the data provided by BELOSLUDOV *et al.* (2002). Figure 4.3 illustrates the diagram presented by the author for the sII empty lattice and propane hydrate.

From Figure 4.3, it is possible to observe a considerable divergence between the simulated volume for a propane hydrate and the experimental data. Thus, we have chosen not to work with the empty lattice simulated volume provided by the BELOSLUDOV *et al.* (2002), but to use the difference between the simulated propane hydrate and the empty lattice unit cell edges – referred to as Δa in Figure 4.3 – to estimate an optimal value for a_0^{uc} empirically.

Even though the Pshift model parameterization does not comprehend more than one type of objective function, the Fobj_1 minimization was achieved step-by-step, using the Interstitial model's optimal parameters as initial guesses and attending the following procedure (which is illustrated by Figure 4.4):

1. Estimate a_0^{uc} empirically;
2. estimate σ_j , ε_j/k_B , $\Delta\mu_{w,00}^{EL-PW}$, and $\Delta\bar{H}_{w,00}^{EL-PW}$ for $j = c3, ic4$;
3. estimate $\ln(\kappa_{R,small})$;
4. estimate $\ln(\kappa_{R,large})$;
5. if necessary, return to step 2 until convergence.

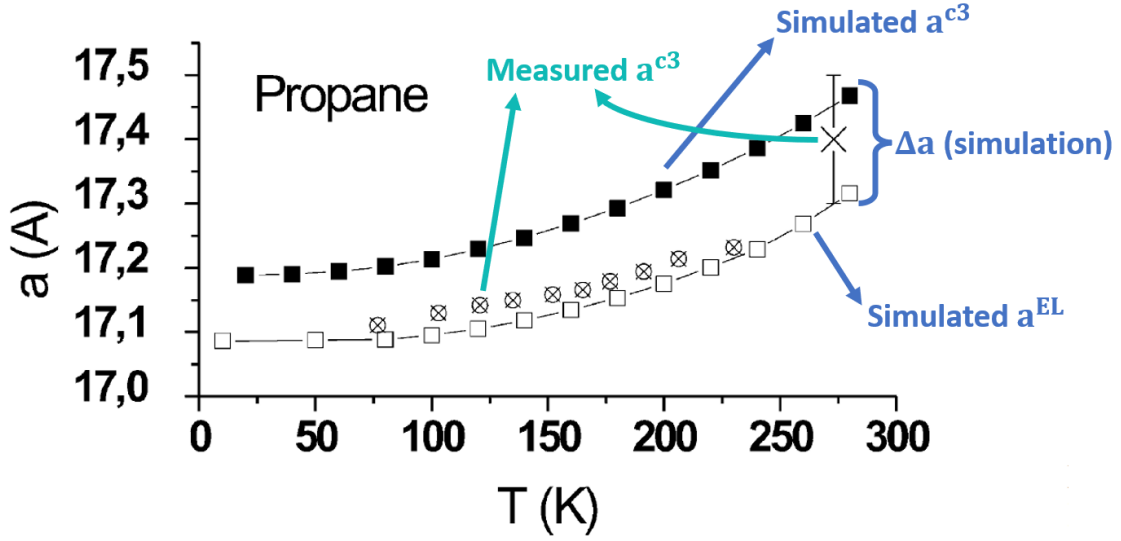


Figure 4.3: Unit cell parameter for sII hydrate of propane and empty lattice of structure sII at fixed atmospheric pressure. The blue arrows highlight BELOSLUDOV *et al.* (2002)’s simulation results: the solid black squares represent the simulated cell parameter for the propane hydrate, and the white squares depict the simulated empty lattice for structure sII. The green arrows point out the experimental data found in the literature by BELOSLUDOV *et al.* (2002). Adapted from BELOSLUDOV *et al.* (2002).

The first step consisted of estimating the optimal value for a_0^{uc} by indirectly using the volumetric data provided by BELOSLUDOV *et al.* (2002). In this manner, we have implemented a more empirical optimization methodology, that comprised of testing values for a_0^{uc} between 17.13 Å – figure provided by KLAUDA and SANDLER (2000) – and 17.03 Å – which is, approximately, 17.13 Å minus the unit cell edge difference ($\Delta a \approx 0.1$ Å) taken from Figure 4.3.

It is worth mentioning that the cage radii obtained experimentally in standard conditions (\underline{R}_0) varied along with a_0^{uc} during this empirical estimation procedure. For the a_0^{uc} estimation, it is desired to maintain \underline{f}_0 , which is the ratio between \underline{R}_0 and a_0^{uc} . In other words, we applied a simple rule of three to modify \underline{R}_0 . To illustrate this procedure, let us take the \underline{R}_0 associated with $a_0^{uc} = 17.13$ Å: [3.91 Å, 4.73 Å].

$$\underline{f}_0 = \frac{[3.91 \text{ \AA}, 4.73 \text{ \AA}]}{17.13 \text{ \AA}} = [0.23, 0.28] \quad (4.25)$$

When $a_0^{uc} = 17.03$ Å, to maintain $\underline{f}_0 = [0.23, 0.28]$ we must work with a new $\underline{R}_0 = [3.89, 4.70]$.

Subsequently, the guest-dependent and dissociation parameters were regressed against experimental equilibrium data by minimizing $\text{Fobj_1}_{global}^{eq}$. These parame-

ters are then used as input for the next steps.

Afterward, the small and large cages' compressibility in log scale ($\ln \kappa_R$) were separately estimated as it was noticed during the parameterization that there was a significant correlation between them. The small and large cavities' compressibility were estimated by minimizing the global version of Fobj_1 in steps 3 and 4, respectively.

Finally, since the guest-dependent, dissociation, and some of the lattice parameters are co-dependent, for good fitting, some of the estimated parameters are reiterated in step 2, and the procedure is repeated until convergence is reached.

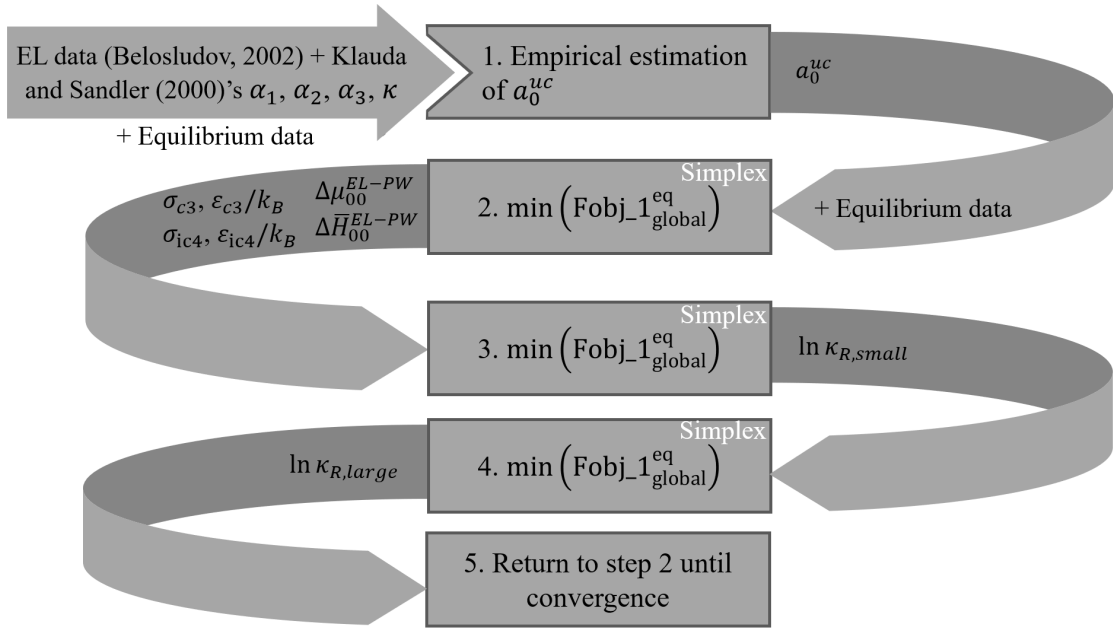


Figure 4.4: Pshift model parameter estimation methodology flowchart.

Chapter 5

Results and discussion

This chapter's goal is to present and discuss the obtained results from the thermodynamic modeling implementation, namely the Interstitial and the Pshift models.

The first section aims at validating the thermodynamic modeling by presenting how the implemented models perform concerning the available data in the literature. Hydrates of sI structure were prioritized in the validation process by virtue of their greater information availability in the literature — specifically, pure methane and ethane hydrates. Bearing in mind that we do not intend to reproduce KLAUDA and SANDLER (2000)'s implementation, our results will not be compared to theirs. Alternatively, we aim to validate our own interpretation of KLAUDA and SANDLER (2000)'s approach against the available experimental data.

Subsequently, the main contributions of the present work are introduced: pure sII hydrates equilibrium curves, as well as the optimal parameters obtained for the Interstitial and the Pshift models.

Finally, a stability analysis is carried out to investigate the feasibility of building mixed hydrates equilibrium curves with the parameters used to assemble the pure hydrates diagrams previously demonstrated.

5.1 Thermodynamic model validation

Prior to implementing the Pshift model to obtain phase equilibrium and volume diagrams for sII hydrates, it is fundamental to validate the thermodynamic modeling with the available data in the literature. Therefore, before the new contributions of this work are demonstrated, results that already exist in the literature

were reproduced.

First, the Interstitial model was applied to build phase diagrams for pure methane and ethane sI hydrates. Afterward, the same plots are assembled through the Pshift model implementation.

Henceforth, the molecules that promote hydrate formation involved in this research, such as methane, ethane, propane, and isobutane, will be referred to as c1, c2, c3, and ic4, respectively.

5.1.1 Interstitial model validation

Since the Interstitial model employment to predict the hydrate phase is part of this research's scope, its validation is indispensable. In this sense, Figures 5.1 and 5.2 illustrate how equilibrium temperature of c1 and c2 hydrates behave throughout a specific pressure range.

Even though there are some Kihara parameter sets in the literature, we opted not to use them. Firstly, for the more straightforward case – which is the Interstitial model validation for sI hydrates –, the empirical correlation purported by Equation 3.86 was sufficient. Furthermore, for the sII hydrates phase equilibrium calculation, we preferred to estimate the Kihara parameters to obtain the best possible Interstitial model adjustment to compare to the Pshift model simulations. Therefore, we used an alternative approach to compute the Langmuir coefficients in this section.

Instead of using the equation based on the free volume integral to calculate the Langmuir coefficients, we employed the empirical correlation described by Equation 3.86 with the parameters estimated by MUNCK *et al.* (1988). The square well function was used to model guest-host interaction. In other words, the same adopted strategy by PARRISH and PRAUSNITZ (1972).

From Figures 5.1 and 5.2, one can observe that although the equilibrium simulation does not rigorously agree with all experimental points, the equilibrium temperature behavior predominantly follows the tendency noticed in the experiments until approximately 2000 bar of pressure. Near the conditions where the equilibrium retrograde behavior is observed, the simulations diverge substantially from the experimental data, consistently underestimating the equilibrium temperatures at pressures over 2000 bar. This discrepancy is probably a consequence of negligence concerning the approach's constraints. Despite the promising results obtained by PARRISH and PRAUSNITZ (1972), the authors indeed warn about the Equation 3.86 restrictions: according to them, this equation must only be applied to calculate

the Langmuir coefficients for temperatures between 260 K and 300 K.

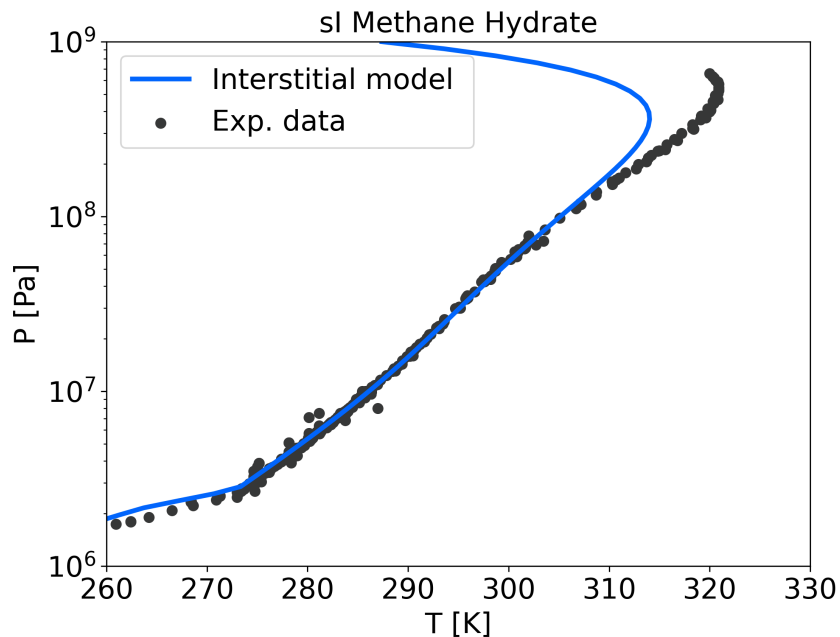


Figure 5.1: I-H-V and LW-H-V phase equilibria prediction for CH_4 hydrate using the Interstitial model. Experimental data from NIST in KROENLEIN *et al.* (2015).

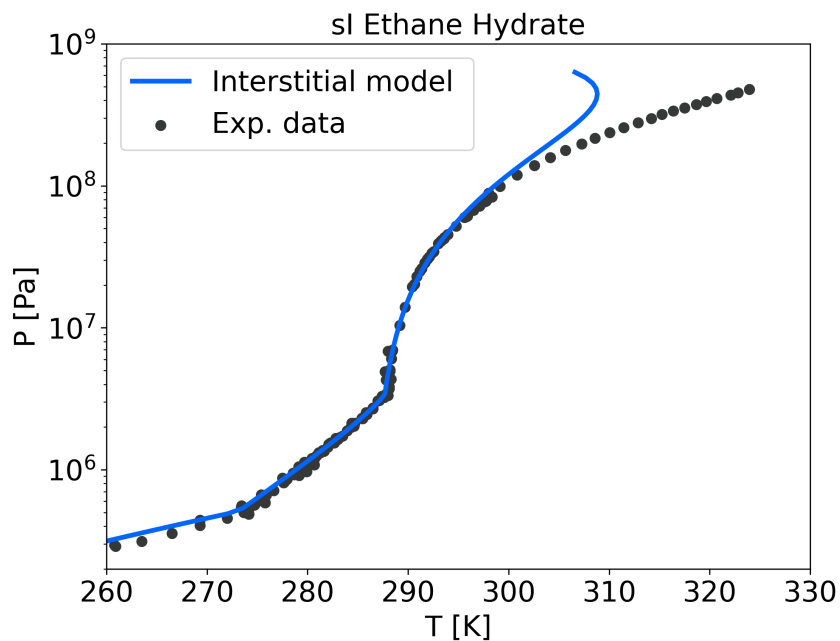


Figure 5.2: I-H-LHc, LW-H-LHc and LW-H-V phase equilibria prediction for C_2H_6 hydrate using the Interstitial model. Experimental data from NIST in KROENLEIN *et al.* (2015).

In conclusion, it is reasonable to assume that the implementation carried out in this work for the Interstitial model was successful, as the equilibrium curves mostly

agree with the experimental data.

5.1.2 Pshift model validation

Similar to the Interstitial model validation, equilibrium curves for sI hydrates were assembled using the Pshift model. Nevertheless, as the Kihara parameters were available, we could compute the Langmuir coefficients through the free volume integral. Thus, the Langmuir coefficients used to built the equilibrium curves portrayed by Figures 5.3 and 5.4 were calculated through Equation 3.94.

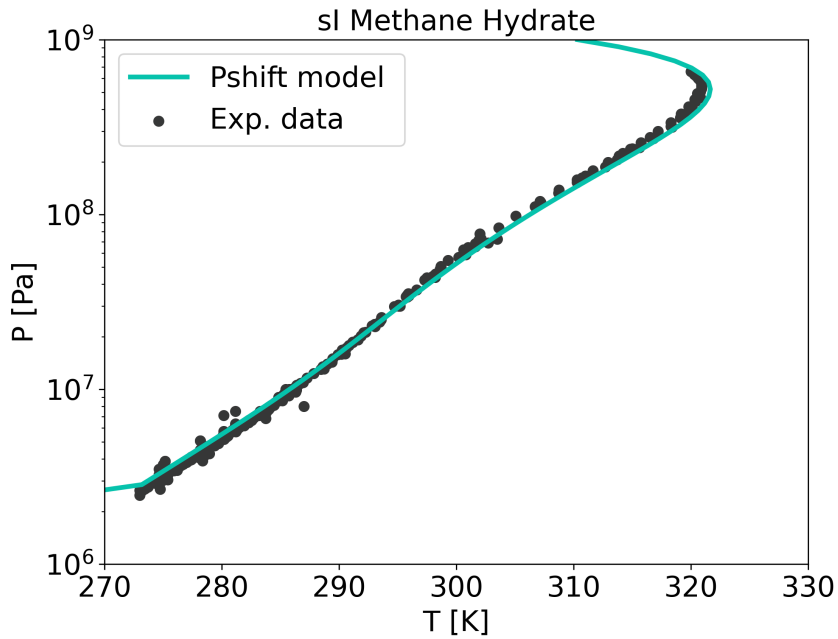


Figure 5.3: LW-H-V phase equilibria prediction for CH_4 hydrate using the Pshift model. Experimental data from NIST in KROENLEIN *et al.* (2015).

From Figures 5.3 and 5.4, one can quickly notice that there is a nearly perfect fit between the equilibrium simulation and the experimental data – as it was expected from a proper Pshift model implementation with the parameters reported by SEGTOVICH *et al.* (2022). Including the retrograde behavior region for the c1 hydrate. Contrarily to what was observed in Figure 5.1, the Pshift model implementation with its optimal parameters (SEGTOVICH *et al.*, 2022) is plainly capable of predicting the methane hydrate equilibrium at very high pressures.

Therefore, we can conclude that the implementation carried out in this work for the Interstitial model was also successful. The next step consists of regressing the parameters for new systems: c3 and ic4 pure hydrates (structure sII).

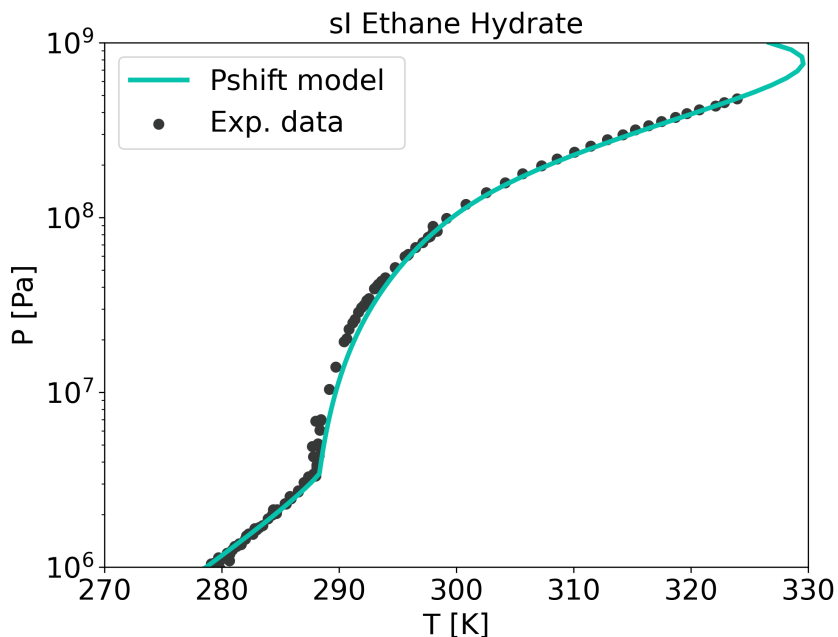


Figure 5.4: LW-H-LHc and LW-H-V phase equilibria prediction for C_2H_6 hydrate using the Pshift model. Experimental data from NIST in KROENLEIN *et al.* (2015).

5.2 Results for pure sII hydrates

Both models' implementation has been validated; thus, we can generate new diagrams to examine how pure sII hydrates equilibria behave at high pressures. Furthermore, this section scrutinizes the parameterization outcomes for each model.

5.2.1 Interstitial model

5.2.1.1 Interstitial model optimal parameters

In consonance with the procedure covered by Section 4.5.4.1, the Interstitial model parameterization was performed in two steps: minimization of F_{obj_1} (Equation 4.21) by using the PSO method – an heuristic global minimum search method – followed by the minimization of F_{obj_2} (Equation 4.22) through the Nelder-Mead method – a direct local minimum search method. Table 5.1 lists the initial guess and optimal value found for all the parameters involved in the estimation. Moreover, aiming to facilitate the methodology reproduction, parameters that did not take part in the parameterization – but are essential to adjust the model – were also included in Table 5.1.

By including F_{obj_2} in the parameterization, we could contemplate the intrinsic experimental fluctuations for the temperature and pressure measurements

within the optimization problem. In this sense, the so-called reconciliation parameters were also estimated and their optimal values are exhibited in Figures 5.5 and 5.6 as orange points.

Table 5.1: Optimal parameters for sII hydrates predicted by the Interstitial model (after simplex method optimization).

Parameter		Initial guess (after PSO)	Optimal value	Status
Guest-dependent parameters	a_{c3}	-	0 Å	Fixed
	σ_{c3}	4.259 Å	3.749 Å	Estimated
	ε_{c3}/k_B	184.6 K	201.6 K	Estimated
	a_{ic4}	-	0 Å	Fixed
	σ_{ic4}	2.740 Å	3.797 Å	Estimated
	ε_{ic4}/k_B	338.0 K	202.1 K	Estimated
Dissociation parameters	$\Delta\mu_{w,00}^{EL-PW}$	886.5 J/mol	814.8 J/mol	Estimated
	$\Delta\bar{H}_{w,00}^{EL-PW}$	-6113.0 J/mol	-5702.8 J/mol	Estimated
	$\Delta\bar{C}_{p,w,00}^{EL-PW}$	-	-39.16 J/(mol·K)	Fixed
Lattice parameters	a_0^{uc}	-	17.13 Å	Fixed
	α_1	-	2.249e-4	Fixed
	α_2	-	2.013e-6	Fixed
	α_3	-	1.009e-9	Fixed
	κ_{hyd}	-	1.098e-10 Pa ⁻¹	Fixed
	$\kappa_{R,small}$	-	0 Pa ⁻¹	Fixed
	$\kappa_{R,large}$	-	0 Pa ⁻¹	Fixed

5.2.1.2 Equilibrium diagrams

This section is designed to demonstrate the sII hydrates equilibria simulations generated by the Interstitial model.

Here we used the free volume integral, differing from the preferred strategy used to calculate the Langmuir coefficients within the Interstitial model implementation to predict sI hydrates equilibria. The parameterization provided the necessary parameters to use Equation 3.94 instead of the empirical correlation described by Equation 3.86.

Figures 5.5 and 5.6 show how the equilibrium temperature predicted by the Interstitial model behaves with pressures ranging from 1 bar to 1000 bar. Moreover,

since a data reconciliation procedure was carried out along with the parameterization, Figures 5.5 and 5.6 also display the experimental data before (dark gray points) and after the reconciliation (orange points).

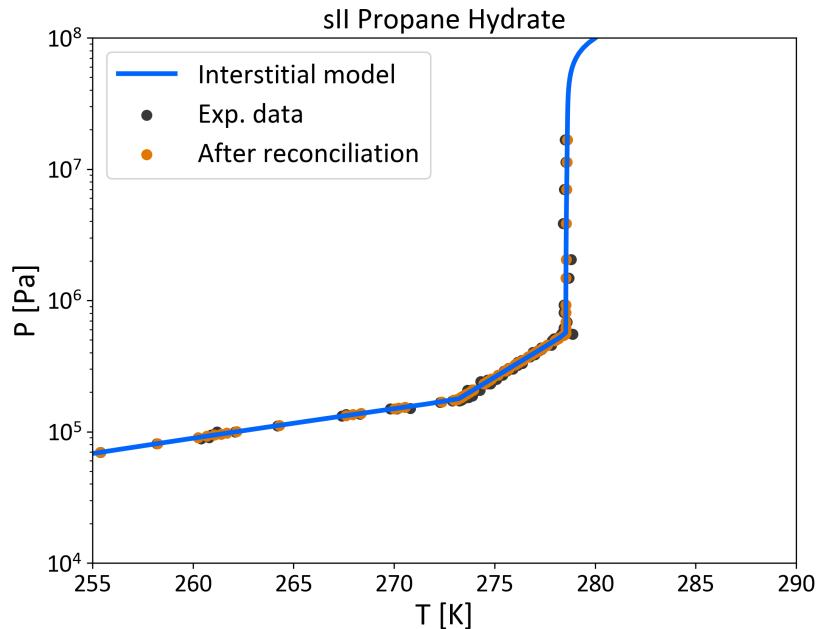


Figure 5.5: I-H-LHc, LW-H-LHc and LW-H-V phase equilibria prediction for C_3H_8 hydrate using the Interstitial model. The dark gray points represent the experimental data obtained from NIST in KROENLEIN *et al.* (2015). The orange points illustrate the experimental data after reconciliation.

For the propane hydrate, Figure 5.5 shows an excellent agreement between the simulated equilibrium and the available data in the literature. No significant disparity between the experimental data before and after reconciliation can be observed.

Likewise, Figure 5.6 shows that the isobutane hydrate equilibrium prediction adjusts reasonably well to the experimental data after reconciliation. However, a slight divergence can be noticed between the dark gray and orange points in Figure 5.6. In other words, assuming the modeling is well implemented, a higher degree of uncertainty associated with ic4 hydrates equilibrium measurements should be expected compared to c3 hydrates experiments. Nevertheless, since the standard deviation associated with hydrate equilibrium experiments is not available in the literature, we can only make educated guesses about the measurement errors of such experiments. The estimated values for the variances related to temperature and pressure measurements (V_T and V_P) are displayed in Table 5.2.

In conclusion, despite the minor discrepancy mentioned above for the isobutane hydrate simulation, it is safe to say that the thermodynamic modeling was successfully implemented. Thus, ratifying the results presented in Section 5.1. Nev-

ertheless, some comments about the data reconciliation results must be made.

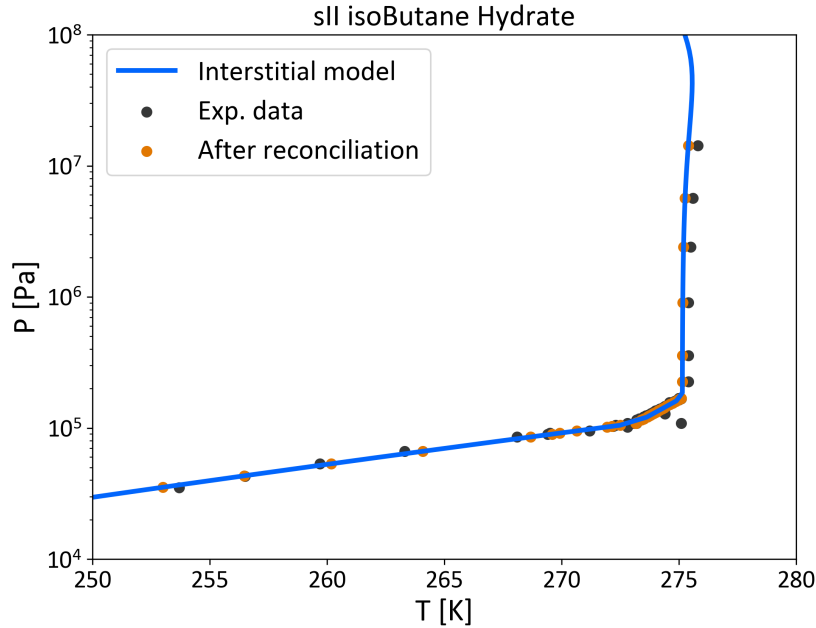


Figure 5.6: I-H-LHc, LW-H-LHc and LW-H-V phase equilibria prediction for iC_4H_{10} hydrate using the Interstitial model. The dark gray points represent the experimental data obtained from NIST in KROENLEIN *et al.* (2015). The orange points illustrate the experimental data after reconciliation.

First, by analyzing the figures presented by Table 5.2 one can notice that estimated value for the pressure variance is excessively high, producing a standard deviation of approximately 1.4 GPa. Second, from Figure 5.6 it is possible to observe that the reconciliation of the experimental points measured at high pressures yielded a systematic adjustment, which conflicts with the hypothesis that considered that the experimental error followed a Gaussian distribution. Therefore, although the parameterization enabled a reasonable agreement between the simulation and the experimental data, the strategy must be revised to incorporate some fundamental concepts in the calculation.

Table 5.2: Regressed temperature and pressure-related variances.

Parameter	Estimated value
$\ln V_T$	0.7057
$\ln V_P$	42.175

5.2.2 Pshift model

5.2.2.1 Pshift model optimal parameters

Following the procedure introduced by Section 4.5.4.2, the optimal parameters for the Pshift model were estimated using the Interstitial model optimal parameters (presented in Table 5.1) as initial guesses. As explained in the section mentioned above, all the parameters involved in the parameterization were estimated by minimizing Fobj_1 through the Nelder-Mead optimization method, except for a_0^{uc} , whose optimal value was empirically obtained.

Even though the Pshift parameterization methodology is not as robust as the one devised to optimize the Interstitial model, the latter model's optimal parameters employment as initial guesses compensates for the more empirical approach used to optimize the Pshift model.

Figure 5.7 depicts the results of empirical estimation procedure devised to locate the optimal a_0^{uc} for the Pshift model. We did not include all the diagrams generated in the a_0^{uc} estimation process because the others would not bring any useful information. Thus, we focused on showing how the simulation fits the experimental data for the superior (17.13 Å) and inferior (17.03 Å) bounds.

With respect to Figure 5.7, subplots (a), (b) and (c) demonstrate equilibrium and volumetric curves for c3 and ic4 hydrates applying $a_0^{uc} = 17.13$ Å. While subplots (d), (e) and (f) show equilibrium and volumetric curves for c3 and ic4 hydrates applying $a_0^{uc} = 17.03$ Å. In addition, subplots (a) and (d) present equilibrium curves, subplots (b) and (e) display $P \times a^{uc}$ at 273 K, and subplots (c) and (f) exhibit $T \times a^{uc}$ at 1 atm.

Since the value of a_0^{uc} greatly influences the parameterization, different optimal parameters were obtained for each case. Tables 5.3 and 5.4 show these optimal parameters sets.

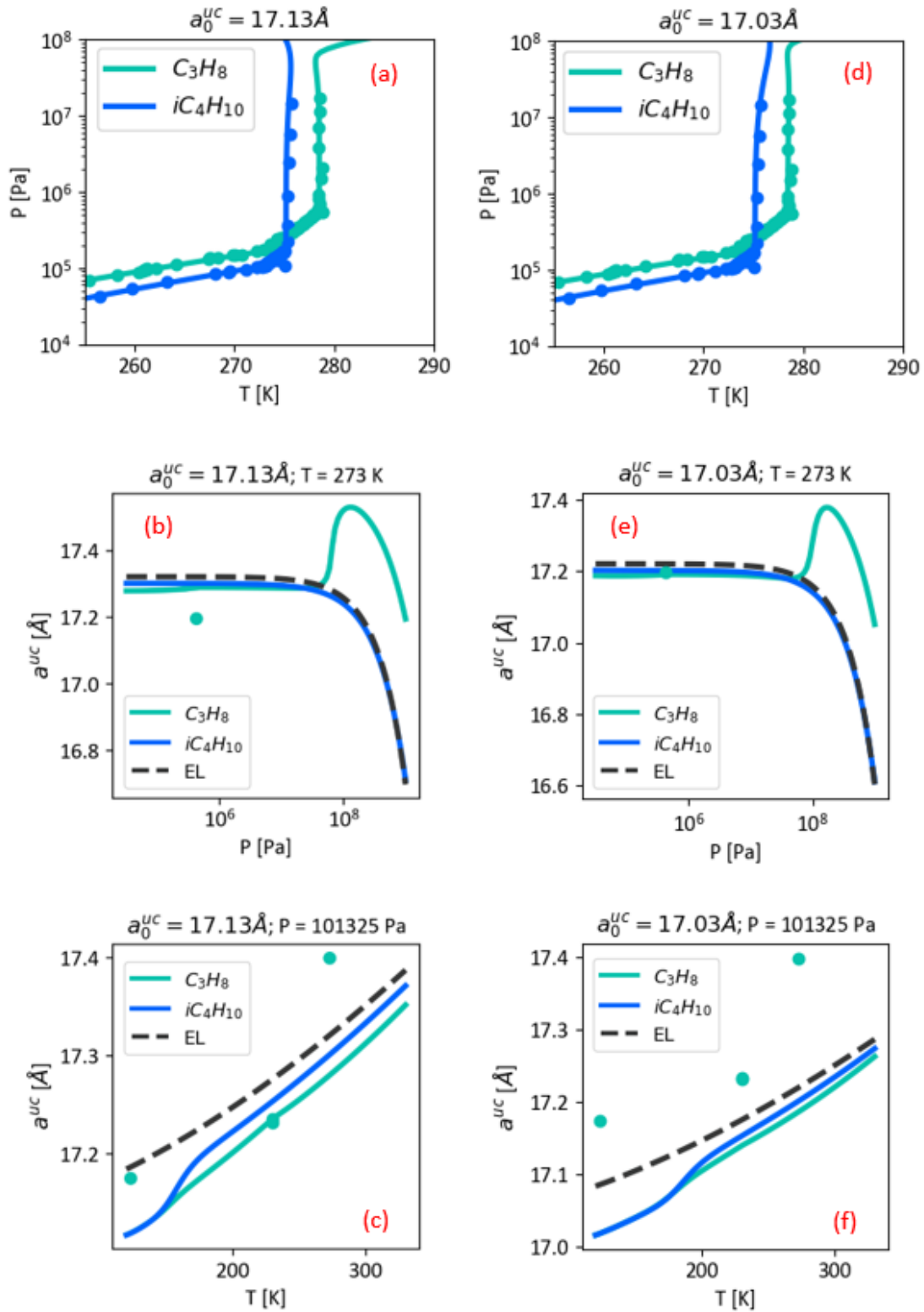


Figure 5.7: Pshift model's equilibrium and volume prediction of sII empty lattice, propane, and isobutane hydrates for different values of a_0^{uc} . The solid green lines represent the propane hydrate simulations, the solid blue lines represent the isobutane hydrate simulations, and the dashed dark gray lines represent the sII empty lattice simulations. Green points represent experimental data related to propane hydrates, and blue points represent experimental data related to isobutane hydrates.

Based on the diagrams displayed by subplots (a) and (d) in Figure 5.7, it is clear for both a_0^{uc} (and \underline{R}_0) values that the equilibrium simulations are in good agreement with the experimental data. On the other hand, the same conclusion cannot be drawn for the volumetric diagrams. For $a_0^{uc} = 17.13 \text{ \AA}$, subplot (b) shows that the model over-predicts the c3 hydrate volume at a constant temperature, while subplot (c) reveals that the simulation agrees with two measurements at constant pressure. For $a_0^{uc} = 17.03 \text{ \AA}$ the simulation responds very differently: subplot (e) reveals that the model correctly predicts the only available experimental point at a constant temperature, whereas subplot (f) shows that the simulation considerably under-predicts the c3 hydrate volume at constant pressure.

Table 5.3: Optimal parameters for sII hydrates predicted by the Pshift model for $a_0^{uc} = 17.13 \text{ \AA}$.

Parameter	Initial guess	Optimal value	Status	
Guest-dependent parameters	a_{c3}	-	0 \AA	Fixed
	σ_{c3}	3.749 \AA	3.806 \AA	Estimated
	ε_{c3}/k_B	201.6 K	200.7 K	Estimated
	a_{ic4}	-	0 \AA	Fixed
	σ_{ic4}	3.797 \AA	4.057 \AA	Estimated
	ε_{ic4}/k_B	202.1 K	182.4 K	Estimated
Dissociation parameters	$\Delta\mu_{w,00}^{EL-PW}$	814.8 J/mol	828.3 J/mol	Estimated
	$\Delta\bar{H}_{w,00}^{EL-PW}$	-5702.8 J/mol	-5508.4 J/mol	Estimated
	$\Delta\bar{C}_{p,w,00}^{EL-PW}$	-	-39.16 J/(mol·K)	Fixed
Lattice parameters	a_0^{uc}	17.13 \AA	17.13 \AA	Fixed
	α_1	-	2.249e-4	Fixed
	α_2	-	2.013e-6	Fixed
	α_3	-	1.009e-9	Fixed
	κ_{hyd}	-	1.098e-10 Pa^{-1}	Fixed
	$\kappa_{R,small}$	1.098e-10 Pa^{-1}	1.104e-10 Pa^{-1}	Estimated
	$\kappa_{R,large}$	1.098e-10 Pa^{-1}	1.098e-10 Pa^{-1}	Estimated
	$R_{0,small}$	3.910 \AA	3.910 \AA	Fixed
$R_{0,large}$	4.730 \AA	4.730 \AA	Fixed	

In other words, both parameter sets seem to be equivalently good for predicting hydrate equilibrium and equally inefficient for simulating hydrate volume simultaneously. This is evidence of the high correlation between the parameters when regressed against limited experimental data. Despite the good amount of pure hydrate equilibrium data, to reduce the parameter correlation, it is crucial to employ

a more diverse data set in the parameterization: (more) volume data, occupation data, dissociation enthalpy data, and mixed hydrate equilibrium data.

Table 5.4: Optimal parameters for sII hydrates predicted by the Pshift model for $a_0^{uc} = 17.03 \text{ \AA}$.

Parameter	Initial guess	Optimal value	Status	
Guest-dependent parameters	a_{c3}	-	0 \AA	Fixed
	σ_{c3}	3.749 \AA	3.773 \AA	Estimated
	ε_{c3}/k_B	201.6 K	175.7 K	Estimated
	a_{ic4}	-	0 \AA	Fixed
	σ_{ic4}	3.797 \AA	4.002 \AA	Estimated
	ε_{ic4}/k_B	202.1 K	161.9 K	Estimated
Dissociation parameters	$\Delta\mu_{w,00}^{EL-PW}$	814.8 J/mol	828.4 J/mol	Estimated
	$\Delta\bar{H}_{w,00}^{EL-PW}$	-5702.8 J/mol	-5512.5 J/mol	Estimated
	$\Delta\bar{C}p_{w,00}^{EL-PW}$	-	$-39.16 \text{ J/(mol}\cdot\text{K)}$	Fixed
Lattice parameters	a_0^{uc}	17.03 \AA	17.03 \AA	Fixed
	α_1	-	$2.249\text{e-}4$	Fixed
	α_2	-	$2.013\text{e-}6$	Fixed
	α_3	-	$1.009\text{e-}9$	Fixed
	κ_{hyd}	-	$1.098\text{e-}10 \text{ Pa}^{-1}$	Fixed
	$\kappa_{R,small}$	$1.098\text{e-}10 \text{ Pa}^{-1}$	$1.104\text{e-}10 \text{ Pa}^{-1}$	Estimated
	$\kappa_{R,large}$	$1.098\text{e-}10 \text{ Pa}^{-1}$	$1.098\text{e-}10 \text{ Pa}^{-1}$	Estimated
	$R_{0,small}$	3.887 \AA	3.887 \AA	Fixed
	$R_{0,large}$	4.702 \AA	4.702 \AA	Fixed

Interestingly, both parameter sets anticipate the lattice contraction for propane and isobutane hydrates for a wide pressure range. More about crystallography will be discussed in the following sections.

Since there is not an unequivocally correct optimal parameter set, we chose, for practical effects, the one presented by Table 5.3 to carry on with the discussion.

5.2.2.2 Equilibrium diagrams

After validating the Pshift model implementation and estimating its optimal parameters (listed in Table 5.3), it is time to study this model's ability to predict sII hydrates' formation. For that reason, $P \times T$ diagrams were assembled to illustrate the conditions in which pure propane and isobutane hydrates are formed. Figures 5.8

and 5.9 show the obtained equilibrium curves for c3 and ic4 hydrates, respectively.

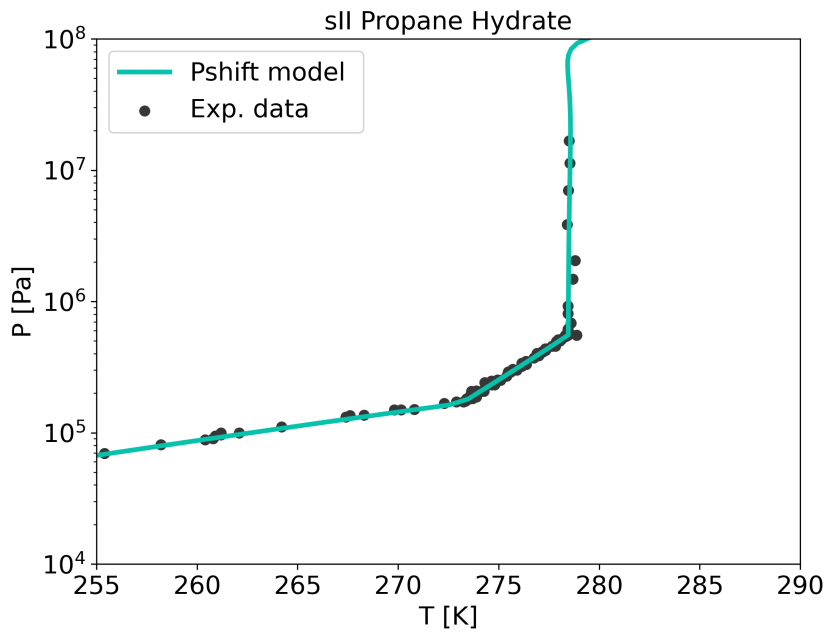


Figure 5.8: I-H-LHc, LW-H-LHc and LW-H-V phase equilibria prediction for C₃H₈ hydrate using the Pshift model. Experimental data from NIST in KROENLEIN *et al.* (2015).

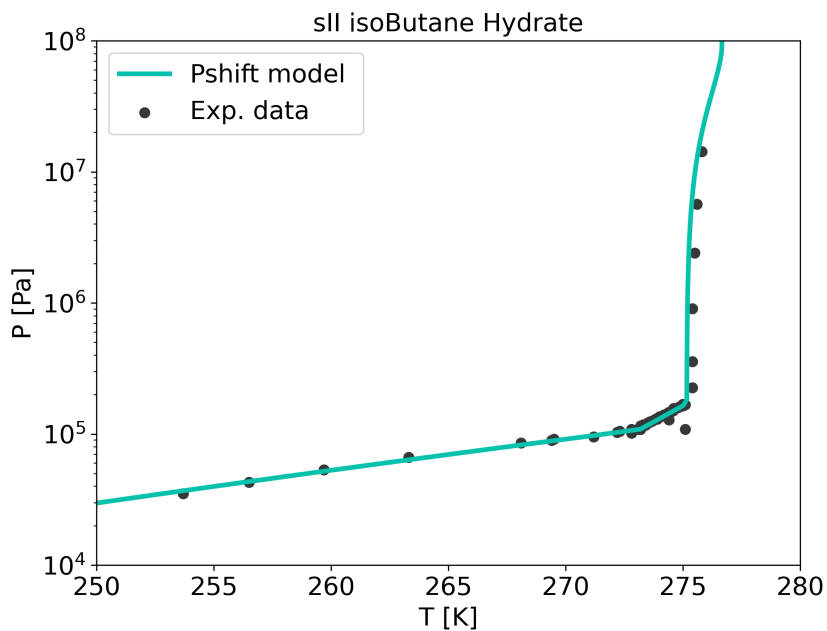


Figure 5.9: I-H-LHc, LW-H-LHc and LW-H-V phase equilibria prediction for iC₄H₁₀ hydrate using the Pshift model. Experimental data from NIST in KROENLEIN *et al.* (2015).

From the equilibrium curves depicted by Figures 5.8 and 5.9, it is clear that

the Pshift model adjusts almost perfectly to the available experimental data for propane hydrates. For isobutane hydrates, although there is a slight deviation between the predicted equilibrium temperature and the one observed in the experiments in the LW-H-V phase equilibrium region, the model mostly concurs with the available experimental data. This solid agreement between the sII hydrates' simulation and experiments indicates proper thermodynamic modeling and parameterization methodology implementation.

5.2.2.3 Volume diagrams

In addition to the equilibrium curves presented in the previous sections, plots that correlate the hydrate's lattice unit cell parameter with pressure (at a constant temperature) and temperature (at a fixed pressure) were built. Since these plots indirectly provide information about the hydrate volume, they are referred to as "volume diagrams" in this work.

Even though the main objective of this research is to expand the Pshift model's ability to simulate hydrates formation, it is essential to investigate how accurately can the Pshift model predict the hydrates' volume. While the equilibrium curves provide a great deal of information about the hydrate dissociation, the volume diagrams give us vital data about the hydrate's crystallography. With this information, it is possible to anticipate if the guests are causing the lattice to expand or shrink regarding the hydrate's reference state.

Since there is virtually no usable volumetric experimental data available in the literature for sII hydrates¹, the quantitative analysis of the volume diagrams is problematic. This unavailability causes a bias in the parameterization procedure, favoring equilibrium data over volumetric. Consequently, the optimal parameters presented in Table 5.3 may not adjust the model satisfactorily regarding the – very scarce – volumetric experimental data. Hence, we intend to discuss the hydrate volume simulations from a qualitative perspective.

Figures 5.10 and 5.11 show the unit cell parameter as a function of pressure (at 273 K), and as a function of temperature (at 101 325 Pa), respectively.

Both Figures 5.10 and 5.11 show that c3 and ic4 hydrates' unit cell edge lengths are smaller compared to the empty lattice, except when they are submitted to very

¹HESTER *et al.* (2007) presented a considerable amount of propane hydrate thermal expansion experimental points at atmospheric pressure in their work. However, these measurements were taken at the fixed occupation ratio found for the highest temperature (230 K). In this sense, except for the 230 K point, all the others are considered meta-stable, and our model is not properly fit to represent this kind of data. Therefore, we decided only to use the highest temperature measurement from the HESTER *et al.* (2007) experimental data.

high pressures at 273 K. For the isobutane, the lattice expansion is quite subtle, but it is possible to observe the solid blue line crossing the dashed dark gray line at approximately 1×10^4 bar.

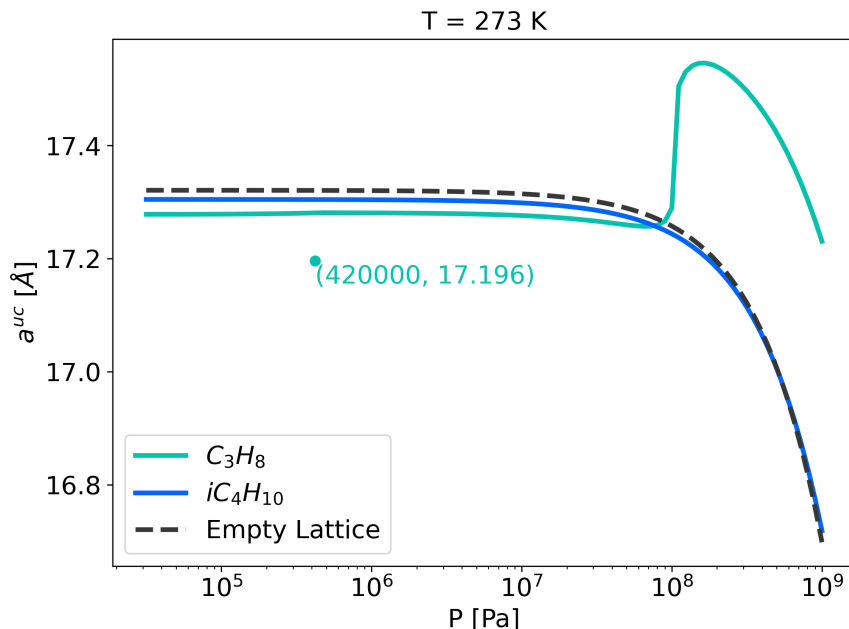


Figure 5.10: Unit cell parameter versus pressure for C_3H_8 and iC_4H_{10} hydrates (green and blue lines, respectively), and empty lattice (dark gray dashed line) at 273 K using the Pshift model. The green point portrays the propane hydrate experimental data from KOH *et al.* (1996).

By applying the reasoning explained in Section 3.5, these graphs indirectly reveal that propane and isobutane molecules at least fit loosely within the large cavities, which, in this case, contributes more to the contraction effect than the small cage since, at a fixed pressure, these pure hydrates have a smaller volume than the hypothetical sII empty lattice. Considering the isochoric perspective – illustrated in Figure 3.2 –, a negative pressure shift should be expected for both hydrates for most temperature and pressure conditions, according to our simulations. However, not all equilibrium points should present a negative pressure shift since, for very high pressures, Figure 5.10 shows that the hydrates have a higher volume than the empty lattice (i.e., positive pressure shift).

As anticipated, nothing can be inferred about the Pshift model’s capability to predict sII hydrates’ volume. A quick look to Figures 5.10 and 5.11 reveals that the tuned parameter set presented by Table 5.3 could not represent adequately the volumetric experimental data.

On the one hand, the model could qualitatively predict the lattices’ edge length as a function of temperature and pressure. The expected thermal expansion ap-

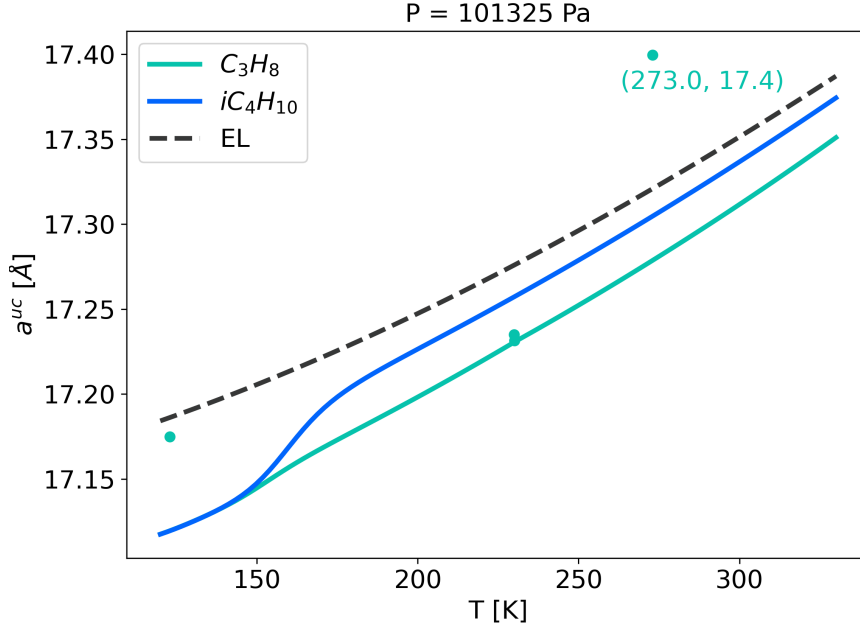


Figure 5.11: Unit cell parameter versus temperature for C_3H_8 and iC_4H_{10} hydrates (green and blue lines, respectively), and empty lattice (dark gray dashed line) at 273 K using the Pshift model. The green points portray the propane hydrate experimental data from KIRCHNER *et al.* (2004), HESTER *et al.* (2007) and BELOSLUDOV *et al.* (2002).

peared for isobaric experiments, and the lattice compression could be identified at very high pressures for isothermal measurements. Moreover, most experiments displayed in Figures 5.11 and 5.10 indicates that the c3 and ic4 hydrates would have a lower volume than the empty lattice, converging our model’s simulations.

By studying Figure 5.10 some intriguing phenomena are unveiled. First, we focus on the propane hydrate plot (green line). At moderate conditions, the propane hydrate volume is almost unaffected by pressure increments since it remains constant until approximately 5×10^7 Pa (or 500 bar). Two phenomena co-occur as the system pressure increases: guest adsorption is favored, and the crystalline lattice is compressed. Interestingly, right about 1×10^3 bar, a lattice swelling can be observed for the propane hydrate. In this region, the guest adsorption promotion phenomenon is believed to overwhelm lattice compression, and the crystalline structure expands to accommodate the new guests until a certain pressure. Along with the lattice, the cavities swell, facilitating propane molecules’ adsorption within the small cages. This phenomenon is called gate-opening.

As the pressure increases and the hydrate gets saturated, the guest adsorption loses intensity until it reaches a point where it becomes to be less favored than the lattice compression; eventually, at extreme conditions (1×10^3 bar $< P < 1 \times 10^4$ bar),

as the lattice gets compressed, the hydrate volume progressively reduces. At this point, the importance of considering the cavities' compressibility becomes very clear since it is only logical to assume that the cages shrink along with the crystalline structure. At some point, the cages get too small, and the guests are gradually expelled from the lattice. This phenomenon is called gate-closing. For the isobutane hydrate volume simulation (blue plot), Figure 5.10 shows that a different behavior should be expected compared to the propane hydrate at very high pressures: instead of dropping after a peak, the unit cell parameter sharply declines. In other words, according to the Pshift model simulation, ic4 hydrates only present the gate-closing phenomenon at extreme pressures. The isobutane molecules are probably too big to fit inside the small cages, and with all the large cages occupied, because of this steric hindrance, the pressure increase only favors lattice compression, shrinking the crystalline structure. Possibly, this is why no gate-opening phenomenon should be expected for ic4.

The simulations mostly disagree with the experimental data. Unfortunately, we could not satisfactorily adjust the model to the volumetric experimental data. In addition, our isobaric simulation of the propane hydrate edge length strongly diverges from BELOSLUDOV *et al.* (2002)'s. While the author's simulation predicts that the propane hydrate would have a larger volume than the empty lattice, ours suggests otherwise.

Nevertheless, neither is there an agreement between available experimental data in the literature. We have highlighted two points in the volume diagrams to illustrate this discrepancy: the sole experimental point at Figure 5.10 (from KOH *et al.* (1996) and the point located in the upper right quadrant in Figure 5.11 (from BELOSLUDOV *et al.* (2002)). The text near the above-mentioned points represents their coordinates, for instance: Figure 5.10's point is situated at approximately 4.2 bar and 17.2 Å (measured at 273 K), and 5.11's point is located at 273 K and 17.4 Å (measured at 1 bar). Assuming that, at moderate conditions, the pressure does not affect dramatically the lattice edge length – which, based on Figure 5.10, seems a reasonable assumption –, these two points should agree to very similar a^{uc} value. However, a considerable difference between these two measurements is observed.

Some alternative scenarios were simulated for exploratory research purposes to enrich the discussion. Figure 5.12 depict the equilibrium and volume predictions for c3 and ic4 hydrates under a special condition: the guest molecules are not allowed to occupy the small cavities mathematically – which is a hypothesis used in the square well approach of PARRISH and PRAUSNITZ (1972) and MUNCK *et al.* (1988), where parameters A and B for c3 and ic4 in the small cages are hard-coded to zero,

and not fitted. For this calculation, we fixed the propane and isobutane molecules' soft-core parameter (σ) at higher values than the small cage radius. First, for case 1, we fixed σ_{c3} and σ_{ic4} at 4.0 Å and 4.1 Å, respectively. Then, for case 2, the same variables were set at 4.2 Å and 4.3 Å. For both cases, the other parameters were re-estimated – those are displayed in Table 5.5. With this constraint, we hope to force the hydrate lattice expansion and demonstrate that the analysis employed to verify lattice compression or expansion depends considerably on the used parameters.

Table 5.5: Optimal parameters for sII hydrates predicted by the Pshift model for special cases 1 and 2.

Parameter		Optimal value Case 1	Optimal value Case 2	Status
Guest-dependent parameters	a_{c3}	0 Å	0 Å	Fixed
	σ_{c3}	4.000 Å	4.200 Å	Fixed
	ε_{c3}/k_B	400.2 K	352.8 K	Estimated
	a_{ic4}	0 Å	0 Å	Fixed
	σ_{ic4}	4.100 Å	4.300 Å	Fixed
	ε_{ic4}/k_B	388.0 K	360.6 K	Estimated
Dissociation parameters	$\Delta\mu_{w,00}^{EL-PW}$	3429.3 J/mol	3123.3 J/mol	Estimated
	$\Delta\bar{H}_{w,00}^{EL-PW}$	-2681.9 J/mol	-3071.5 J/mol	Estimated
	$\Delta\bar{C}p_{w,00}^{EL-PW}$	-39.16 J/(mol·K)	-39.16 J/(mol·K)	Fixed
Lattice parameters	a_0^{uc}	17.13 Å	17.13 Å	Fixed
	α_1	2.249e-4	2.249e-4	Fixed
	α_2	2.013e-6	2.013e-6	Fixed
	α_3	1.009e-9	1.009e-9	Fixed
	κ_{hyd}	1.098e-10 Pa ⁻¹	1.098e-10 Pa ⁻¹	Fixed
	$\kappa_{R,small}$	1.104e-10 Pa ⁻¹	1.104e-10 Pa ⁻¹	Estimated
	$\kappa_{R,large}$	1.098e-10 Pa ⁻¹	1.098e-10 Pa ⁻¹	Estimated
	$R_{0,small}$	3.910 Å	3.910 Å	Fixed
	$R_{0,large}$	4.730 Å	4.730 Å	Fixed

With respect to Figure 5.12, subplots (a), (b) and (c) demonstrate c3 and ic4 hydrates equilibrium and volumetric curves for case 1. While subplots (d), (e), and (f) show c3 and ic4 hydrates equilibrium and volumetric curves for case 2. In addition, subplots (a) and (d) present equilibrium curves, subplots (b) and (e) display $P \times a^{uc}$ at 273 K, and subplots (c) and (f) exhibit $T \times a^{uc}$ at 1 atm.

From the volume diagrams depicted in subplots (e) and (f) of Figure 5.12, it is possible to detect the hydrate expansion very clearly. Before, when the guests

were allowed to occupy the small cavities, the ic4 was too big to fit such cages, while c3 molecules were too small to expand them (according to our simulations, the propane molecules fit loosely within the small cages). By forbidding the guests to fill the small cavities and considerably enlarging the c3 and ic4 soft-core parameters, we observed the lattice expansion – taking the empty lattice as reference –, which is represented by a positive pressure shift. In other words, the case 2 parameter set makes the model simulates c3 and ic4 hydrates whose guests fit tightly within the large cages.

To summarize, this trial is decent evidence that the employed parameters deeply influence the interpretation of hydrate volume simulation diagrams. Therefore, it is reasonable to affirm that the parameterization procedure and the experimental data quality and quantity substantially impact the study of such diagrams. More reliable volume data is required for a sound estimation.

5.3 Stability analysis

All the simulations so far concern pure hydrates, i.e., hydrates of which guests of the same species occupy the cavities. Nevertheless, we rarely encounter a pure hydrate within the engineering systems when it comes to natural gas clathrates. Usually, natural gas hydrates are composed of more than one guest species since the natural gas streams are multi-component.

According to SLOAN JR and KOH (2007), natural gas molecules consist of methane, ethane, propane, and carbon dioxide. Hence, to represent the natural gas hydrates as close as possible to their natural state, it is crucial to study mixed hydrates as well.

Differently from single hydrates, clathrates with multiple guest species can occur in more than one configuration for the same vapor composition. For instance, for a specific vapor composition, a mixed hydrate can stabilize with the sI structure at low temperatures, while the sII configuration appears at high temperatures, or vice-versa. Therefore, a stability analysis is required to determine the most stable configuration for a specific condition. Otherwise, we would need to guess the correct structure to select the appropriate parameter set, which is impossible!

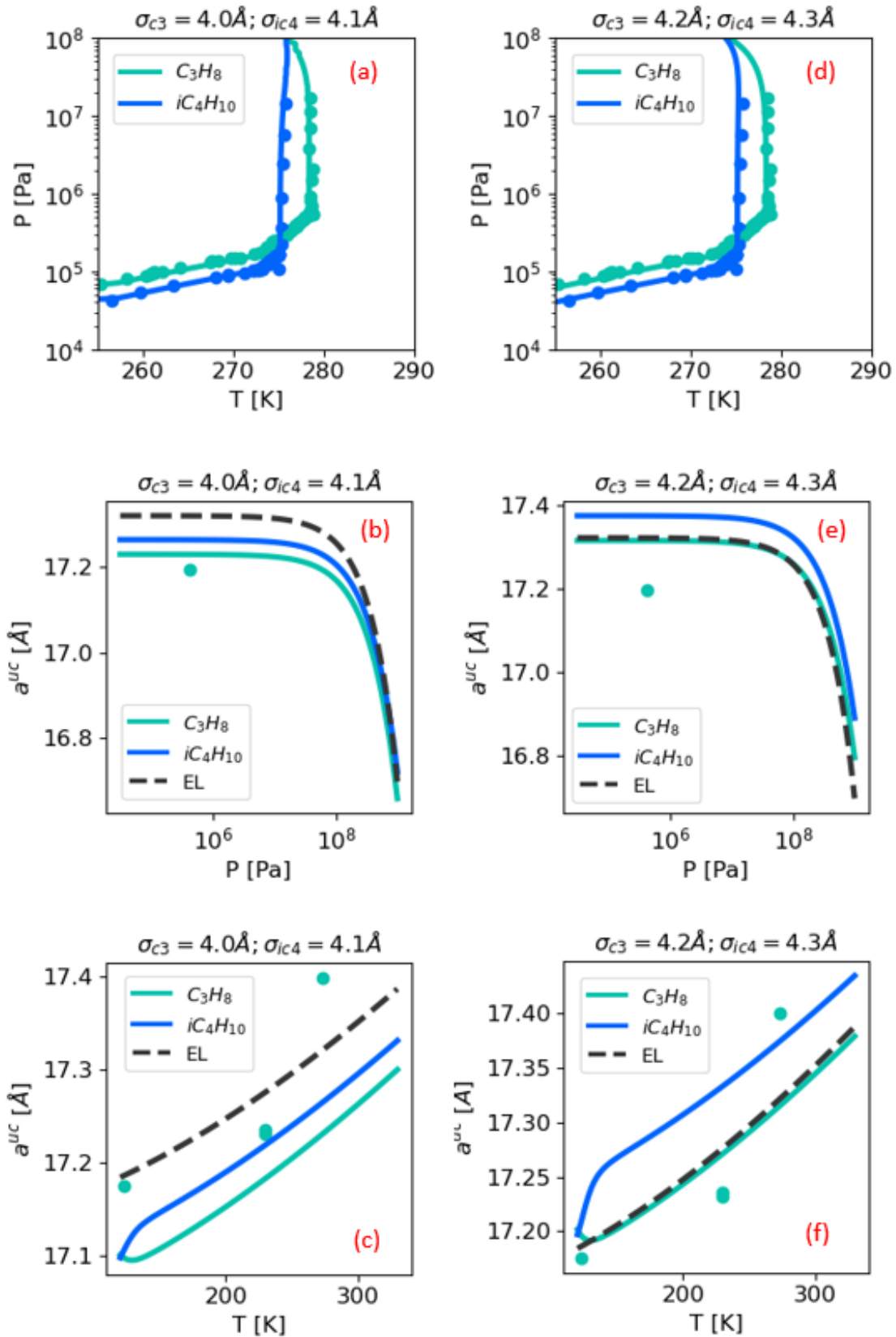


Figure 5.12: Pshift model's equilibrium and volume prediction of sII empty lattice (EL), c3, and ic4 hydrates if the guest molecules were not allowed to occupy the small cavities. The solid green lines represent the c3 hydrate simulations, the solid blue lines represent the ic4 hydrate simulations, and the dashed dark gray lines represent the sII EL simulations. The points represent the experimental data: green for c3 hydrates and blue for ic4 hydrates.

In this sense, as discussed in 4.3, PARRISH and PRAUSNITZ (1972) developed an algorithm that eliminates the necessity of structure deduction by indicating the most stable configuration for a given temperature, pressure, and composition. We have used a modified version of PARRISH and PRAUSNITZ (1972)'s method. By comparing the resultant equilibrium temperature – instead of pressure – we could generate some equilibrium diagrams for mixed hydrates using both Interstitial and Pshift models.

5.3.1 Interstitial model mixed hydrates prediction

As mentioned, we could not find the Kihara parameters for sI hydrates in the literature that were optimized regarding the Interstitial model. Thus, we have resorted to employing the empirical correlation described by Equation 3.86 with the parameters provided by MUNCK *et al.* (1988). We are looking to represent sI and sII forming molecules simultaneously in the thermodynamic model; hence, we adopted the same approach for both guest types: calculating the Langmuir coefficients through the above-mentioned empirical correlation.

Figures 5.13, 5.14 and 5.15 respectively depict the phase equilibrium curves for systems of which vapor compositions are:

- 50% CO₂ + 50% C1 (system A);
- 10% CO₂ + 90% C1 (system B);
- 90% C1 + 10% C2 (system C).

These systems were selected because there was a greater experimental data availability associated with these compositions in the literature.

Figures 5.13 to 5.15 portray scenarios in which the sII configuration (represented by the blue line) occurs for lower temperatures, while the sI structure (represented by the green line) is the most stable one for higher temperatures. These diagrams perfectly illustrate the importance of the PARRISH and PRAUSNITZ (1972)'s algorithm.

Even though there are not many experimental points, it is possible to observe a good agreement between the simulation and the experiments in Figures 5.13 to 5.15. Moreover, no evidence in the literature could contradict our simulations regarding these three systems (A, B, and C). In other words, we did not find the hydrate configuration for all the experimental points, but for the ones we verified, the structure predicted by the model converges with the one observed in the laboratory.

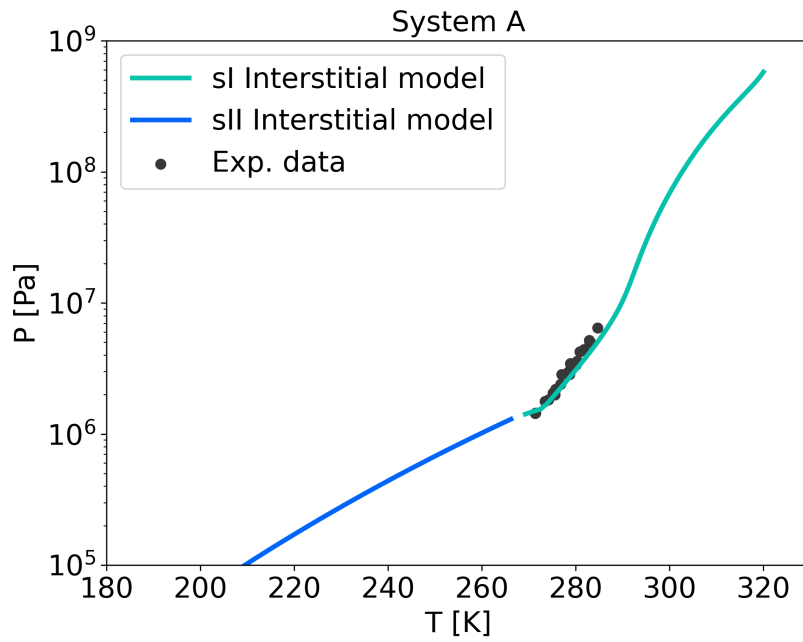


Figure 5.13: Interstitial model's phase equilibrium prediction for a $\text{CH}_4 + \text{CO}_2$ hydrate (50% mol methane). The green line represents the equilibrium simulation of an sI hydrate, and the blue line the equilibrium simulation of an sII hydrate. Experimental data from NIST in KROENLEIN *et al.* (2015).

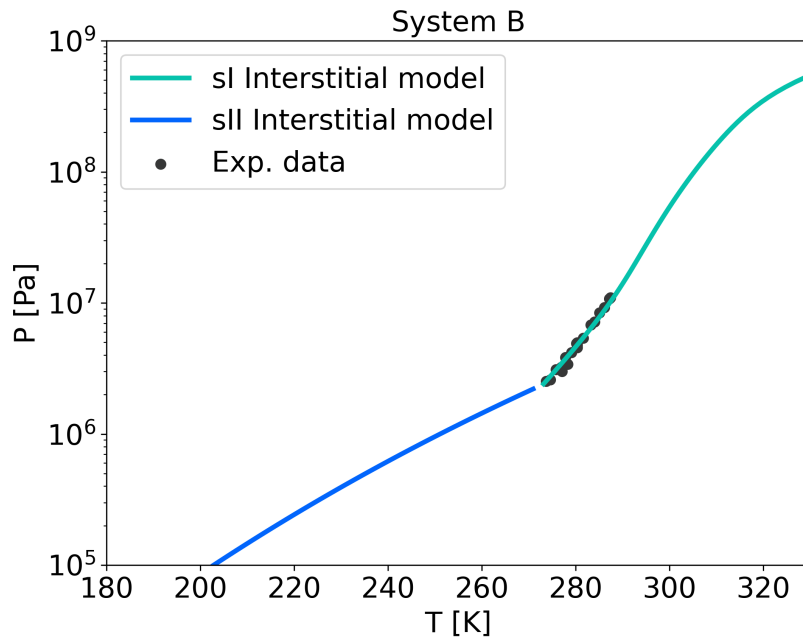


Figure 5.14: Interstitial model's phase equilibrium prediction for a $\text{CH}_4 + \text{CO}_2$ hydrate (90% mol methane). The green line represents the equilibrium simulation of an sI hydrate, and the blue line the equilibrium simulation of an sII hydrate. Experimental data from NIST in KROENLEIN *et al.* (2015).

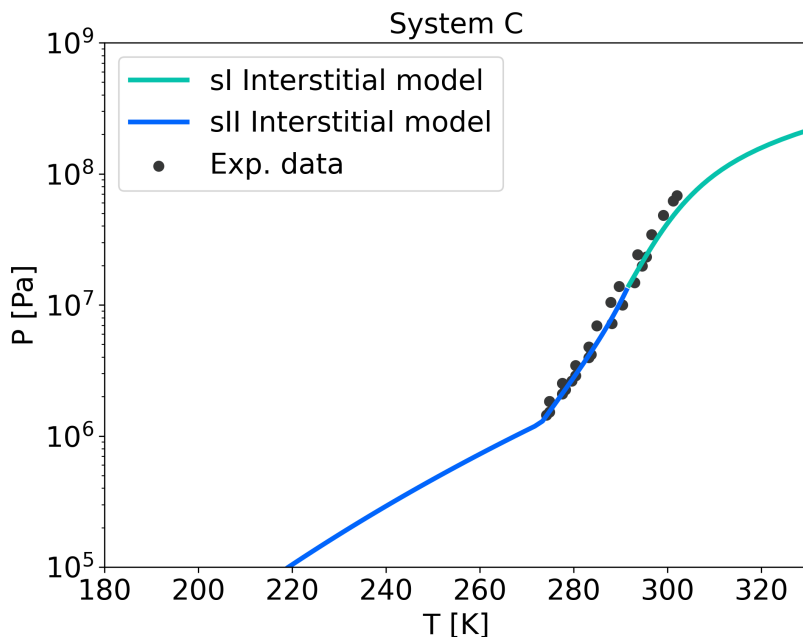


Figure 5.15: Interstitial model’s phase equilibrium prediction for a $\text{CH}_4 + \text{C}_2\text{H}_6$ hydrate (90% mol methane). The green line represents the equilibrium simulation of an sI hydrate, and the blue line the equilibrium simulation of an sII hydrate. Experimental data from NIST in KROENLEIN *et al.* (2015).

5.3.2 Pshift model mixed hydrates prediction

The mixed hydrates equilibrium diagrams obtained via the Pshift model are displayed here. Contrary to the approach implemented for the Interstitial model, the Langmuir coefficients were computed via free volume integral; i.e., we employed the SEGTOVICH *et al.* (2022)’s sI hydrates tuned parameters with our optimal parameters for sII-type hydrates in the calculation of the Langmuir coefficients and the phase equilibrium algorithm.

Figures 5.16 to 5.18 respectively depict the phase equilibrium curves for systems of which vapor compositions are given by the above-mentioned systems A, B, and C.

Examining the two models makes it possible to identify similarities and disparities. On the one hand, like the Interstitial model, the Pshift model fits adequately to systems’ A and B experimental data, as shown by Figures 5.16 and 5.17. Furthermore, both Pshift and Interstitial models predict the correct hydrate configuration of the available experimental data: structure sI.

On the other hand, Figures 5.16 and 5.17 show that the Pshift model anticipates that the hydrate would present structure sI at temperatures below the quadruple point, which diverges from the Interstitial model’s prediction. Moreover,

for system C the Pshift model could not represent the experiments. Not only does the simulation overestimate the equilibrium temperature, but also it predicts a different structure compared to the Interstitial model.

This performance discrepancy might be associated with multiple elements. Nevertheless, since we firmly believe that both the thermodynamic modeling and the PARRISH and PRAUSNITZ (1972)’s algorithm is implemented correctly – which is ratified by the results displayed in the previous sections – this inaccurate simulation might be related to the parameter set selected to execute the calculation.

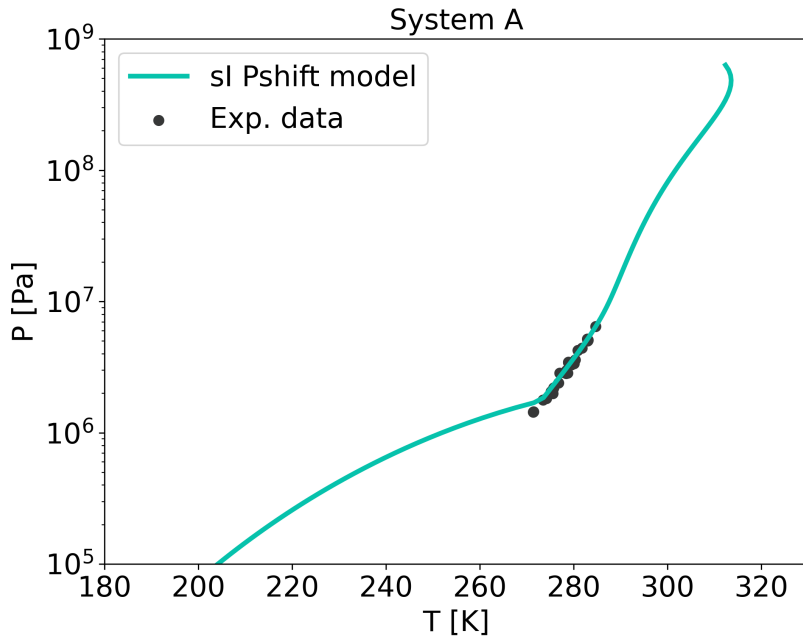


Figure 5.16: Pshift model’s phase equilibrium prediction for a $\text{CH}_4 + \text{CO}_2$ hydrate (50% mol methane). Experimental data from NIST in KROENLEIN *et al.* (2015).

As demonstrated in Section 5.1, the tuned parameters presented by SEGTOVICH *et al.* (2022) are, indeed, optimal to make the Pshift model reproduce some pure sI hydrates phase equilibria. Likewise, as exhibited in Section 5.2, our parameterization procedure outcomes also promote a good fit between the Pshift model simulation and the sII hydrate experimental data. However, both parameter estimation methodologies mainly focused on devising an optimization problem that would produce the optimal parameters for the hydrate structure experimentally encountered, with no restrictions regarding any alternative configuration. For instance, to adjust the model to propane and isobutane experimental data, we did not include any restrictions for the sI structure. In other words, the parameterization procedure was oriented to the most thermodynamically stable structure and delivered the optimal parameters accordingly.

Nonetheless, when the PARRISH and PRAUSNITZ (1972)’s algorithm is ap-

plied, and the hydrate is simulated for both structures, the model might anticipate the less thermodynamically favored lattice configuration if it presents a higher equilibrium temperature than the other – which is the used criterion to determine the equilibrium structure. As there were no constraints regarding the "wrong" structure in the optimization problem for both approaches – ours and SEGTOVICH *et al.* (2022)'s –, the tuned parameters are perfectly capable of representing pure hydrate phase equilibria (by predicting the "correct" configuration), but the same cannot be affirmed for mixed hydrates.

Since there is limited information about the most stable configuration of the equilibrium measured in the experiments, it is delicate to affirm whether our optimal parameters promote or not the simulation of the most stable structure for every system composition. However, Figure 5.18 is sufficient to affirm that the parameterization procedure needs to be more robust to incorporate the complexity of mixed hydrates.

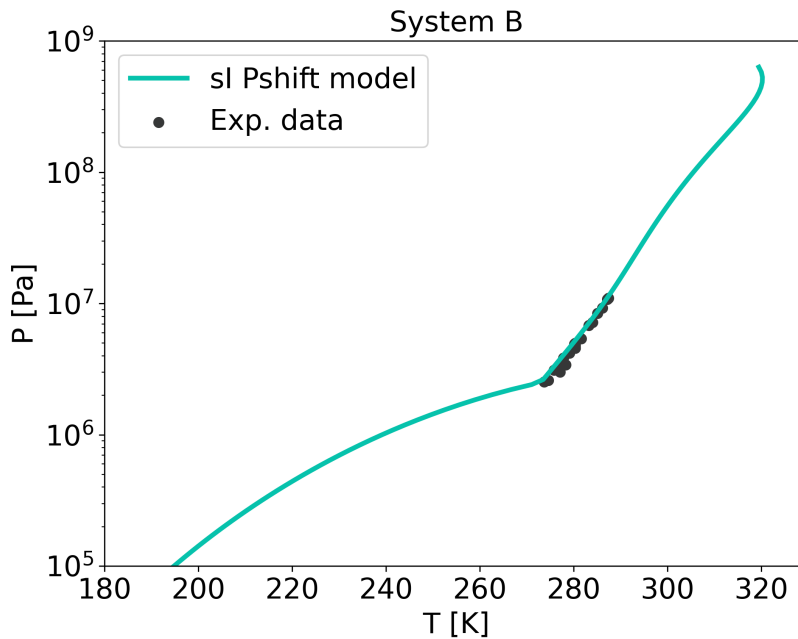


Figure 5.17: Pshift model's phase equilibrium prediction for a $\text{CH}_4 + \text{CO}_2$ hydrate (90% mol methane). Experimental data from NIST in KROENLEIN *et al.* (2015).

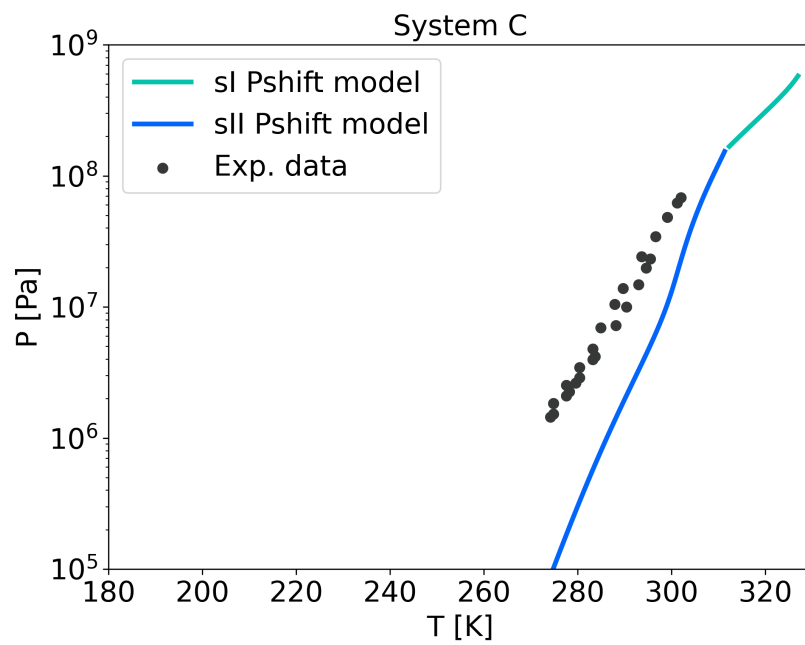


Figure 5.18: Pshift model's phase equilibrium prediction for a $\text{CH}_4 + \text{C}_2\text{H}_6$ hydrate (90% mol methane). The green line represents the equilibrium simulation of an sI hydrate, and the blue line the equilibrium simulation of an sII hydrate. Experimental data from NIST in KROENLEIN *et al.* (2015).

Chapter 6

Conclusions and suggestions

Here, we implemented the Interstitial and Pshift models to predict sII hydrates equilibria and volume by analyzing $P \times T$ diagrams and the unit cell parameter behavior with temperature and pressure. Furthermore, we estimated the above-mentioned models' parameters for sII hydrates.

From the results presented in the previous chapter, it is clear that the Pshift model was successfully implemented and that the tuned parameters promote a decent fit between the phase equilibria simulation and the experimental data. Nevertheless, due to the sparse availability of sII hydrate volumetric data in the literature, the optimal parameters mentioned above have proven inadequate to accurately describe sII hydrates' volume. Even so, the Pshift model could qualitatively reproduce some interesting crystallographic features, which might help understand the many variables that affect the volume of natural gas hydrates.

Even though the Pshift model implementation has yielded promising results, we still have a long journey regarding mixed hydrate simulation. The Pshift model-PARRISH and PRAUSNITZ (1972)'s algorithm combination yields decent results for some specific systems and might be a very appealing alternative to predict mixed hydrates phase equilibria. However, the results presented in Chapter 5 have shown that the parameterization methodology immensely impacts the model's behavior.

Considering the results, we have some suggestions for future research regarding the hydrate phase equilibrium calculation framework.

- The inclusion of experimental data from mixed hydrates equilibrium, dissociation enthalpy (as in MEDEIROS *et al.* (2020)), and cage occupancy in the parameter estimation would be handy to discorrelate parameters. From the mixed hydrates equilibrium results, it is known that the parameters have a

great influence on their prediction. Therefore, incorporating mixed hydrates experimental data would help us decide the proper parameter for pure hydrates.

- We believe that performing more experiments for reliable cage occupancy data and volume data is essential to improve the quantity and quality of sII hydrate volumetric experimental data.
- Moreover, the employment of an algorithm to compute how the hydrate volume behaves with temperature at fixed θ and P (canonical meta-stable calculation) to represent the isobaric volume data would enable the use of many already available $T \times a^{uc}$ experimental points.
- We consider that implementing a parametric statistical analysis to examine the estimated parameters' statistical quality would help us perform a more thorough investigation of the parameterization results.
- Finally, we believe that elaborating a more robust optimization problem by including constraints regarding the less thermodynamically stable configuration in the mixed hydrate equilibrium calculation would hinder the structure misprediction.

References

- BALLARD, A. L., SLOAN, E. D., 2004, “The next generation of hydrate prediction: Part III. Gibbs energy minimization formalism”, *Fluid Phase Equilibria*, v. 218, n. 1, pp. 15–31. ISSN: 03783812. doi: 10.1016/j.fluid.2003.08.005.
- BALLARD, A. L., SLOAN JR, E. D., 2002, “The next generation of hydrate prediction I. Hydrate standard states and incorporation of spectroscopy”, *Fluid Phase Equilibria*, v. 194–197, pp. 371–383.
- BARRER, R. M., EDGE, A. V. J., 1967, “Gas hydrates containing argon, krypton and xenon: kinetics and energetics of formation and equilibria”, *Proceedings of the Royal Society of London. Series A. Mathematical and Physical Sciences*, v. 300, n. 1460, pp. 1–24. ISSN: 0080-4630. doi: 10.1098/rspa.1967.0154.
- BARRER, R. M., STUART, W. I., 1957, “Non-stoichiometric clathrate compounds of water”, *Proceedings of the Royal Society of London. Series A. Mathematical and Physical Sciences*, v. 243, n. 1233, pp. 172–189. ISSN: 0080-4630. doi: 10.1098/rspa.1957.0213.
- BELOSLUDOV, V. R., INERBAEV, T. M., SUBBOTIN, O. S., et al., 2002, “Thermal expansion and lattice distortion of clathrate hydrates of cubic structures I and II”, *Journal of Supramolecular Chemistry*, v. 2, n. 4-5, pp. 453–458. ISSN: 14727862. doi: 10.1016/S1472-7862(03)00072-8.
- BHAWANGIRKAR, D. R., ADHIKARI, J., SANGWAI, J. S., 2018, “Thermodynamic modeling of phase equilibria of clathrate hydrates formed from CH₄, CO₂, C₂H₆, N₂ and C₃H₈, with different equations of state”, *Journal of Chemical Thermodynamics*, v. 117, pp. 180–192. ISSN: 10963626. doi: 10.1016/j.jct.2017.09.024. Disponível em: <<https://doi.org/10.1016/j.jct.2017.09.024>>.

- CARSTENS, C., 2019. “Industrial Application of Clathrate Hydrates”. Disponível em: <<https://www.energy.gov/sites/prod/files/2019/06/f63/MHAC%20Chris%20Carstens.pdf>>. Acessado em: 08-mar-2022.
- ESLAMIMANESH, A., MOHAMMADI, A. H., RICHON, D., et al., 2012, “Application of gas hydrate formation in separation processes: A review of experimental studies”, *Journal of Chemical Thermodynamics*, v. 46, pp. 62–71. ISSN: 00219614. doi: 10.1016/j.jct.2011.10.006. Disponível em: <<http://dx.doi.org/10.1016/j.jct.2011.10.006>>.
- FOURNAISON, L., DELAHAYE, A., CHATTI, I., 2004, “GENERAL RESEARCH CO 2 Hydrates in Refrigeration Processes”, *Carbon*, pp. 6521–6526.
- HAMMERSCHMIDT, E. G., 1934, “Formation of Gas Hydrates in Natural Gas Transmission Lines”, *Industrial and Engineering Chemistry*, v. 26, n. 8, pp. 851–855. ISSN: 00197866. doi: 10.1021/ie50296a010.
- HESTER, K. C., HUO, Z., BALLARD, A. L., et al., 2007, “Thermal expansivity for sI and sII clathrate hydrates”, *Journal of Physical Chemistry B*, v. 111, n. 30, pp. 8830–8835. ISSN: 15206106. doi: 10.1021/jp0715880.
- HIELSCHER, S., VINŠ, V., JÄGER, A., et al., 2018, “A new approach to model mixed hydrates”, *Fluid Phase Equilibria*, v. 459, pp. 170–185. ISSN: 03783812. doi: 10.1016/j.fluid.2017.12.015.
- HILL, T. L., 1986, *An Introduction to Statistical Thermodynamics*. 1st ed. New York, Dover Publications, Inc. ISBN: 9780486652429.
- HOLDER, G. D., CORBIN, G., PAPADOPOULOS, K. D., 1980, “Thermodynamic and Molecular Properties of Gas Hydrates from Mixtures Containing Methane, Argon, and Krypton”, *Ind. Eng. Chem. Fundam.*, , n. 19, pp. 282–286.
- HOLDER, G. D., ZETTS, S. P., PRADHAN, N., 1988, “Phase behavior in systems containing clathrate hydrates: A review”, *Reviews in Chemical Engineering*, v. 5, n. 1-4, pp. 1–70. ISSN: 01678299. doi: 10.1515/REVCE.1988.5.1-4.1.
- HSIEH, M. K., TING, W. Y., CHEN, Y. P., et al., 2012, “Explicit pressure dependence of the Langmuir adsorption constant in the van der Waals-Platteeuw model for the equilibrium conditions of clathrate hydrates”, *Fluid Phase Equilibria*, v. 325, pp. 80–89.

- HWANG, M. J., HOLDER, G. D., ZELE, S. R., 1993, "Lattice distortion by guest molecules in gas-hydrates", *Fluid Phase Equilibria*, v. 83, n. C, pp. 437–444. ISSN: 03783812. doi: 10.1016/0378-3812(93)87048-6.
- IEA, 2019. "World Energy Outlook 2019". Disponível em: <<https://www.iea.org/reports/world-energy-outlook-2019>>. Acessado em: 08-mar-2022.
- JOHN, V. T., PAPADOPOULOS, K. D., HOLDER, G. D., 1985, "A Generalized Model for Predicting Equilibrium Conditions for Gas Hydrates", *AIChE Journal*, v. 31, n. 2, pp. 252–259.
- KHAN, M. N., PETERS, C. J., KOH, C. A., 2019, "Desalination using gas hydrates: The role of crystal nucleation, growth and separation", *Desalination*, v. 468, n. July, pp. 114049. ISSN: 00119164. doi: 10.1016/j.desal.2019.06.015. Disponível em: <<https://doi.org/10.1016/j.desal.2019.06.015>>.
- KIRCHNER, M. T., BOESE, R., BILLUPS, W. E., et al., 2004, "Gas hydrate single-crystal structure analyses", *Journal of the American Chemical Society*, v. 126, n. 30, pp. 9407–9412. ISSN: 00027863. doi: 10.1021/ja049247c.
- KLAUDA, J. B., SANDLER, S. I., 2000, "A fugacity model for gas hydrate phase equilibria", *Industrial and Engineering Chemistry Research*, v. 39, n. 9, pp. 3377–3386.
- KOH, C. A., SAVIDGE, J. L., TANG, C. C., 1996, "Time-resolved in-situ experiments on the crystallization of natural gas hydrates", *Journal of Physical Chemistry*, v. 100, n. 16, pp. 6412–6414. ISSN: 00223654. doi: 10.1021/jp960094s.
- KROENLEIN, K., MUZNY, C., KAZAKOV, A., et al., 2015. "Clathrate Hydrate Physical Property Database". Disponível em: <<https://gashydrates.nist.gov/>>. Acessado em: 15-mar-2022.
- KUHS, W. F., CHAZALLON, B., RADAELLI, P. G., et al., 1997, "Cage occupancy and compressibility of deuterated N₂-clathrate hydrate by neutron diffraction", *Journal of Inclusion Phenomena and Molecular Recognition in Chemistry*, v. 29, n. 1, pp. 65–77. ISSN: 09230750. doi: 10.1023/A:1007960217691.
- LENNARD-JONES, J. E., DEVONSHIRE, A. F., 1937, "Critical phenomena in gases I", *Proc. R. Soc. London. Ser. A - Math. Phys. Sci.*, v. 163, pp. 53–70. ISSN: 00280836. doi: 10.1098/rspa.1937.0210.

- LEVINE, I. N., 2014, *Quantum Chemistry*. 7 ed. Nova Iorque, Pearson. ISBN: 978-0-321-80345-0.
- MAKOGON, Y. F., HOLDITCH, S. A., PERRY, K. F., et al., 2004, “Gas hydrate deposits: Formation and development”, *Proceedings of the Annual Offshore Technology Conference*, v. 2, pp. 1534–1541. ISSN: 01603663. doi: 10.4043/16677-ms.
- MAKOGON, Y. F., 1997, *Hydrates of hydrocarbons*. Tulsa, PennWell Books.
- MAKOGON, Y. F., 2010, “Natural gas hydrates - A promising source of energy”, *Journal of Natural Gas Science and Engineering*, v. 2, pp. 49–59.
- MARSHALL, D. R., SAITO, S., KOBAYASHI, R., 1964, “Hydrates at high pressures: Part I. Methane-water, argon-water, and nitrogen-water systems”, *AIChE Journal*, v. 10, n. 2, pp. 202–205. ISSN: 15475905. doi: 10.1002/aic.690100214.
- MCKOY, V., SINANOĞLU, O., 1963, “Theory of dissociation pressures of some gas hydrates”, *The Journal of Chemical Physics*, v. 38, n. 12, pp. 2946–2956. ISSN: 00219606. doi: 10.1063/1.1733625.
- MCQUARRIE, D. A., 1976, *Statistical Mechanics*. New York, Harper & Row.
- MEDEIROS, F. D. A., 2018, *Hydrate Enthalpy of Dissociation from Statistical Thermodynamics*. PhD Thesis.
- MEDEIROS, F. D. A., SEGTOVICH, I. S. V., TAVARES, F. W., et al., 2020, “Sixty Years of the van der Waals and Platteeuw Model for Clathrate Hydrates - A Critical Review from Its Statistical Thermodynamic Basis to Its Extensions and Applications”, *Chemical Reviews*, v. 120, n. 24, pp. 13349–13381.
- MUNCK, J., SKJOLD-JORGENSEN, S., RASMUSSEN, P., 1988, “Computations of the Formation of Gas Hydrates.” *Society of Petroleum Engineers of AIME, (Paper) SPE*, v. 43.
- NG, H.-J., ROBINSON, D. B., 1980, “A Method for Predicting the Equilibrium Gas Phase Water Content in Gas-Hydrate Equilibrium”, *Ind. Eng. Chem. Fundam.*, , n. 19, pp. 33–36.
- PARRISH, W. R., PRAUSNITZ, J. M., 1972, “Dissociation Pressures of Gas Hydrates Formed by Gas Mixtures”, *Industrial and Engineering Chemistry Process Design and Development*, v. 11, n. 1, pp. 26–35.

- PRATT, R. M., BALLARD, A. L., SLOAN, E. D., 2001, “Beware of singularities when calculating clathrate hydrate cell potentials!” *AIChE Journal*, v. 47, n. 8, pp. 1897–1898.
- RASOOLZADEH, A., SHARIATI, A., 2016, “Considering double occupancy of large cages in nitrogen and oxygen hydrates at high pressures”, *Fluid Phase Equilibria*, v. 434, pp. 107–116. ISSN: 03783812. doi: 10.1016/j.fluid.2016.11.028. Disponível em: <<http://dx.doi.org/10.1016/j.fluid.2016.11.028>>.
- SCHWAAB, M., PINTO, J. C. U., 2007, *Análise de dados experimentais I: fundamentos de estatística e estimação de parâmetros*. 1 ed. Rio de Janeiro, E-papers. ISBN: 8576500884.
- SEGTOVICH, I. S. V., 2018, *Thermodynamic modeling of compressible hydrates and calculations of multiphase equilibrium diagrams*. PhD Thesis.
- SEGTOVICH, I. S. V., MEDEIROS, F. D. A., TAVARES, F. W., 2022, “Physical-Chemical Properties of Compressible Clathrates: A Natural Pressure Shift by Extending the van der Waals and Platteeuw Model”, *Journal of Physical Chemistry C*, v. 126, n. 5, pp. 2839–2856. ISSN: 19327455. doi: 10.1021/acs.jpcc.1c09715.
- SLOAN, E. D., KHOURY, F. M., KOBAYASHI, R., 1976, “Water Content of Methane Gas in Equilibrium with Hydrates”, *Industrial and Engineering Chemistry Fundamentals*, v. 15, n. 4, pp. 318–323. ISSN: 01964313. doi: 10.1021/i160060a016.
- SLOAN JR, E. D., KOH, C. A., 2007, *Clathrate Hydrates of Natural Gases*. Boca Raton, CRC Press.
- VAN DER WAALS, J. H., PLATTEEUW, J. C., 1959, “Clathrate Solutions”. In: *Advance in Chemical Physics*, v. II, John Wiley & Sons, pp. 1–57, Amsterdam.
- VELUSWAMY, H. P., KUMAR, A., SEO, Y., et al., 2018, “A review of solidified natural gas (SNG) technology for gas storage via clathrate hydrates”, *Applied Energy*, v. 216, n. February, pp. 262–285. ISSN: 03062619. doi: 10.1016/j.apenergy.2018.02.059. Disponível em: <<https://doi.org/10.1016/j.apenergy.2018.02.059>>.
- WARRIER, P., KHAN, M. N., SRIVASTAVA, V., et al., 2016, “Overview: Nucleation of clathrate hydrates”, *Journal of Chemical Physics*, v. 145,

n. 21. ISSN: 00219606. doi: 10.1063/1.4968590. Disponível em: <<http://dx.doi.org/10.1063/1.4968590>>.

YIN, Z., LINGA, P., 2019, “Methane hydrates: A future clean energy resource”, *Chinese Journal of Chemical Engineering*, v. 27, pp. 2026–2036.

ZHANG, W., WANG, Y., LANG, X., et al., 2017, “Performance analysis of hydrate-based refrigeration system”, *Energy Conversion and Management*, v. 146, pp. 43–51. ISSN: 01968904. doi: 10.1016/j.enconman.2017.04.091. Disponível em: <<http://dx.doi.org/10.1016/j.enconman.2017.04.091>>.